R-05-82

Scale dependence and estimation of rock thermal conductivity

Analysis of upscaling, inverse thermal modelling and value of information with the Äspö HRL prototype repository as an example

Jan Sundberg, Pär-Erik Back, Geo Innova AB

Göran Hellström, Lund University

December 2005

Svensk Kärnbränslehantering AB
Swedish Nuclear Fuel
and Waste Management Co
Box 5864
SE-102 40 Stockholm Sweden
Tel 08-459 84 00
+46 8 459 84 00
Fax 08-661 57 19
+46 8 661 57 19

ISSN 1402-3091
SKB Rapport R-05-82

Scale dependence and estimation of rock thermal conductivity

Analysis of upscaling, inverse thermal modelling and value of information with the Äspö HRL prototype repository as an example

Jan Sundberg, Pär-Erik Back, Geo Innova AB

Göran Hellström, Lund University

December 2005

Preface

This report is based on the results of a suite of investigations with the main objective to get a better understanding of the scale of thermal processes and decrease the uncertainties in a Thermal Site Descriptive Model. Most of the work has been done in association with the Prototype Repository at Äspö Hard Rock Laboratory. However, parts of the data come from the site investigation at the Simpevarp area.

Göran Hellström has been involved in the modelling of significant scale and the inverse modelling at the prototype repository. Except the authors, other participants in the project have been Anna Bengtsson and Märta Ländell, Geo Innova AB.

A reference group has been connected to the project consisting of: Johan Andersson, Rolf Christiansson, Lars O Ericsson and Harald Hökmark.

Summary

The thermal properties of the rock affects the resulting temperature on the canister and on the surrounding buffer, and is thus an important parameter in determining the repository layout in order to meet thermal demands. Of main interest is the thermal conductivity, since it directly influences the design of a repository. This report is a result of the SKB RD&D programme. In the programme, research and development on the area of heat transport and thermal properties are described /SKB 2004/.

The overall objective of the project is to reduce the uncertainties in thermal data used in the dimensioning and design of a repository for final disposal of the nuclear waste produced in Sweden. The project is also meant to increase the knowledge of scale effects, anisotropy and inhomogeneity, establish a model/compilation of the different uncertainties present regarding thermal properties and determine the scale of the variation of thermal properties that significantly influence the temperature on the canister (the scale where difference no longer are levelled out).

In the site descriptive projects (e.g. /SKB 2005/) thermal properties are modelled for different rock types and geological domains. The thermal conductivity for a rock type is based on small scale laboratory measurements which can give rather high variability. There is a need for upscaling of thermal properties to the scale of interest for the thermal design of a repository, in order to decrease the variability due to small scale determinations. If the rock is relatively homogeneous, variation in thermal conductivity at a small scale is averaged out at a larger scale.

The scale at which variations of thermal conductivity is significant for the maximum temperature on the canister has been investigated by numerical modelling. The result shows that below a scale of approximately 1–2 m, variation in thermal conductivities is mainly levelled out due to the size of the canister. Consequently it is possible to upscale small scale thermal conductivity values into at least 1–2 m scale when assessing the maximum temperature. However, the appropriate scale for thermal conductivity data depends on the method of modelling.

The scale dependence for laboratory measurements of thermal conductivity with different sensor size has been investigated on samples from Äspö HRL. The difference in results seems to be non significant.

In earlier project a relationship between density and thermal conductivity has been observed /Sundberg 2002/. Within the density range of Ävrö granite, the thermal conductivity is inversely proportional to density. By the use of density logging, the relationship makes it possible to predict the spatial variability of conductivity in the rock mass. In this report, a physical explanation is suggested of the relationship, based on magma composition and mineralogy.

In the prototype repository at Äspö HRL, measurements of the temperature increase, caused by the heat generated from the canisters, have been conducted. Earlier, measurements of the rock thermal properties in the repository have been conducted in laboratory and in situ. A prognosis model of the thermal properties has been established based on these data. The prognosis model is evaluated towards values calculated through inverse modelling. The inverse modelling is based on an iterative process where a fitting of measured and calculated temperatures is performed with a numerical model. There is good agreement between

prognosis of thermal conductivity in the prototype repository and the result from inverse modelling based on 37 different temperature sensors. The rather low thermal conductivity in the prototype repository is verified. Some sensors seem to be influenced by water movements and get a higher evaluated thermal conductivity. However, the evaluation shows that the initial conditions before the heating started where not stable, regarding temperature and water movements.

Different types of variograms can be used to analyse the spatial distribution of conductivities, preferably calculated from density loggings (semi variograms of thermal conductivity), and the spatial distribution of rock types (indicator variograms). The main challenge is to determine the spatial variability in rock domains where Ävrö granite is absent or subordinate. In order to model the spatial variability for these domains in a reliable way more measurements are required, especially for the dominating rock types.

A methodology for upscaling of thermal conductivity from measurement scale to a significant scale for the canister has been developed. The variance is reduced when the scale increases but for some rock types the decrease in variance is low, mainly because of the high large-scale spatial variability. The model has been used in the ongoing site descriptive models in Oskarshamn and Forsmark. Uncertainties in the whole process have been analysed. The largest uncertainty is the representativity of the boreholes.

A Value of Information Analysis (VOIA) has been performed in order to estimate the value of additional investigations by studying how the new information reduces uncertainty in the mean thermal conductivity. Field measurements in a relevant scale yields the highest while producing an improved relationship between density and thermal conductivity is the most cost-efficient alternative of the four investigated ones.

Sammanfattning

Bergets termiska egenskaper påverkar temperaturen på kapslarna och den omgivande bufferten, och är därför en väsentlig parameter vid bestämning av förvarets utformning, med hänseende på termiska krav. Särskilt intressant är den termiska konduktiviteten, därför att den direkt påverkar utformningen av förvaret. Denna rapport är ett resultat av SKB:s FUD-program. I programmet beskrivs forskning och utveckling inom området värmetransport och termiska egenskaper /SKB 2004/.

Det generella syftet med projektet är att reducera osäkerheterna i de termiska data som används vid dimensionering och utformning av slutförvaret för kärnavfall producerat i Sverige. Projektet ska också öka kunskapen om effekter av skala, anisotropi och inhomogenitet, upprätta en modell/sammanställning av olika osäkerheter som finns för termiska egenskaper och beräkna skalan för de termiska egenskapernas variation som signifikant påverkar temperaturen på kapseln (skalan där skillnader i konduktivitet inte längre utjämnas).

I de platsbeskrivande modellerna (t ex /SKB 2005/) beskrivs de termiska egenskaperna för olika bergarter och geologiska domäner. Det kan finnas en stor variabilitet i värmeledningsförmågan baserat på småskalig laboratoriemätning. Det finns därför ett behov av att skala upp egenskaperna till en skala som är relevant för den termiska dimensioneringen av ett förvar. Om en bergart är homogen kommer småskalig variation i värmeledningsförmåga att utjämnas i en större skala.

Den skala för vilken variationer i termisk konduktivitet är relevant för den maximala temperaturen på kapseln, har undersökts med hjälp av numerisk modellering. Resultaten visar att vid en skala under 1–2 m så är variationen i värmeledningsförmåga i huvudsak utjämnad. Sålunda kan man skala upp småskaliga bestämningar av värmeledningsförmåga till åtminstone 1–2 m när maximal temperatur beräknas för kapseln. Till vilken skala det är lämpligt att skala upp resultat till är beroende av den metod som används för simulering av maximal temperatur.

Skalberoendet för laboratoriemätningar av termisk konduktivitet med olika sensorstorlekar har undersökts på prover från Äspö HRL. Skillnaden i resultaten verkar inte vara signifikanta.

I tidigare projekt har ett samband mellan densitet och termisk konduktivitet observerats /Sundberg 2002/. I densitetsintervallet för Ävrögranit, är termisk konduktivitet omvänt proportionell mot densiteten. Genom att använda densitetsloggningar, blir det möjligt att, genom detta samband, förutsäga konduktivitetens rumsliga variation i bergmassan. I denna rapport framläggs en fysikalisk förklaring till sambandet, baserad på magmasammansättning och mineralogi.

I prototypförvaret vid Äspö HRL, har mätningar av temperaturökningen, orsakat av värmeavgivningen från kapslarna, utförts. Tidigare har mätningar av berget termiska egenskaper i förvaret utförts på laboratorium och in situ. En prognostisk modell av de termiska transportegenskaperna har tagits fram baserat på dessa data. Den prognostiska modellen utvärderas mot värden beräknade genom inversmodellering. Inversmodelleringen baseras på en iterativ process där anpassning av uppmätta och beräknade temperaturer utförs i en numerisk modell. Överensstämmelsen mellan prognosen för termisk konduktivitet i prototypförvaret och resultaten från inversmodelleringen (baserad på 37 olika temperatursensorer) är god. Den relativt låga termiska konduktiviteten i prototypförvaret verifieras. Några sensorer

verkar ha påverkats av vattenrörelser och erhåller en högre utvärderad värmeledningsförmåga. Värderingen visar att förhållandena innan uppvärmningen startade inte var stabila, beträffande temperatur och vattenrörelser.

Olika typer av variogram kan användas för att analysera den rumsliga fördelningen för konduktivitet, företrädesvis beräknad från densitetsloggningar (semivariogram för termisk konduktivitet), och den rumsliga fördelningen för bergarter (indikatorvariogram). Den största utmaningen är att utvärdera den rumsliga variationen i bergartsdomäner där Ävrögranit inte finns eller endast finns i liten mängd. För att modellera den rumsliga variationen för dessa domäner på ett tillförlitligt sätt, behövs fler mätresultat, främst för de dominerande bergarterna.

En metodik för uppskalning av termisk konduktivitet från mätskala till en skala relevant för kapslarna, har utvecklats. Variansen reduceras när skalan ökar, men för några bergarter är variansminskningen liten, främst beroende på den stora storskaliga rumsliga variationen. Modellen har använts i det pågående arbetet med de platsbeskrivande modellerna för Oskarshamn och Forsmark. Osäkerheter för hela processen har analyserats. Den största osäkerheten är representativiteten för borrhålen.

En datavärdesanalys har utförts för att uppskatta värdet av ytterligare undersökningar, genom att studera hur den nya informationen skulle reducera osäkerhet i medelvärdet för termisk konduktivitet. Fältmätningar i en relevant skala ger högst värde, medan förbättring av sambandet mellan densitet och termisk konduktivitet är det mest kostnadseffektiva alternativet av de fyra som undersökts.

Contents

1 Introduction

1.1 General

The thermal properties of the rock mass affects the possible distance, both between canisters and between deposition tunnels, and therefore puts requirements on the necessary repository volume. Of primary interest is the thermal conductivity, since it directly influences the design of a repository. This report is a result of the SKB RD&D programme. In the programme, research and development within the area of heat transport and thermal properties are described /SKB 2004/.

The Swedish Nuclear Fuel and Waste Management Co (SKB) have established a prototype repository at the Äspö HRL since several years for final disposal of nuclear waste produced in Sweden /SKB 2005b/. Canisters have been installed in the rock mass with a heat emission simulating the effect of the radioactive waste. A number of investigations have been conducted and a monitoring programme has been established. Measurements of thermal properties have earlier been conducted within and outside of the prototype repository both as field and laboratory measurements /Sundberg and Gabrielsson 1999/. Further, a number of temperature sensors have been installed in the rock mass with different geometric configurations in relation to the canisters. The prototype repository gives opportunities to study the confidence in prognosis models of thermal conductivities together with scale effects.

This report presents three different ways of acquiring thermal conductivity values; from direct measurements with the TPS method, from estimations based on density loggings and a relationship between density and thermal conductivity, and from inverse modelling using temperature measurements from the prototype repository. Further, the identified scale effects of the thermal properties are described and a methodology is presented for thermal modelling at large scales in order to handle the scale effects. Uncertainties in data and thermal modelling are evaluated and used in a value of information analysis in order to evaluate the worth of additional measurement and investigation alternatives. Further the scale for the variation of the thermal properties that influence a canister significantly is investigated.

Some of the statistical concepts used in the report deserve clarification. Both the arithmetic mean and the geometric mean are used in the report. The former is referred to as “the mean” while the geometric mean always is denoted as “the geometric mean”. Whenever standard deviations are calculated from measurements, the data set is regarded as a sample from the population and consequently one degree of freedom is lost.

1.2 Scale and determination of thermal properties

1.2.1 Scale of thermal processes in a repository

The thermal function of a repository can be studied at different scales, exemplified in Figure 1-1. In order to describe the influence from natural climatic conditions above ground on the thermal conditions in a repository, mean values and deviations of thermal transport properties for the whole rock mass is adequate. However, for the local temperature field around canisters a much better understanding of the spatial variability of thermal properties

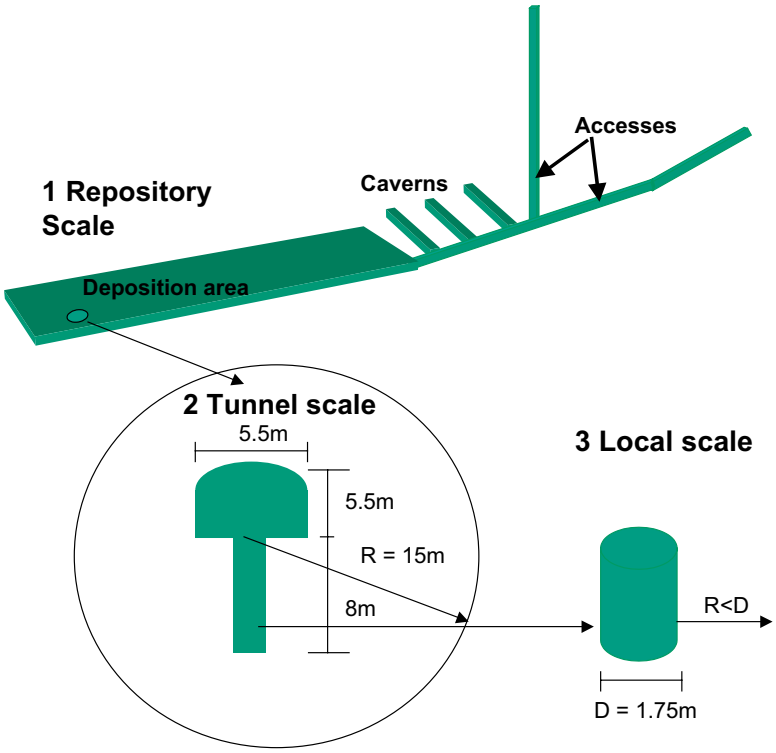

Figure 1-1. *Illustration of the various scales of importance for rock mechanics considerations for siting and constructing a KBS-3 repository /from Andersson et al. 2002/.*

is needed. The sensitivity of the canister temperature for changes in thermal properties is highest in the area close to the canister. It is therefore of special interest to analyse the variation in thermal properties in the rock mass at the scale 3–20 m (canister deposition scale and up to tunnel scale). Small-scale variations in thermal properties are mainly evened out at this scale.

Preliminary, the following scales are believed to be relevant:

- 1–10 m for the thermal function of the canister (canister or local scale),
- 10–100 m for the thermal function of the tunnel (tunnel scale),
- 100–1,000 m for the thermal function of the whole repository (repository scale).

Of special interest is the scale for thermal function of a canister. In Chapter 3 the significant scale of the canister is calculated. Computer simulations are made in order to investigate what scale of variation of thermal properties that influences the temperature of the canister.

1.2.2 Scale of variations and spatial variability in rock

Rock forming minerals have different thermal properties, see i.e. /Sundberg 1988/. The different minerals exist at a micro- or millimetre scale. Thus, there is a rather large variation in thermal properties at this scale. If the rock is fine-grained, isotropic and homogeneous, the variations have to a large degree been evened out at the cm-scale. Therefore, this small-scale variability is of minor importance for rock samples of larger scale.

However, even for a homogeneous igneous rock there is always a variation in thermal properties due to chemical variations in the original magma. This “within rock type” variability may occur at the 1–100 m scale and differs significantly between different rock types.

The most significant type of spatial variability is of course the variation in thermal properties between different rock types, the so called “between rock type” variability. This variation coincides with the appearance of the various rock types, typically at a scale from 0.1 m (dykes) up to several hundred meters (dominating rock types).

1.2.2 Scale of determinations of thermal properties

Determinations of thermal properties are made in different scales. Determinations of thermal properties in the laboratory are often made at the cm-scale. The use of different sensors sizes for such small-scale measurements are made in Chapter 4. Spatial variations in chemistry and mineralogy, which influence the thermal conductivity of rock, also influence the density. A relationship between density and thermal conductivity has been established for certain rock types and permits the use of density logs for determination of the spatial variability of thermal conductivity within the rock mass. This is discussed further in Chapter 5. For the prototype repository it also possible to back-calculate the thermal properties of the rock mass from the measured temperature distribution, see Chapter 6.

1.3 Upscaling

If the rock is relatively homogeneous, variation in thermal conductivity at a given scale is averaged out at a certain distance (a larger scale). If the rock is anisotropic and heterogeneous, a larger variation will exist at the small scale but not necessarily at the larger scale.

There is a need for upscaling of thermal properties to the scale of interest, in order to decrease the variability due to small scale determinations. In this report, an upscaling methodology is developed and described in Chapter 7.

The upscaling process must take into account the spatial variability within a rock type due to mineralogical and chemical changes in the magma. Furthermore, another type of variability is due to the presence of different rock types within a lithological domain. The variability is more pronounced where the difference in thermal conductivity is large between the most common rock types of the domain. A large variability of this type can also be expected in a domain of many different rock types. This type of variability is only reduced significantly when the scale becomes large compared to the spatial occurrence of the rock. This latter type of variability is subsequently referred to as “between rock type”.

1.4 Uncertainties and value of information

In general, a good description of uncertainties and if possible, the quantification of these, may strengthen the results and conclusions of a thermal model. In Chapter 8 an uncertainty model for the prototype repository is presented. These are uncertainties that may introduce variability (or bias) in addition to the spatial variability handled in earlier chapters. This combined variation due to spatial variability and lack-of-knowledge uncertainty is managed in Chapter 9. The lack-of-knowledge uncertainty can be reduced by investigations and a model with the objective to identify efficient investigation strategies is presented. It utilises value of information analysis and makes it possible to compare the value of different methods of determining the thermal conductivity. The methodology is applied using the prototype repository as an example.

1.5 Rock type nomenclature

The nomenclature of rock types is different at the Äspö Hard Rock laboratory compared tothe Simpevarp and Laxemar site description projects /SKB 2005/. The main difference is that at the Äspö HRL, the Ävrö granite (Simpevarp nomenclature) is divided into Ävrö granite and Äspö diorite (Äspö nomenclature). This may cause some confusion but the reason to the simplified rock type nomenclature in the Site dscription projects is that the different types of Ävrö granite are very hard to distinguish by eye.

2 Objective and scope

The overall objective of this project is to reduce the uncertainties in thermal data used in the dimensioning and design of a repository for final disposal of the nuclear waste produced in Sweden. This is of importance since reducing the uncertainty means that the possible distance, both between canisters and deposition tunnels may be reduced. In order to reach this objective, knowledge needs to be gained and different methods need to be tested and evaluated. A number of sub-goals have been formulated for the project:

As regards knowledge three goals have been identified. The project proposes to:

- increase the knowledge of scale effects, anisotropy and inhomogeneity,
- establish a model/compilation of the different uncertainties present regarding thermal properties,
- determine the scale below which variation in thermal properties do not have a significant influence on the temperature on the canister (the scale below where variations in properties are levelled out).

Four purposes are stated regarding methods. The project is meant to:

- investigate scale effects at laboratory measurements,
- more profoundly study the methods for density loggings with an investigation of the relationship between density and thermal conductivity (reason and understanding),
- test inverse modelling as a tool to verify a prognosis model of thermal properties for the prototype repository,
- develop a method to evaluate the use of additional information/data (value of information analysis),
- develop a methodology of upscaling thermal properties to a relevant scale.

3 Significant scale for thermal processes around canisters

3.1 Introduction

An important aspect in the performance of a nuclear waste repository is the thermal exposure of the canister and the buffer material. The maximum canister and buffer temperature must be kept below a certain design temperature limit. The evolution of the canister temperature depends to a large extent on the thermal properties of the surrounding bentonite, rock mass and possible air gaps /Hökmark and Fälth 2003/. The canister temperature is most sensitive to the thermal properties of the material close to the canister, i.e. possible air gaps, the bentonite buffer and the rock nearest the canister borehole. An important issue concerns the level of detail or scale at which the thermal conductivity of the rock must be known and how an uncertainty relates to the ability to predict the maximum possible temperature.

Thus, one source of uncertainty in the thermal modelling is at which scale thermal conductivity is significant for the heat emitted from the canister. The significant scale is believed to be in the interval 1–10 m. Below the significant scale of thermal conductivity variations, the temperature on the canister surface is levelled out. To reduce this uncertainty and get a better understanding of the thermal process around a canister, numerical simulation have been made.

In this study, the thermal conductivity of the rock matrix is randomized in order to study the influence of scale of heterogeneity in thermal conductivity on the maximum canister temperature.

The objective of the modelling is to define the scale for which variations of thermal conductivity is significant for the temperature on the canister, and not to evaluate how large the temperature variation could be in different scales.

3.2 Numerical model

The model repository consists of nine deposition holes with copper canisters surrounded by a bentonite buffer. The deposition holes have been drilled from a tunnel, which has been backfilled with a mixture of bentonite and crushed rock. The deposition boreholes are drilled vertically from the tunnel and placed along a straight horizontal line. The standard spacing between the deposition boreholes is 6 m. It is assumed that identical repositories are placed parallel to the model repository.

A three-dimensional finite difference model of the prototype repository (canisters, buffers, tunnel, etc) is used to calculate the transient temperature increase due to the heat generation in the canisters. The numerical model of the repository uses an explicit finite difference scheme. The code has been developed based on models previously used for underground thermal energy storage applications /Eftring 1990/ and it has been extended to accommodate the geometry of the repository, see inverse modelling in Chapter 6.

The simulated ground region encompasses a parallelepipedical volume of 40×156×120 m^3 (approx. 750,000 m^3) and is described with a grid using 54×271×59 = 863,406 cells for the numerical simulation scheme. The numerical grid has a fine resolution close to the canisters and the cell size expands outwards. The surrounding repositories are modelled by assuming a vertical symmetry plane at mid-distance between the repositories. There is no heat flow across these planes. The other boundaries are set a distance where the boundary conditions will not influence canister temperatures during the simulated time span.

3.3 Assumptions and method

The geometry and dimensions of canister and deposition boreholes as well as materials used in this study is based on the prototype repository. The tunnels above the deposition holes are backfilled with a mixture of bentonite (30%) and crushed rock. The thermal conductivity of the rock mass is assumed to be normal distributed with a mean value of 2.8 W/(m×K) and a standard deviation of 0.35 W/(m×K). This assumption is not strictly valid for the Ävrö granite. However, this is of secondary interest since the main objective of the modelling is to evaluate the scale of variation and not to evaluate how large the absolute temperature variation could be for different scales.

The gaps between canister and bentonite buffer and between bentonite and borehole wall are assumed to be filled with air and have thermal resistances that give a combined temperature difference of about 16°C. Approximately this value was measured for a “dry” canister at the prototype repository /Goudarzi and Johannesson 2004/.

The thermal properties of the different materials involved in the large-scale thermal process are assumed to be homogeneous with exception of the thermal conductivity of the rock. The thermal properties are given in Table 3-1.

The heterogeneity of the rock thermal conductivity is modelled by dividing a ground region, which is slightly larger than the considered ground region for the simulation, into cubes of a certain size and assigning a random thermal conductivity value (normal distribution with average value 2.8 (W/(m×K)) and standard deviation 0.35 W/(m×K)) to each cube. The numerical grid used for the simulation is then placed into this three-dimensional matrix of cubes. Both grids use a cartesian coordinate system. The axes are parallel, but the origins of the two grids do not coincide. The relative location of the origin is placed at random, which means that the cubes are located differently in each simulation. The initial temperature is assumed to be 15°C everywhere.

Table 3-1. Thermal properties of the materials involved in the thermal process.

	Thermal conductivity (W/(m×K))	Volumetric heat capacity (MJ/(m^3×K))
Canister	15.0	4.00
Buffer	1.1	3.40
Backfill in tunnel	1.5	2.50
Rock	Random*	2.20

* Normal distribution with average value 2.8 (W/(m×K)) and standard deviation 0.35.

The time-dependent heat generation in the canisters is /Hökmark and Fälth 2003/:

$$P(t) = P(0)\sum_{i=1}^{7} a_i \exp(-t/t_i) \qquad \text{Equation 3-1}$$

where t is time after deposition and the coefficients t_i and a_i are given by:

Different scales of the heterogeneity of the rock mass were modelled by varying the size of the cubic division of the ground. Five different side lengths of the cubes were used: 1, 2, 5, 10 and 20 m. Thirty simulations were performed for each scale. The simulation gives the maximum volume average temperature for each of the nine canisters. The time to reach the maximum temperature is about ten years.

3.4 Results

The results for the thirty simulation cases for each scale are given in Figure 3-1 to Figure 3-5. The serie number represent a canister. Canister 5 is in the middle and should have the highest temperature (series 5 with bold line). The thermal conductivity is randomly assigned to successively larger and larger scale in the different figures, and therefore the temperature variation is increased in larger scales.

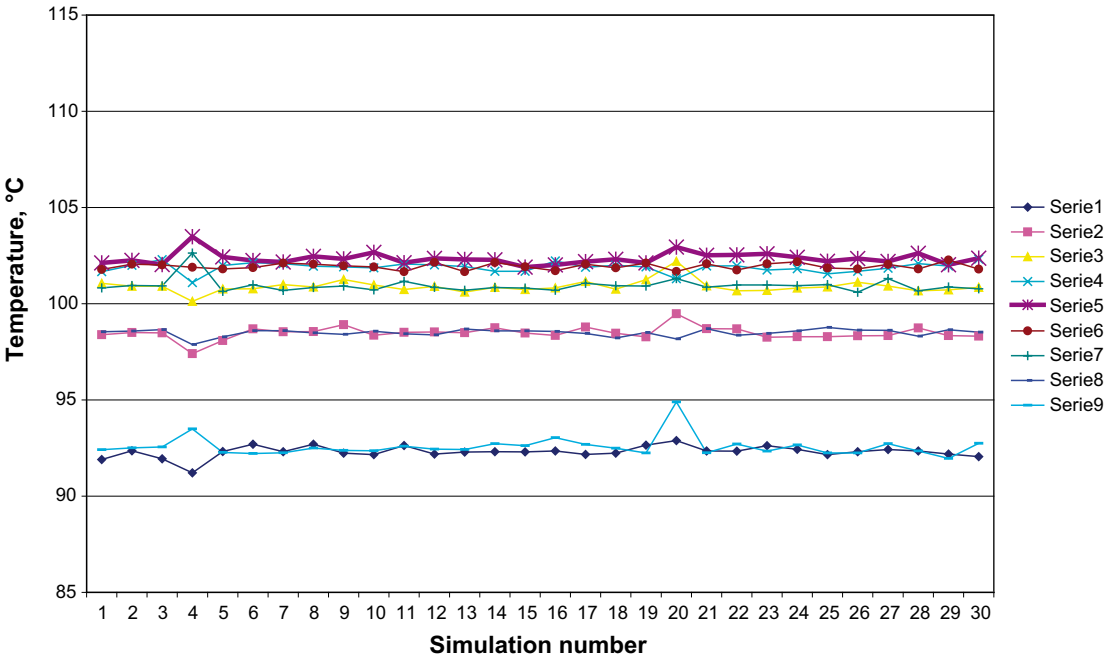

Figure 3-1. *Maximum volume average temperature for each of the nine canisters for the thirty simulated cases. Thermal conductivity values are randomly assigned in the 1 m scale.*

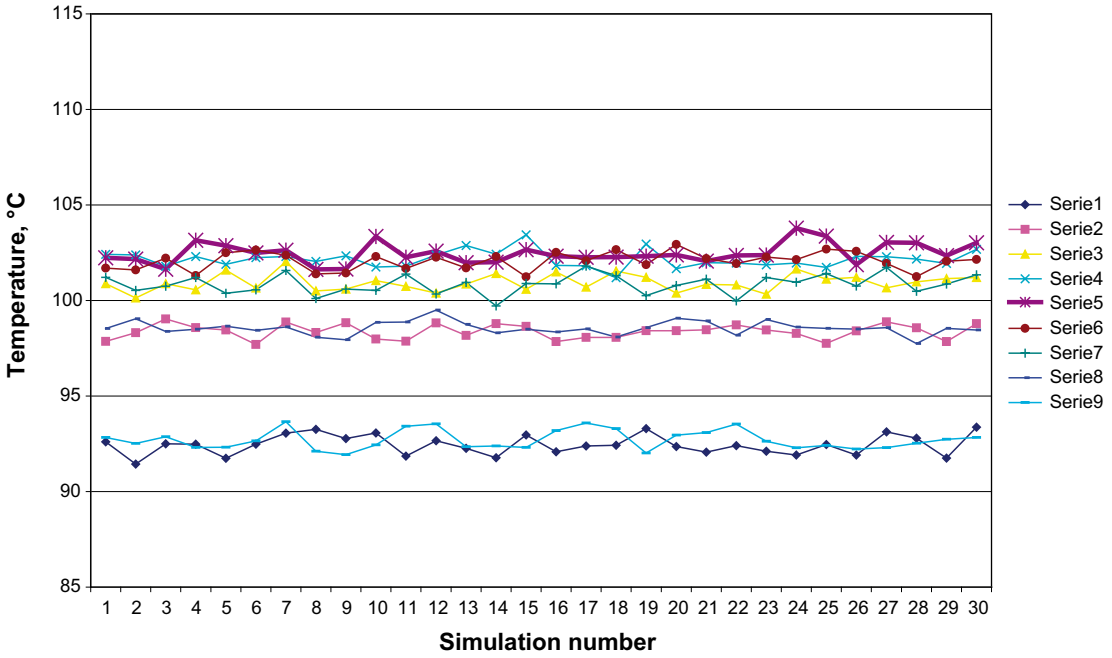

Figure 3-2. *Maximum volume average temperature for each of the nine canisters for the thirty simulated cases. Thermal conductivity values are randomly assigned in the 2 m scale.*

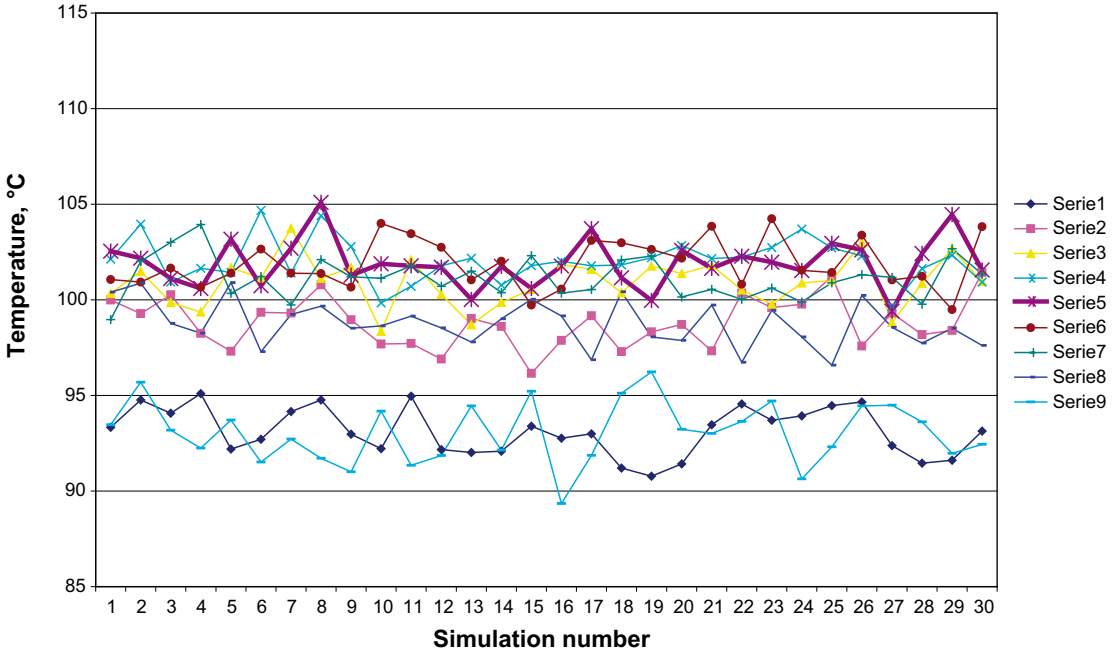

Figure 3-3. *Maximum volume average temperature for each of the nine canisters for the thirty simulated cases. Thermal conductivity values are randomly assigned in the 5 m scale.*

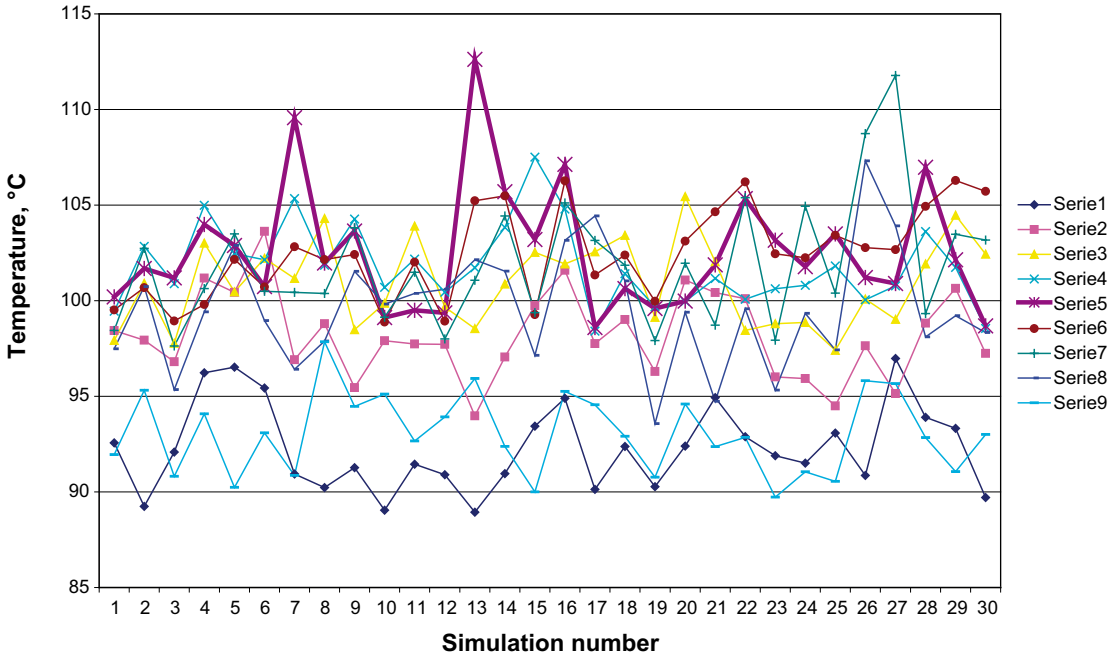

Figure 3-4. *Maximum volume average temperature for each of the nine canisters for the thirty simulated cases. Thermal conductivity values are randomly assigned in the 10 m scale.*

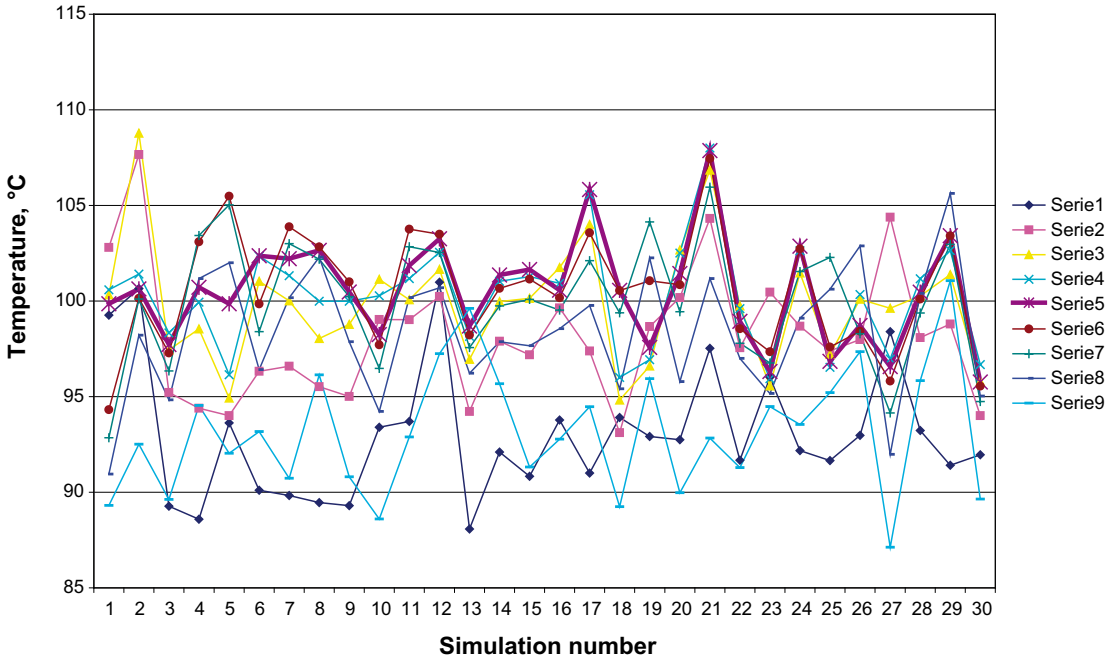

Figure 3-5. *Maximum volume average temperature for each of the nine canisters for the thirty simulated cases. Thermal conductivity values are randomly assigned in the 20 m scale.*

On the 1 m scale, the influence of the relative position of the canisters is easily visible. The maximum temperature is lowest for the outer canisters (1 and 9) and highest for the central canisters (5). The other canisters fall in between these values as expected. Each deposition borehole may potentially involve roughly 40–90 of the cubes with randomly distributed thermal conductivity. The thermal behaviour of deposition borehole therefore responds to a surrounding rock that statistically has an average thermal conductivity that should be fairly close to mean value of normal distribution. The variation in maximum temperature for each canister is relatively small.

As the scale of the cubes becomes larger, the statistical variation of the thermal conductivity around a deposition borehole increases. The temperature gradients in the rock in the immediate surrounding of the borehole are inversely proportional to the local thermal conductivities. On the 10 m scale, a whole canister may actually be completely located inside a cube with one value of the thermal conductivity. The local heat transfer properties in the surrounding rock and the resulting maximum canister temperature may then vary drastically from case to case. When the scale increases further beyond the scale of the deposition boreholes (> 10 m scale), the likelihood of a having one or several boreholes (canisters) within one cube increases. For these extreme cases, however, the thermal conductivity in the vicinity will be about the same, but there will be an influence due to differing thermal conductivities at some distance from the borehole.

For larger scales the number of cubes to which thermal conductivity values are assigned becomes smaller. This means that more extreme values are expected for larger scales. In Figure 3-6 the numbers of "property cubes" in the model for each simulation are shown.

The sorted deviation of the maximum average temperature for each of the nine canisters from the average maximum temperature for the thirty simulated cases on 2 m and 10 m scale is shown in Figure 3-7 and Figure 3-8. The slope will vary depending on scale. The slopes obtained for different canisters are fairly similar for values around the mean value for each scale.

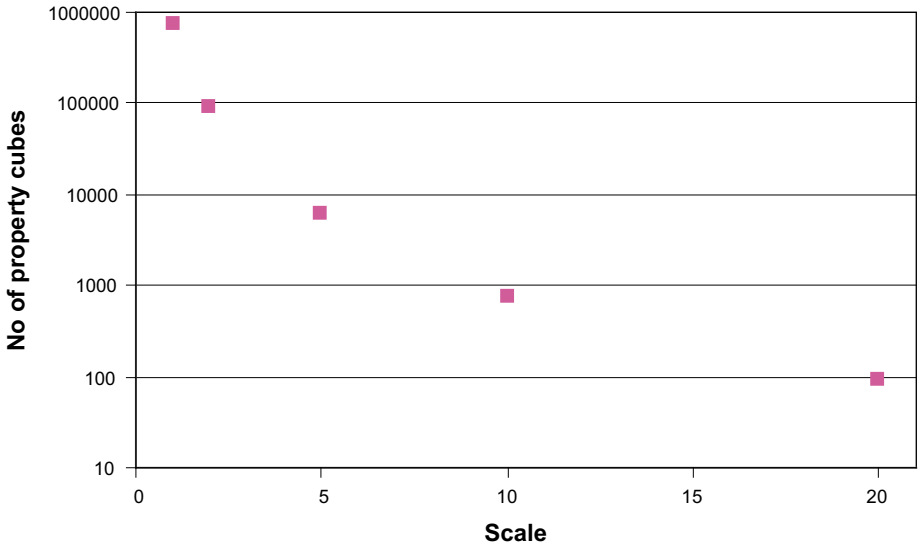

Figure 3-6. *Visualization of the number of property areas (cubes) in the total model volume (750,000 m³).*

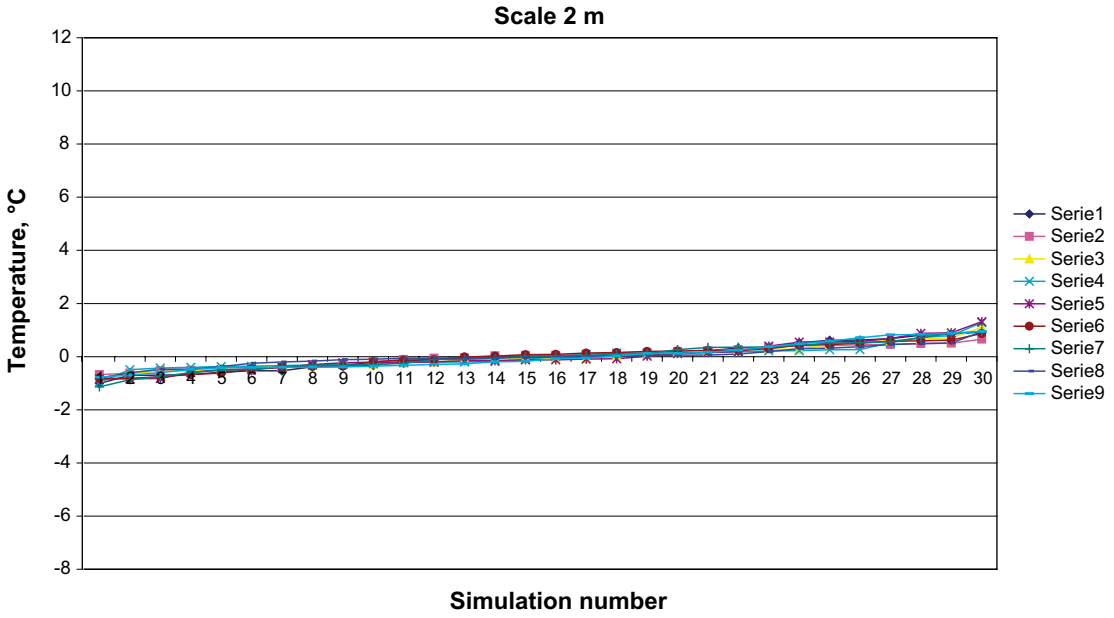

Figure 3-7. *Sorted deviation of maximum average temperature for each of the nine canisters for the thirty simulated cases. Thermal conductivity values are randomly assigned in the 2 m scale.*

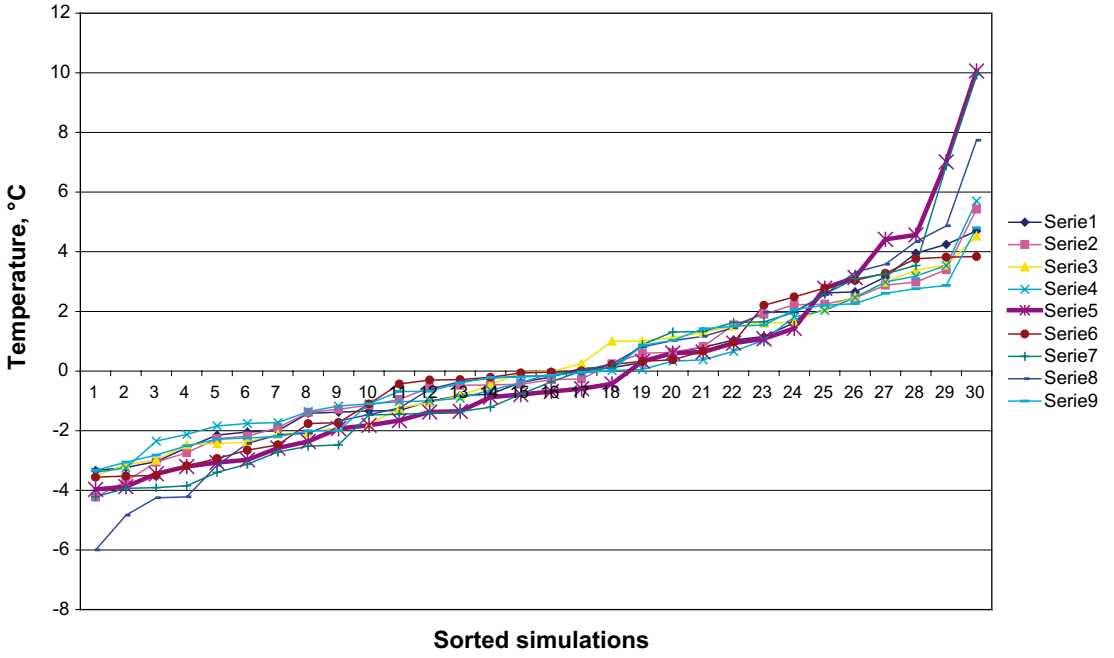

Figure 3-8. *Sorted deviation of maximum average temperature for each of the nine canisters for the thirty simulated cases. Thermal conductivity values are randomly assigned in the 10 m scale.*

3.5 Evaluation

In Figure 3-9 and Figure 3-10 the mean temperature and standard deviation for each scale and canister are shown. The mean temperatures for the three canisters in the middle are similar. The somewhat lower temperature for the 20 m scale is probably a result of the rather limited number of property areas for this scale, see Figure 3-6. If the number of simulation for the 20 m scale were increased this discrepancy would probably be lower. The temperature for canister 1 and 9, with canisters at only one side, is approximately 10°C lower.

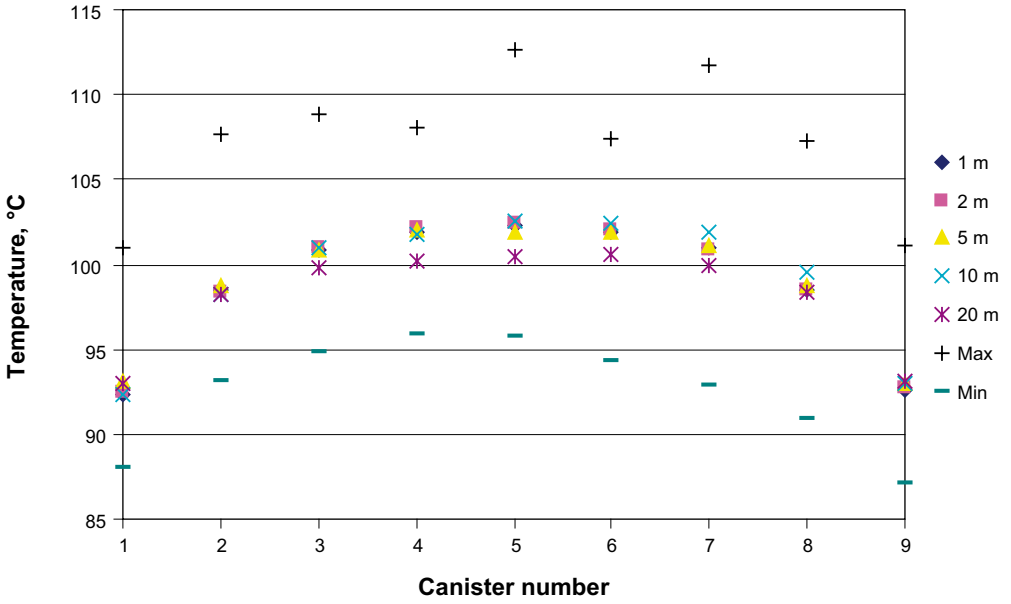

Figure 3-9. *Mean temperature for each canister at different scales. In addition, maximum and minimum temperatures are shown for the individual simulations.*

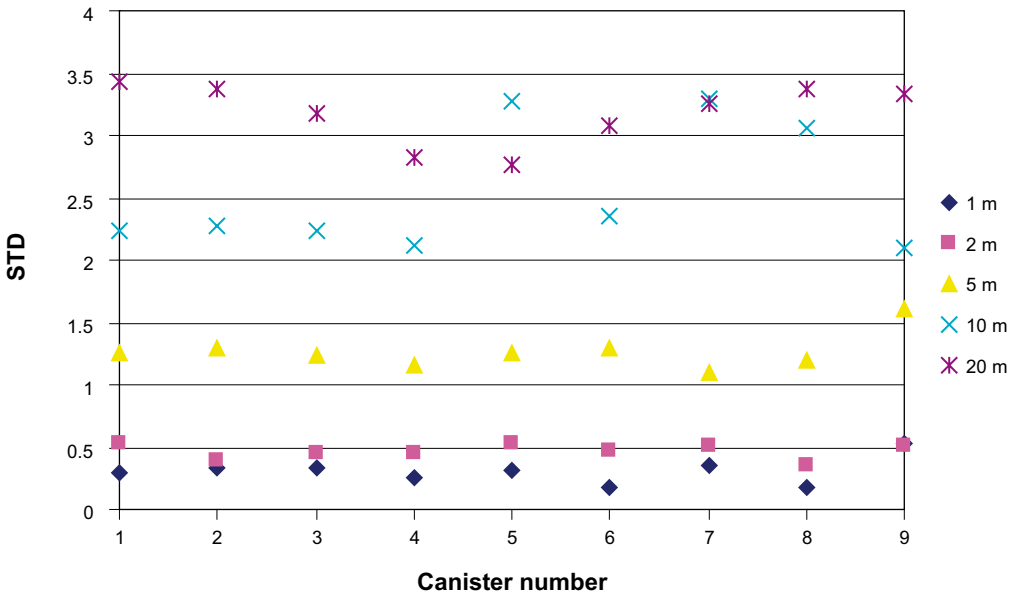

Figure 3-10. *Standard deviation for each canister at different scales.*

The standard deviation shows no trend according to canister placement. The minima for the central canisters at the 20 m scale may be a result of the limited number of property areas for this scale.

The maximum temperature is of interest and the central canister (no 5) should have the highest possible temperature. In Table 3-2 the mean and max temperature are shown for canister 5. The mean temperature is rather similar at the different scales. However, the maximum temperature increases significantly when the scale is above 2–3 m.

At larger scales (above 10 m) the simulation results are less certain due to the combination of limited number of property areas to which the thermal conductivities are assigned (Figure 3-6), and the limited number of simulations (30).

For further evaluation of the standard deviation, the distribution of the mean canister temperature is assumed to be normal and is evaluated according to the method of randomized sampling /Blom 1970/. For a (statistically) small number of observations this means that extreme values are excluded and that a fitting is performed for the observations within one standard deviation as indicated in Figure 3-11 as an example. This type of evaluation is performed for each canister and scale.

Table 3-2. Mean and maximum temperature for canister 5 at different scales. The result comes from all 30 simulations.

Scale, m	Mean, °C	Max, °C	Max/mean	Std
1	102.4	103.5	1.011	0.309
2	102.5	103.8	1.013	0.537
5	101.9	105.1	1.031	1.252
10	102.6	112.6	1.098	3.283
20	100.5	107.9	1.073	2.755

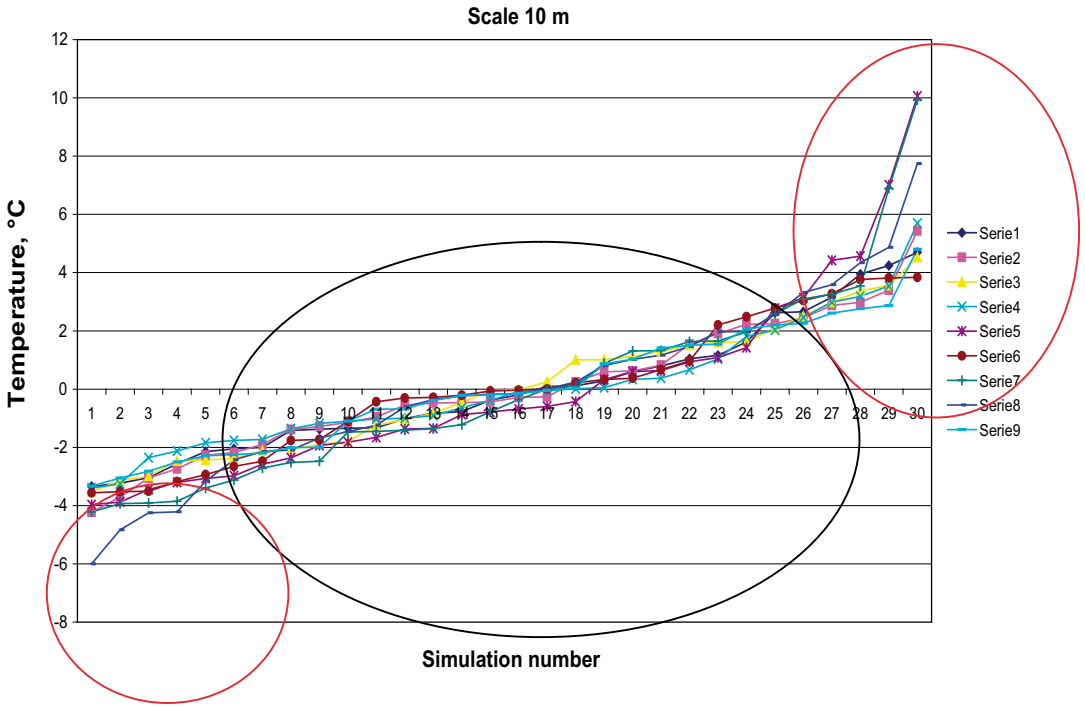

Figure 3-11. *Sorted deviation of maximum average temperature for each of the nine canisters for the thirty simulated cases. 10 m scale. The central part of the curve, used for further evaluation, is indicated.*

The temperature variation based on the average value of one standard deviation for each canister is shown in Figure 3-12. The statistical deviation of the maximum temperature grows until the scale of the heterogeneities is on the order of 8–10 m. This corresponds roughly to the linear dimensions of the canisters. For larger values of the scale the deviation approaches a limiting value that will occur when the whole simulated ground region has a homogeneous thermal conductivity for each simulation). The conductive thermal process will have negligible influence on the surrounding rock at distances larger than 50 m from the canisters during the ten years to reach maximum canister temperatures. Likewise, thermal properties beyond 50 m from the canisters will have negligible influence on the maximum temperature rise in the canisters.

The temperature variation (or standard deviation) is approximately linearly proportional to the scale up to 8–10 m. The slope is depending on the variability in thermal conductivities. For a thermal conductivity distribution with higher standard deviation the slope would be steeper and vice verse.

The relatively small number of simulations for each scale is likely the cause of the irregular shape of the curves for the canisters in Figure 3-12. The average value of all canisters uses more observations and is more regular. It is probably a more reasonable representation of how the temperature variation depends on the scale.

Temperature variation based on the average value for all canisters for each scale is shown in Figure 3-13. The dotted lines indicate the maximum and minimum temperature variation.

The temperature variation according to Figure 3-13 is used to derive Table 3-3, which gives an estimated maximum average temperature of canister 5 for different scales. The mean temperature is chosen to be 102.5 for all scales. The maximum temperature that will be exceeded in 1% (p=0.01, +2.58σ) or 0.1% (p=0.001, +3.29σ)) of the cases is stated.

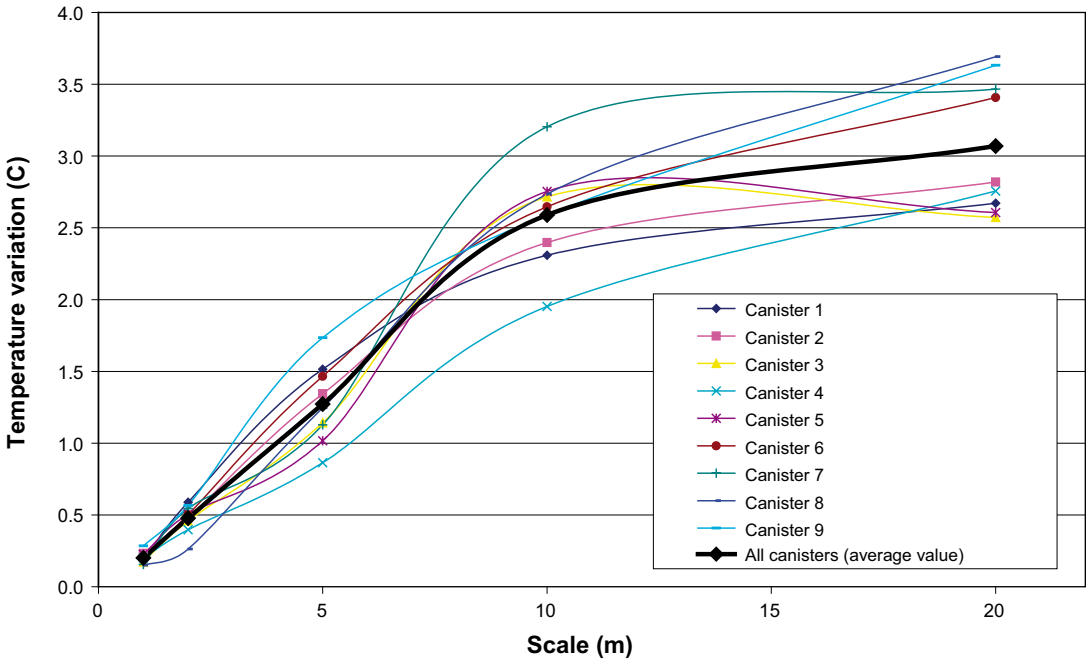

Figure 3-12. *Temperature variations based on average value of one standard variation for each canister.*

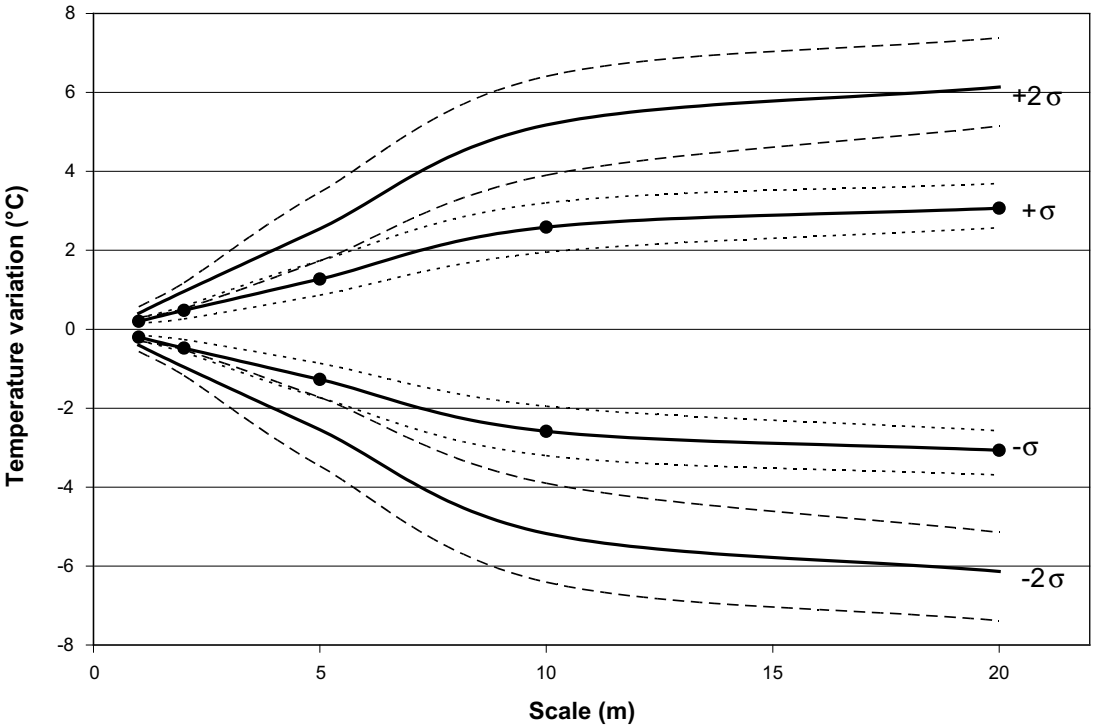

Figure 3-13. *Temperature variations at one and two standard deviations based on average values for each scale for all canisters. The dotted lines show the temperature variation based on the min and max standard deviation.*

Table 3-3. Mean and maximum temperature for canister 5 at different scales. The standard deviation has been evaluated from all canisters. The maximum temperature that will be exceeded in 1% (p=0.01) or 0.1% (p=0.001) of the cases is stated.

Scale, m	Mean, °C	Max (p=0.01)	Max (p=0.001)
1	102.5	103.0	103.2
2	102.5	103.7	104.1
5	102.5	105.8	106.7
10	102.5	109.2	111.0
20	102.5	110.4	112.6

Some conclusions from the simulations:

- The maximum temperature is relatively insensitive to variations in a scale below 2–3 m.
- The temperature variation (or standard deviation) increases linearly up to scales of 8–10 m, which approximately corresponds to the linear dimension of the canister (4.5 m). The slope is a function of the standard deviation of the thermal conductivity distribution. For larger scales the variation increases more slowly.
- Evaluation of larger scales (above 10 m) has uncertainties according to the limited number of property areas (cubes) to which the thermal conductivities are assigned, in combination with the limited number of simulations.
- The simulations are based on a constant value of the standard deviation of the thermal conductivity distribution. In reality, upscaling of thermal properties would decrease the variability of the distribution for larger scales. This would of course influence the shape of the curves in Figure 3-12.

4 Small-scale measurements and upscaling

4.1 Introduction

Measurements in the laboratory of the two properties thermal conductivity (λ) and thermal diffusivity (κ) have been conducted by the TPS (Transient Plane Source) method /Gustafsson 1991/ using two different sensor sizes. The purpose of the measurements was to study scale effects of the thermal properties. Hot Disk AB has performed the TPS measurements on samples from borehole KA2599G01. An attempt to investigate the variability in repeated TPS measurements for the same sample has also been carried out by Hot Disk AB. Determinations of density and porosity have been performed for the same samples by the Swedish National Testing and Research Institute (SP).

Result reports from the above stated measurements are presented in Appendix A–C.

4.2 Methods

4.2.1 Sampling design

The sampling layout was designed with the objective of allowing scale factors of thermal properties to be examined. The rock type distribution of the drill core from borehole KA2599G01 has been described in /Sundberg 2002/. According to Äspö nomenclature the chosen part of the drill core (4.33–24.92 m) was determined as Äspö diorite. The rock types of the samples has been revised to Ävrö granite in accordance with Simpevarp nomenclature /SKB 2005/, see Table 6-1.

Three sample groups with five samples in each were taken along the drill core. The individual samples were taken 0.1 m apart and the sample groups were located approximately 10 m (9.87 respectively 8.02 m) apart. A sketch of the sampling layout is shown in Figure 4-1.

4.2.2 Laboratory measurements with different sensor sizes

The TPS method can be used for measurements of thermal diffusivity and thermal conductivity of both fluids and solids, from cryogenic temperatures to about 250°C (if the sensor insulation is made of kapton). Measurements of thermal properties using the TPS method has been used before by SKB /Sundberg and Gabrielsson 1999, Sundberg 2002/ and also within the thermal programme of the site investigations.

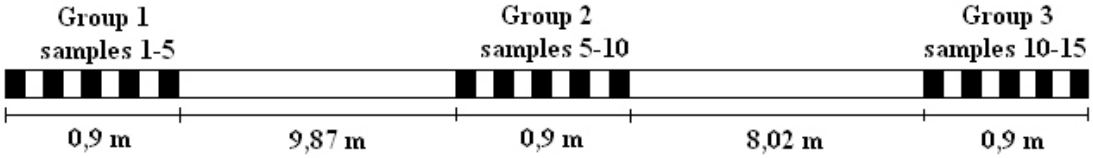

Figure 4-1. *Sketch of the sampling layout along a drill core from borehole KA2599G01. Samples are marked in black.*

Prior to the measurements, the rock samples from the drill core were prepared by cutting the samples in two halves, each with a thickness of about 50 mm. The two intersection surfaces were carefully polished in order to limit the contact resistance between the probe and the sample surface. The samples were also water saturated for at least 7 days which means that all measurements were performed on water saturated samples.

The principle of the TPS instrument is to place a circular probe consisting of a Ni-spiral covered by an insulating material (Kapton) between the two sample pieces. The sensor generates a heat pulse while simultaneously the heating of the specimen is recorded. The heat pulse is selected to achieve a heat increase of 1K at the sample surfaces facing the sensor. The output power and the duration of the pulse are dependent on sample size, material properties and sensor diameter. The thermal properties can be evaluated by using the fact that the resistance for the thin Ni-spiral at any time is a function of its initial resistance, the temperature increase and the temperature coefficient of the resistivity of Nickel. The measured temperatures is stored in the software and by comparing these values to a theoretical solution based on assumptions regarding a plane sensor and an infinite sample in perfect contact with the sensor surface, the thermal diffusivity and thermal conductivity can be determined. The volumetric heat capacity (C_p) can thereafter be calculated.

According to the manufacturer the accuracy of the thermal conductivity measurements is ± 2%, thermal diffusivity ± 5% and specific heat ± 7% /HotDisk 2004/. This is reached if the sample size, sensor diameter, output of power and total time of the temperature measurement is properly selected, and providing the sample is allowed to reach temperature equilibrium before the start of measuring.

In this case two sensor sizes have been used for the TPS measurements in order to investigate different sample volumes. With a larger sample volume the influence from voids, cracks and grains becomes larger. Both of the sensors have been applied to all of the 15 samples.

- Large sensor 4921 (r = 9.719 mm) with an approximate probing depth of 14 mm. Heat pulse duration t_{meas} = 40 s with the power of 0.7 W. (Probing depth calculated from $2\times(\kappa\times t_{meas})^{0.5}$ with a mean κ = 1.23E–6 m^2/s of the rock sample).
- Small sensor 5501 (r = 6.401 mm) with an approximate probing depth of 10 mm. Heat pulse duration 20 s with the power of 0.7 W.

For more detailed result of the method, see Appendix A: TPS measurements of thermal properties, two different sensor sizes.

4.2.1 Density and porosity measurements

The methods of density and porosity determinations have been SS EN 13755, ISRM (1973) section 3. For more detailed descriptions of the methods see Appendix B: Porosity and density measurements of core samples.

4.2.2 Repeated laboratory measurements on the same sample

Samples for repeated measurements were selected after evaluation of the results from the TPS measurements with two sensor sizes, density and porosity measurements. Two samples showing a large difference in results between the two sensor sizes (sample 1 and 5) and two with a small difference (sample 8 and 9) were selected. The samples were planned to be measured five times each and for each measurements the sensor was supposed to be

disconnected and replaced at the supposed same location without marking out the sensor location on the sample piece. The purpose of this measurement was to investigate how the thermal properties vary when the measurements are repeated and if some of the differences between measurements with different sensor size could be addressed to the testing procedure.

4.3 Results

4.3.1 Laboratory measurements with different sensor sizes

Results from TPS measurements on Ävrö granite samples with two different sensor sizes together with density, porosity and rock code classifications are summarized in Table 4-1. The rock code presented in Table 4-1 is the revised rock classification according to Simpevarp nomenclature /Wahlgren 2004/.

Table 4-1. Results from TPS measurements with two sensor sizes (sensor 4921 and 5501) and rock classification. Sensor 5501 is the smaller one.

Sample (no)	Density (kg/m³)	Poro-sity (%)	λ (W/m×K)		κ (mm²/s)		C_p (MJ/m³×K)		Rock code
			4921	5501	4921	5501	4921	5501	
KA2599G01 4.33–4.43 (1)	2,780	0.4	2.390	2.155	1.131	1.314	2.115	1.641	501044
KA2599G01 4.53–4.63 (2)	2,730	0.4	2.927	2.869	1.272	1.322	2.302	2.170	501044
KA2599G01 4.73–4.83 (3)	2,710	0.4	3.004	3.045	1.316	1.323	2.282	2.309	501044
KA2599G01 4.93–5.03 (4)	2,730	0.4	2.860	2.664	1.332	1.464	2.148	1.820	501044
KA2599G01 5.13–5.23 (5)	2,710	0.4	2.909	2.517	1.474	1.761	1.974	1.449	501044
KA2599G01 15.10–15.20 (6)	2,770	0.4	2.551	2.612	1.104	1.120	2.311	2.332	501044
KA2599G01 15.30–15.40 (7)	2,760	0.4	2.621	2.667	1.156	1.124	2.268	2.374	501044
KA2599G01 15.50–15.60 (8)	2,780	0.4	2.568	2.564	1.148	1.129	2.237	2.272	501044
KA2599G01 15.70–15.80 (9)	2,770	0.4	2.534	2.542	1.125	1.130	2.255	2.250	501044
KA2599G01 15.90–16.00 (10)	2,770	0.4	2.496	2.526	1.086	1.083	2.298	2.331	501044
KA2599G01 24.02–24.12 (11)	2,760	0.5	2.613	2.764	1.130	1.127	2.314	2.452	501044[1]
KA2599G01 24.22–24.32 (12)	2,770	0.5	2.550	2.475	1.164	1.095	2.193	2.260	501044
KA2599G01 24.42–24.52 (13)	2,810	0.5	2.599	2.573	1.115	1.071	2.331	2.402	501044[2]
KA2599G01 24.62–24.72 (14)	2,740	0.4	2.812	2.720	1.302	1.240	2.160	2.193	501044[3]
KA2599G01 24.82–24.92 (15)	2,690	0.4	3.699	3.558	1.567	1.651	2.360	2.156	501044[4]

[1)] Strong foliation and epidote filled joints.
[2)] Elements of fine-grained mafic rock type.
[3)] Diffuse elements of red granite.
[4)] mixed with red granite and elements of fine-grained mafic rock type

4.3.2 Repeated laboratory measurements on the same sample

The results of the first measurement set out of five for the same sample were of varying quality and further measurements were not continued. Results of the first measuring set are presented in Appendix C. In Table 4-2 the results of the first measuring set (out of five) is compared with the corresponding measurements from the two sensors measuring (same sample and sensor size). Results from two of the samples were of bad quality (sample 1 and 5), one sample relatively good (sample 9) and one sample gave good results (sample 8).

This was due to the fact that the measuring surfaces were not as smooth as they ought to be. The deformation of the sample pieces meant that they did not fit as closely together as during measurements with two different sensor sizes. An explanation to the deformation may be that after density and porosity measurements the four samples were dried out from water saturation at 105°C. The density and porosity measurements were made after the two sensor measurements but before the repeated measurements. It is possible that the different volume expansion for the minerals has caused the deformation.

For sample 1 and 5 the measuring points ~ 100–200 were used which indicates that there is an air gap between the sample pieces and the sensor. The reason for some measuring points being excluded in the beginning of the transient is that the air layer demands a certain amount of energy to be heated and this heating process takes time. The consequence of having few measuring points from the initial part of the measuring is that it can give incorrect diffusivity values. It is also reasonable to expect a somewhat lower thermal conductivity value if air has an influence on the measurements.

For sample 8 the measuring points 40–200 were used in the calculations, which indicate that the sample pieces could come closer to the sensor than for samples 1 and 5. Sample 8 also seems to be the sample which has the smoothest surface towards the sensor.

The result of sample 9 is something between the two above ways of reasoning.

Observe that measuring points that gave the best fitting model were selected which means a relatively low standard deviation value.

The results indicate that the results for two measurements on the same sample with good or relatively good quality are in reasonably good agreement with each other (difference 1–3%). Due to the problem with deformation of samples, no further evaluation is made.

Table 4-2. Comparison or results from two measuring sets of the same samples with the same sensor size.

Sample	Measurement	λ (W/m×K)	κ (mm²/s)	C_p (MJ/m³×K)	Quality of measurement
1	First meas (2 sensors)	2.155	1.31	1.64	Good
	Second meas (1 out of 5)	2.479	1.085	2.286	Bad
5	First meas (2 sensors)	2.5	1.8	1.4	Good
	Second meas (1 out of 5)	2.994	1.358	2.204	Bad
8	First meas (2 sensors)	2.564	1.129	2.27	Good
	Second meas (1 out of 5)	2.495	1.209	2.063	Good
9	First meas (2 sensors)	2.542	1.130	2.25	Good
	Second meas (1 out of 5)	2.565	1.087	2.359	Relatively good

4.4 Evaluation of results in different scales

4.4.1 Measurement scale

The difference in thermal conductivity measured with two different sensor sizes is illustrated in Figure 4-2. Statistical data of measurement results for both thermal conductivity and heat capacity is presented in Table 4-3 and Table 4-4.

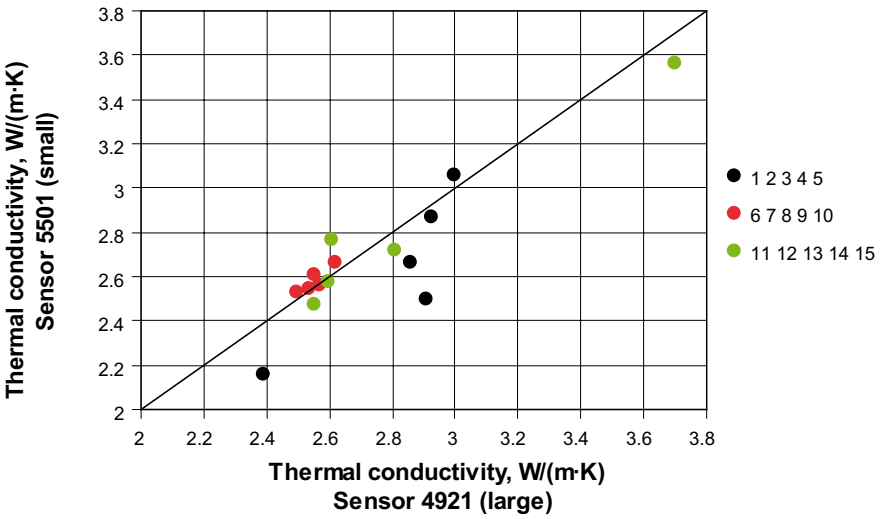

Figure 4-2. *Comparison of thermal conductivity measured with two sensor sizes. Presentation is given with samples divided in sample groups.*

For thermal conductivity there is a tendency that the large sensor gives a slightly higher value than the small sensor. This difference is however not significant at the 5% level (paired t-test). For heat capacity there is also a non-significant tendency for larger values with the large sensor. However, for individual groups of data there is also the opposite tendency. The numbers of measurements are too few to draw any conclusion of how the absolute value of thermal conductivity and heat capacity is affected by the size of the sensor.

Table 4-3. Statistical data of thermal conductivity (W/(m×K)) per sampling group. Sample 15 in group 3 excluded because of ambiguous rock type. Sensor 5501 is the smaller one.

Group	Sample	Sensor 4921	Sensor 5501	Difference (S4921–S5501)/ S4921 (%)
1	1	2.39	2.155	9.8
	2	2.927	2.869	2.0
	3	3.00	3.054	–1.7
	4	2.860	2.66	6.9
	5	2.91	2.5	13.5
	Mean	2.817	2.648	**6.1**
	St. dev	**0.244**	**0.346**	
2	6	2.551	2.61	–2.4
	7	2.62	2.667	–1.7
	8	2.57	2.564	0.1
	9	2.534	2.542	–0.3
	10	2.496	2.526	–1.2
	Mean	2.554	2.582	**–1.1**
	St. dev	**0.046**	**0.057**	
3	11	2.61	2.764	–5.8
	12	2.55	2.475	3.0
	13	2.599	2.573	1.0
	14	2.81	2.720	3.3
	Mean	2.642	2.633	**0.4**
	St. dev	**0.115**	**0.133**	
All data	**Mean**	**2.673**	**2.620**	**1.9**
	St. dev	**0.189**	**0.207**	

Table 4-4. Statistical data of heat capacity (MJ/(m³×K)) per sampling group. Sample 15 in group 3 is excluded because of ambiguous rock type. Sensor 5501 is the smaller one.

Group	Sample	Sensor 4921	Sensor 5501	Difference (S4921–S5501)/ S4921 (%)
1	1	2.11	1.64	22.4
	2	2.30	2.17	5.7
	3	2.28	2.31	–1.2
	4	2.15	1.82	15.3
	5	1.97	1.4	26.6
	Mean	2.162	1.868	**13.8**
	St. dev	**0.135**	**0.374**	
2	6	2.31	2.33	–0.9
	7	2.27	2.37	–4.7
	8	2.24	2.27	–1.5
	9	2.26	2.25	0.215
	10	2.298	2.33	–1.4
	Mean	2.276	2.311	**–1.7**
	St. dev	**0.028**	**0.050**	
3	11	2.31	2.45	–6.0
	12	2.19	2.26	–3.1
	13	2.33	2.40	–3.1
	14	2.16	2.19	–1.5
	Mean	2.248	2.326	**–3.4**
	St. dev	0.085	0.121	
All data	**Mean**	**2.227**	**2.157**	**3.3**
	St. dev	**0.102**	**0.312**	

There is no significant difference in variance between the small and large sensor for the thermal conductivity measurements (Figure 4-3). However, for heat capacity there is a distinct and significant difference in variance, see Figure 4-4. Data from the small sensor have a variance that is 9 times as large as data from the large sensor (3 times as large standard deviation, see Table 4-4). These results are based on all 14 data points. When each group of data in Table 4-3 and Table 4-4 is analysed separately, no significant difference in variance can be identified, neither for thermal conductivity nor heat capacity.

The size of the small sensor (5501) is 1.3 cm^2 and the measurement volume in the rock sample is about 11.3 cm^3. For the large sensor (4921), the size is 3 cm^2 and the measurement volume about 32.9 cm^3. The measurement volume is calculated from an ellipsoid with $r_{x,y}$ = (probing depth + r_{sensor}) and r_z = probing depth.

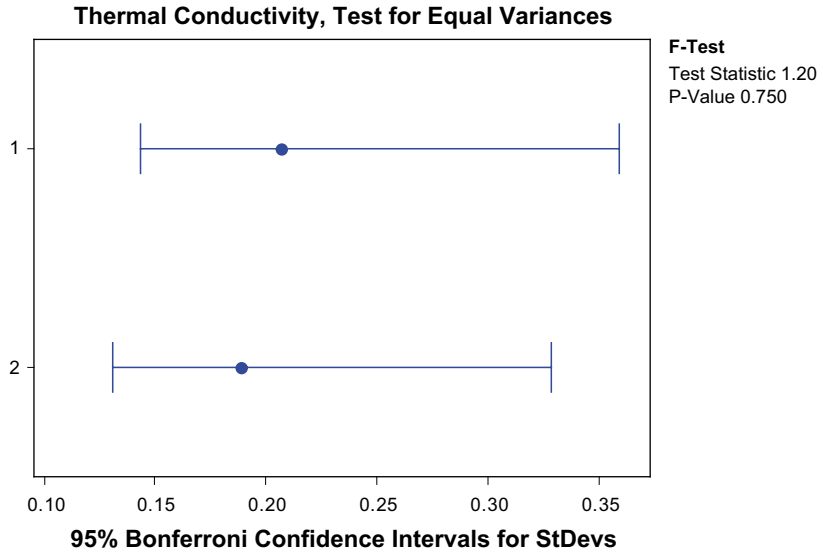

Figure 4-3. *Significance test of equal variances for thermal conductivity with small (1) vs large (2) sensor. Sample 15 in group 3 is excluded.*

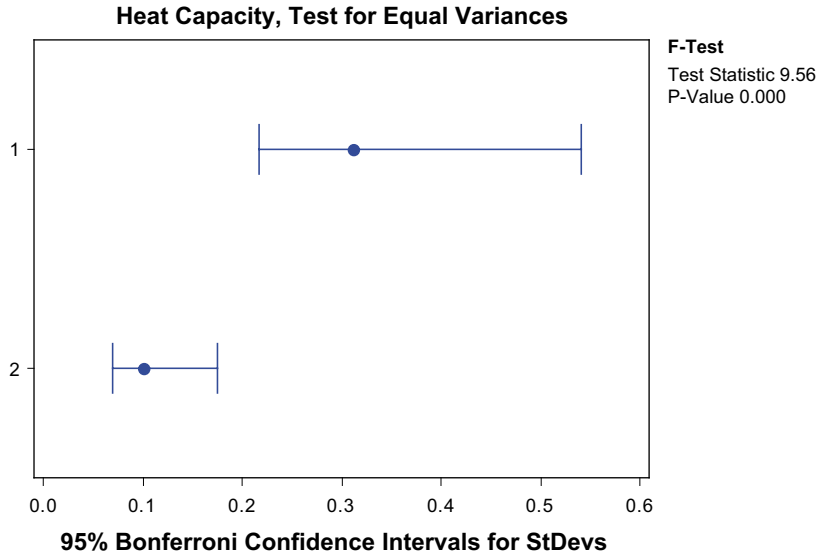

Figure 4-4. *Significance test of equal variances for heat capacity with small (1) vs large (2) sensor. Sample 15 in group 3 is excluded.*

4.4.2 Upscaling to 1 m scale

In order to make possible an upscaling from TPS scale (cm) to 1 m scale, samples were taken in groups with a sampling design as presented in Section 4.2.1. Samples from both Äspö HRL and the Simpevarp subarea were used. By calculating the geometric mean for each group, the effective thermal conductivity at the group scale (1 m support) was estimated. Table 4-5 and Figure 4-5 indicate that the small scale variability (centimetre scale) may be both large and small (st.dev. between 0.06 and 0.36 W/(m×K) within groups). The groups representing the 1 m scale are illustrated in the box plot in Figure 4-5 in grey, 4 values in total.

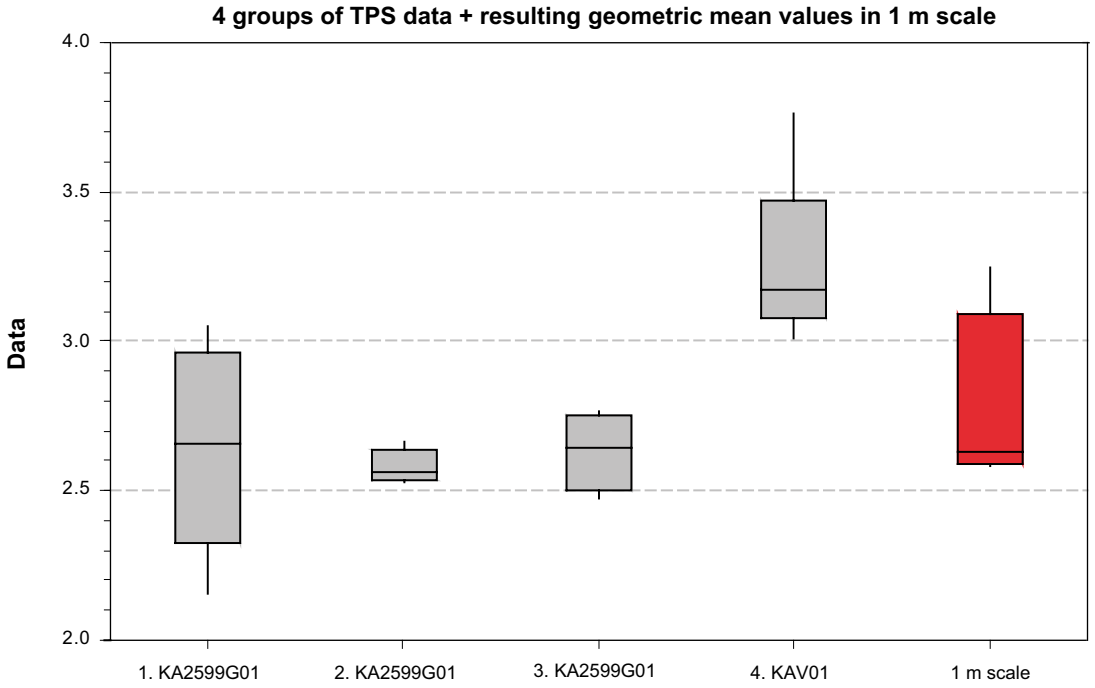

Figure 4-5. *Upscaling of TPS measurements from cm scale to 1 m scale for Ävrö granite (rock code 501044). Four groups of TPS measurements (grey boxes), each representing approximately 1 m, are used to estimate thermal conductivity at the 1 m scale (red box).*

Table 4-5. Estimation of the effective thermal conductivity (W/(m×K)) at the 1 m scale from TPS measurements in the cm scale in rock code 501044 (Ävrö granite). Samples in groups of five from boreholes KA2599G01 (Äspö) and KAV01. One measurement in group 3 is excluded because of ambiguous rock type.

Samples (secup-seclow)	Geometric mean within groups	St dev within groups	Number of samples
KA2599G01 (4.33–5.23)	2.63	0.35	5
KA2599G01 (15.10–16.00)	2.58	0.06	5
KA2599G01 (24.02–24.72)	2.63	0.13	4
KAV01 (508.25–509.26)	3.24	0.29	5
Result for 1 m scale:	**Mean:** **2.77** (arithmetic mean of groups)		
	St.dev: **0.24** (St dev of geometric mean within groups)		

The red box in Figure 4-5 represents variability at the 1 m scale. The mean at the 1 m scale was estimated to 2.77 W/(m×K) and the standard deviation to 0.24 W/(m×K), see Table 4-5. The relatively high standard deviation at the 1 m scale is mainly due to high thermal conductivity values in the samples from KAV01. This indicates that the thermal conductivity of Ävrö granite can differ significantly over large distances. This variability over large distances may be less pronounced for other rock types than Ävrö granite.

No significant difference between data from the centimetre scale and the metre scale can be determined from this limited data set. Therefore, no general conclusions of the scale effects can be drawn from this limited number of TPS measurements. Further analysis of upscaling methodology is discussed in Chapter 7.

4.4.3 Rock type scale

The reason for the variability within a rock type derives from the process of rock formation but also the system of classifying the rock types. This variability cannot be reduced but collecting a large number of samples at varying distances from each other may reduce the uncertainty of the variability, so that reliable variograms can be created. An attempt of this is presented in Figure 4-6, which is constructed from the TPS data presented in Table 4-1 (with an outlier removed, sample No. 15).

An exponential model has been fitted to the data: range 57 m, sill 0.054, and nugget 0.0262. The range is the separation distance where the correlation ceases, i.e. there is no longer an increase in variance. The sill is the variance when no correlation exists, and the nugget is the variance at zero separation distance. The number of data pairs in each lag class is small due to the small number of samples: 26, 45, and 20 for the three lag classes. Therefore, the variogram is highly uncertain. The three lag classes correspond to the three groups of samples in Figure 4-1.

The variability that is indicated in Figure 4-6 is the "within rock type" variability due to spatial variations in composition of the rock. As indicated, the spatial variability increases over distance. There is an increase by a factor of about two from the 1 m scale to the 25 m scale.

Note that Figure 4-6 does not give a reliable picture of the variability below 1 m. Most likely there is a significant drop in variance at separation distances less than 1 m but this has not been investigated.

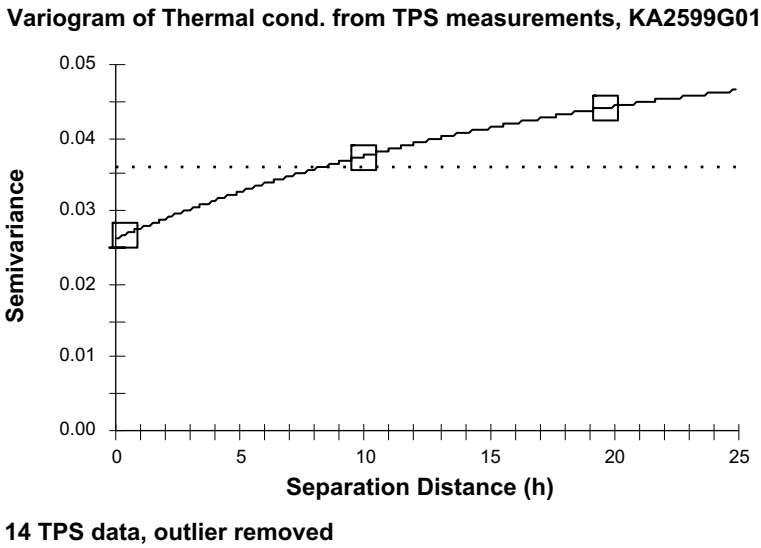

Figure 4-6. *Variogram of thermal conductivity from TPS measurements KA2599G01. The dotted line indicates the total variance* $(W/(m \times K))^2$ *in the data set. Sample 15 in group 3 is excluded.*

5 Estimation of thermal conductivity from small-scale density measurements

5.1 Relationship between density and thermal conductivity

A relationship between density and thermal conductivity was found for granitoid rocks from borehole KA2599G01 at Äspö HRL /Sundberg 2002/. Based on this investigation, a relationship between density and thermal conductivity was used by /Staub et al. 2003/.

Based on additional laboratory measurements /Sundberg and Gabrielsson 1999/, a new, modified relationship was derived in /Sundberg 2003/ with data from both investigations, see Figure 5-1 and Equation 5-1.

$\lambda = 27.265\rho^2 - 156.67\rho + 227.18$ $R^2 = 0.88$ Equation 5-1

The equation was derived based on 20 samples from Äspö HRL (the prototype repository and borehole KA2599G01) including, according to Äspö nomenclature, Äspö diorite, Ävrö granite and Fine-grained granite (one xenolith sample was excluded).

The relationship has been further developed by incorporating additional laboratory measurements on thermal properties. The updated relationship is based on all measurements of Ävrö granite and is presented in Figure 5-1 and Equation 5-2. Classification of the samples has been performed according to Simpevarp nomenclature. New measurements have been made, both within this study (14 samples of Ävrö granite, rock code 501044) and in the Simpevarp site investigation program (41 samples divided between the three rock codes 501030, 501036, and 501044). Samples included in the relationship in Equation 5-1 have been reclassified according to Simpevarp nomenclature and are also included. The updated relationship between density and thermal conductivity for Ävrö granite (501044) is /Sundberg et al. 2005/:

$\lambda = -7.1668\rho + 22.326$ $R^2 = 0.74$ Equation 5-2

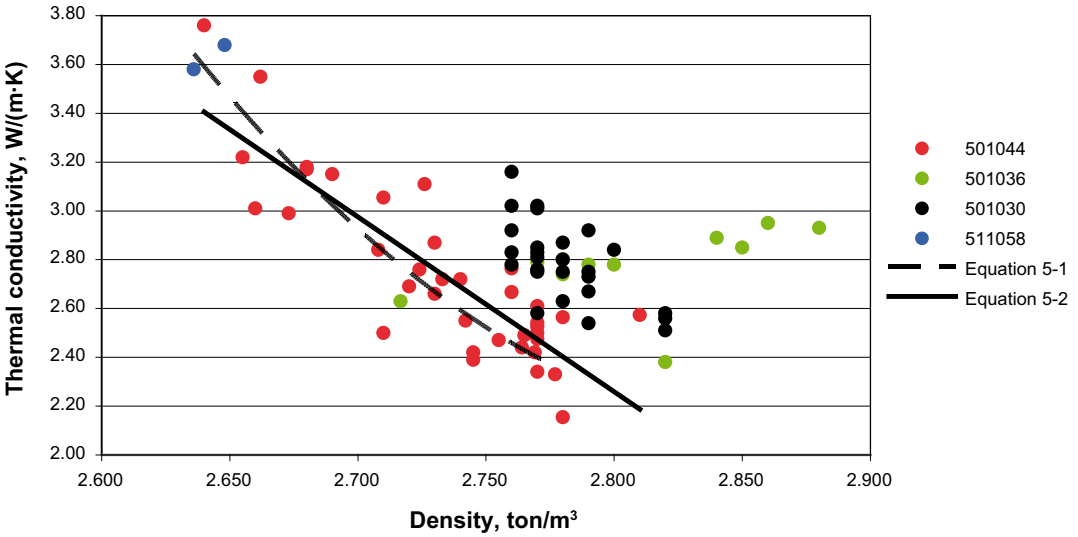

Figure 5-1. *Relationships between density and thermal conductivity. Equations based on rock code 501044 where Equation 5-1 is derived by polynomial regression and Equation 5-2 by linear regression.*

The valid range for density (x) is 2.6–2.85 g/cm^3 and the equation is only applied within this range.

Measurements from the Simpevarp site investigation program of the two rock types Quartz monzodiorite (501036) and Fine-grained dioritoid (501030) are plotted in Figure 5-1 to illustrate the relation between density and thermal conductivity. Samples from these two rock types are not included in the same relationship as the Ävrö granite since they do not show the same trends. Two samples of Fine grained granite (511058) are also included the figure.

The model has been evaluated statistically by calculating both the confidence and prediction interval. The confidence interval indicated in Figure 5-2 by the red dashed line indicates the uncertainty of the model. The interval can be interpreted as the area the model will fall within with 95% probability. The prediction interval shown in Figure 5-2 by a green dashed line shows the uncertainty in predicted thermal conductivity values from density. The interval can be interpreted as the area a prediction of the thermal conductivity will fall within with 95% probability. As Figure 5-2 indicates, the prediction interval is much wider than the confidence interval.

When the relationship in Equation 5-2 is applied to density loggings there are some factors that contribute significantly to the uncertainty in the estimated thermal conductivity data:

1. Uncertainty in the density loggings.
2. Random prediction uncertainty in the model in Equation 5-2.
3. Possible bias in the model in Equation 5-2.

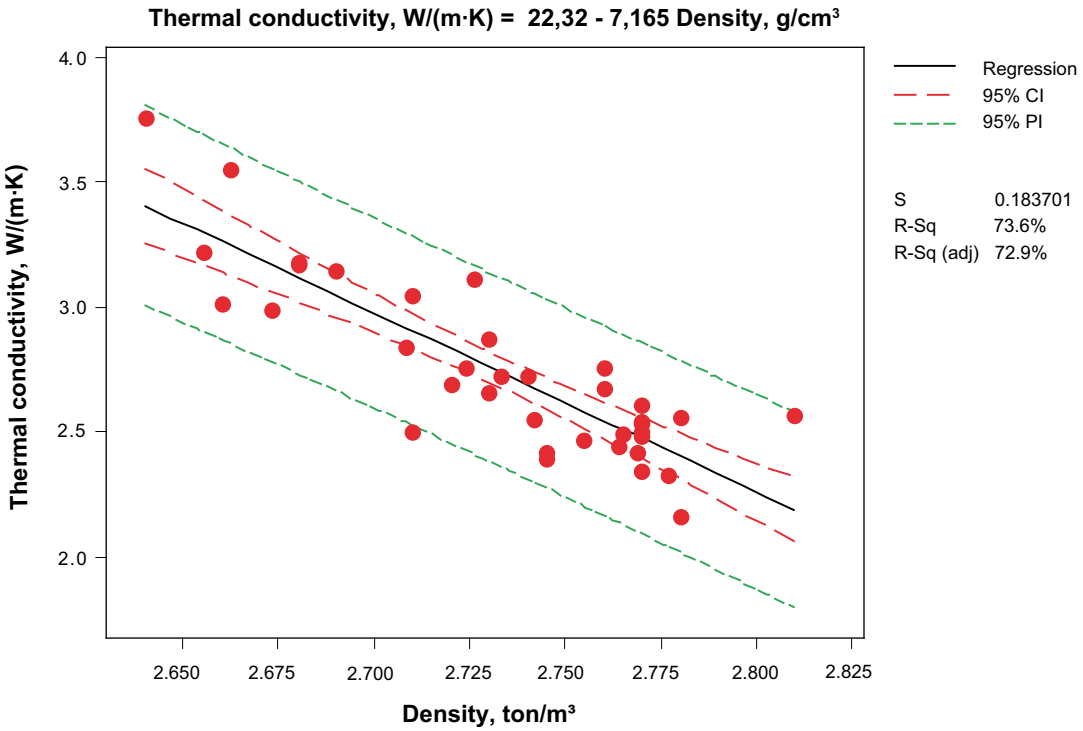

Figure 5-2. *Statistical analysis of the relationship between density and thermal conductivity for Ävrö granite (rock code 501044). The red lines indicate the confidence interval and the green lines the prediction interval.*

There are a number of uncertainties associated with density loggings. These include random errors in the measurement equipment, disturbances in the geology such as fractures etc, bias in the logging data etc. The relative error in density logging data should not exceed 3–5 Kg/m^3, according to SKB:s method description of geophysical logging. In reality, the error is about 10 times this value. The reason for this is under investigation. In addition, the logging data often contains a lot of noise and is therefore filtered. A recalibration is also performed in order to minimise the potential for bias.

The random prediction error that is expected from Equation 5-2 is a result of the heterogeneous composition of the Ävrö granite. It cannot be reduced significantly without further development of the model.

There are indications of a potential bias in the model /Sundberg et al. 2005/. This bias will affect the mean value of estimated thermal conductivities but the magnitude of this bias is not known.

All these uncertainties indicate that the total uncertainty in estimated thermal conductivity data is substantial. The random errors will affect the variance of estimated thermal conductivity, and the bias will affect the mean thermal conductivity. The variance is also affected by the removal of data outside of the valid density range of the regression equation. Although application of the model results in uncertain data there is a major advantage, namely that the spatial correlation of thermal conductivity along a borehole is taken into account, see Chapter 7.

The relationship in Equation 5-2 is applied for calculation of thermal conductivity in the domain modelling approaches described in Chapter 7 and in the Value of Information Analysis (Chapter 9).

5.2 Analysis of relationship

An explanation of the relationship between density and thermal has been sought by investigating porosity dependence, properties of the specific minerals in the Ävrö granite, and by analysing synthetically created “samples” based on the formation of different igneous rock types. Each of these explanations is analysed below.

5.2.1 Effects of porosity

Figure 5-3 illustrates how the density of the core samples depends on the porosity. As illustrated in the figure, there is only a weak relationship between density and porosity within the Ävrö granite (Simpevarp nomenclature). However, the porosity relationship is quite the opposite of what could be expected in order to explain the relationship between density and thermal conductivity. This eliminates one possible explanation of the relationship between density and thermal conductivity.

5.2.2 Mineral properties

Another possible explanation of the relationship between density and thermal conductivity is the mineral properties. For minerals appearing in Ävrö granite (501044) the thermal conductivity has been plotted against density in Figure 5-4.

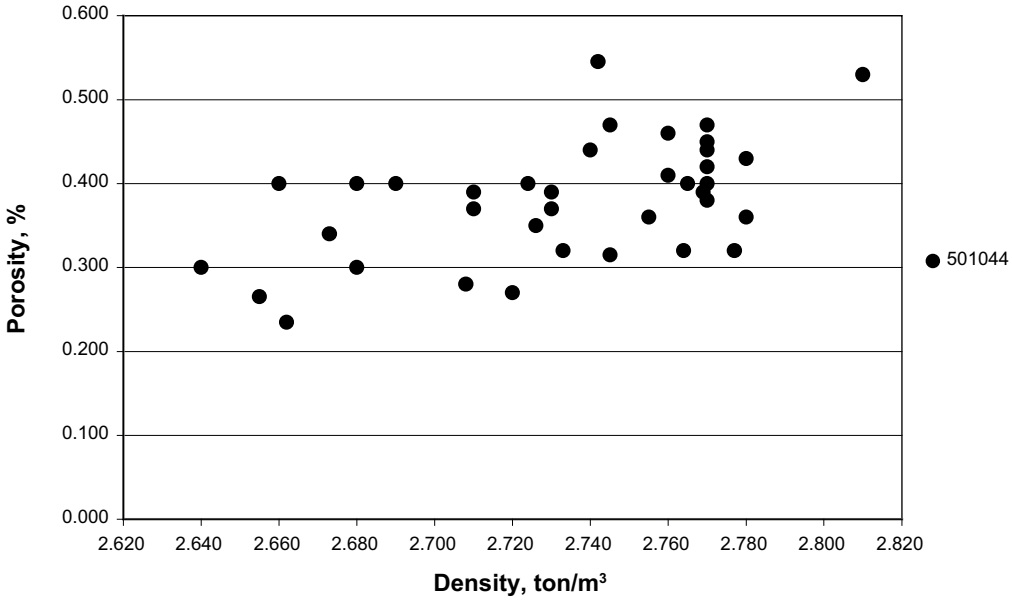

Figure 5-3. *Porosity vs density of measured Ävrö granite (501044) samples.*

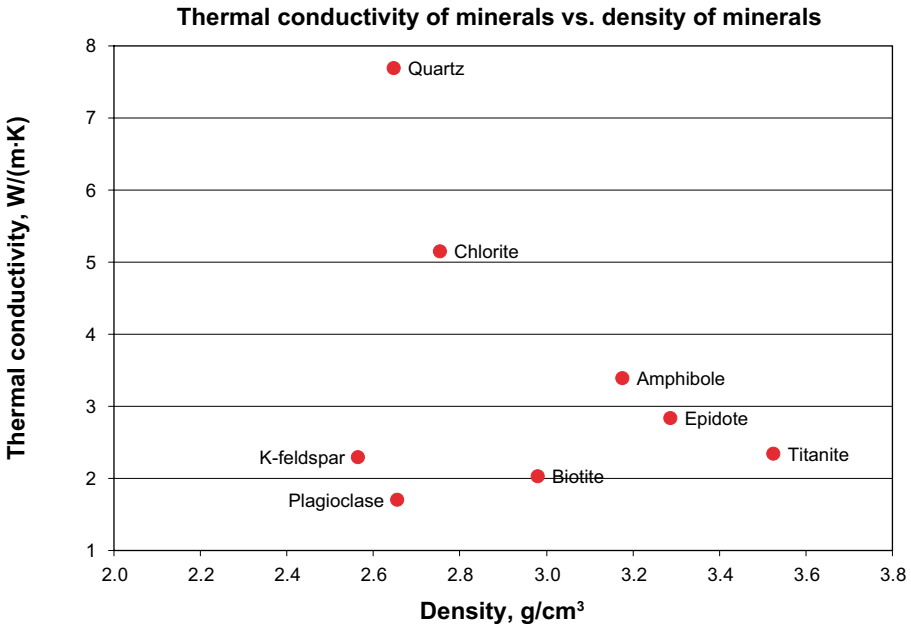

Figure 5-4. *Thermal conductivity of some minerals vs density of minerals /Horai 1971/.*

An explanation of the relationship could be the appearance of low density minerals with high thermal conductivity or high density minerals with low thermal conductivity. The mineral compositions of the dominating rock type Äspö diorite/Ävrö granite have therefore been examined, see Table 5-1. In /Sundberg and Gabrielsson 1999/ the mineral composition of fresh Äspö diorite was determined based on rock samples from the prototype repository. In /Sundberg 2002/ mineral compositions based on core samples from KA2599G01 were determined for Äspö diorite, Ävrö granite and Fine-grained granite (Äspö nomenclature). Äspö diorite and Ävrö granite is named Ävrö granite according to Simpevarp nomenclature.

Table 5-1. Mineral compositions of different rock types together with mineral properties.

	Density mineral (kg/m³)	Therm cond mineral (W/(m×K))	Prototype repository		KA2599G01		
			Fresh Äspö diorite	Fresh Äspö diorite	Äspö diorite	Ävrö granite	Fine-gr granite
Number of samples			2	1	5	3	2
Mean meas density (kg/m³)			2,761	2,770	2,744	2,663	2,642
Opaques	5,000	3.00			0.6	0.3	1
Titanite	3,525	2.34	1	1	1.3	0.4	0.2
Epidote	3,287	2.83	1	7	4	2.5	3
Hornblende	3,183	2.81	7	5			
Amphibole	3,176	3.39			0.2		
Biotite	2,981	2.02	18	15	18	7	3
Sericite	2,852	–	1	1	4	4	10.5
Chlorite	2,755	5.15			0.3	1	0.5
Quartz	2,674	7.69	10	10	12	25	31
Plagioclase	2,652	1.70	52	50	40	28	15
K-feldspar	2,566	2.29	10	10	20	32	36

It is concluded that the relationship between density and thermal conductivity is not the result of a few dominating minerals. More likely, all minerals contribute to the relationship but the contribution of some minerals is believed to be larger, eg. Quartz, plagioclase, biotite and epidote.

5.2.3 Magma composition and mineralogy

A third explanation of the relationship between density and thermal conductivity has been investigated: the mineral compositions of common igneous rocks, schematically illustrated in Figure 5-5. In order to do this, 21 synthetically "samples" were defined, evenly distributed along the horizontal line in Figure 5-5. The mineral composition of each synthetic sample was taken from Figure 5-5. The data is presented in Appendix D in Table D-1. The density and thermal conductivity was calculated for each sample, using mineral properties described in Table D-2 and Table D-3. The thermal conductivity was calculated as the geometric mean of the thermal conductivity of the minerals.

Two different calculations were carried out: (1) with fixed mineral properties of the thermal conductivity for all rock types, and (2) with adjusted (varying) properties of the plagioclase and olivine minerals depending on the silica content in the rock. The latter was performed because thermal conductivity of these two minerals varies when the chemical composition of the minerals changes. For plagioclase, the content of anorthite and albite is estimated to vary from 0–100%, with the lowest content of anorthite on the right hand side in Figure 5-5. The same way of reasoning was applied for the forsterite and fayalite content in the olivine (lowest forsterite content to the right). The same principle of adjustment could also be applied for pyroxene but this was not performed due to lack of reliable mineral data of thermal conductivity. All results are presented in Table D-4 in Appendix D in and in Figure 5-6.

Results of both calculations, with fixed and with adjusted mineral properties, are illustrated in Figure 5-6. The brackets represent the density intervals of the different rock types in Figure 5-1. The relationship between density and thermal conductivity for the Ävrö granite (Equation 5-2) is illustrated in Figure 5-6 with a green line.

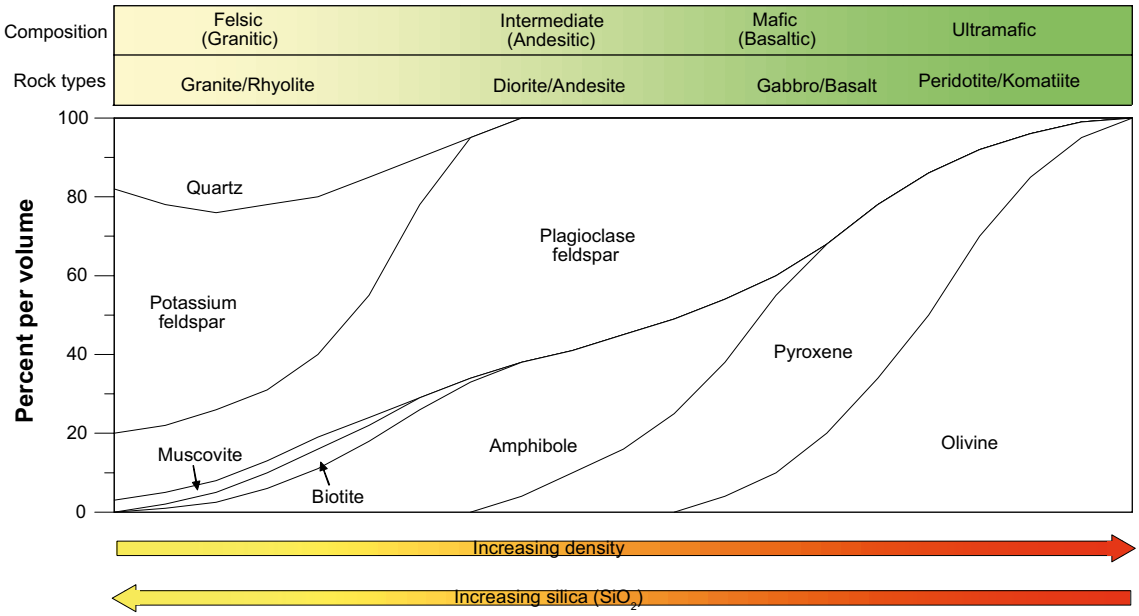

Figure 5-5. *Mineralogy of igneous rocks and the magmas /modified after Tarbuck et al. 2005/.*

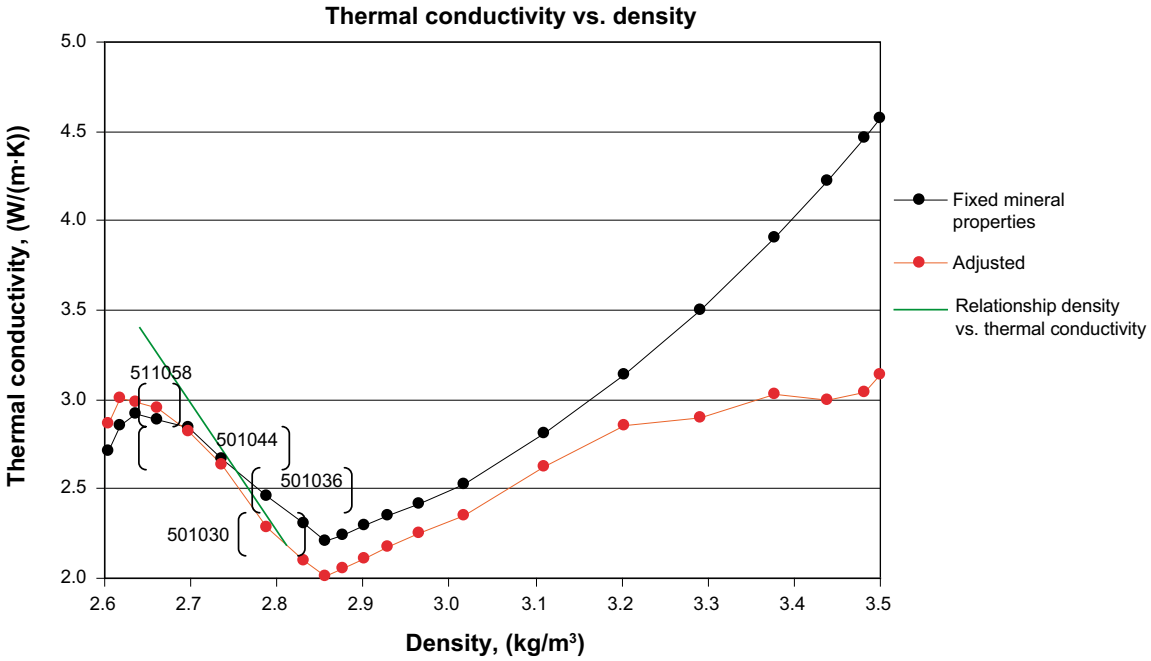

Figure 5-6. *Thermal conductivity vs density for synthetically defined "samples" with different mineral composition. "Fixed mineral properties" refers to thermal conductivity calculated with the same mineral properties for all rock types. For "Adjusted" samples, the relative occurrence of anorthite/albite in plagioclase, and forsterite/fayalite in olivine, respectively, is considered. The brackets represent the density intervals where the studied rock types appear. The green line represents the relationship between density and thermal conductivity for Ävrö granite.*

Figure 5-6 offers an explanation of the relationship between density and thermal conductivity for Ävrö granite (501044). Within the density range of Ävrö granite, the thermal conductivity is inversely proportional to density and the reason is the mineral composition. This is not obvious for the other three rock types, although Fine-grained dioritoid (501030) has a similar tendency but not as pronounced as Ävrö granite.

6 Inverse modelling of thermal conductivity at prototype repository scale

6.1 Introduction

Measurements of thermal properties and temperatures have been conducted within the prototype repository /Sundberg and Gabrielsson 1999/. Measurements has also been made on samples from the nearby borehole KA2599G01 /Sundberg 2002/. A prognosis model of the thermal properties has been established based on these data. The prognosis model is evaluated towards values calculated through inverse modelling. The inverse modelling is based on an iterative process where a fitting of measured and calculated temperatures is performed with a numerical model.

6.2 Instrumentation

Temperature sensors in the rock mass have been placed with a layout described in Figure 6-1. Samples collected for measurements of thermal properties were located in borehole KA2599G01 (drilled vertically from the gallery in Äspö HRL at chainage 2,599 m) and also several short boreholes from both the inner and outer section of the prototype repository.

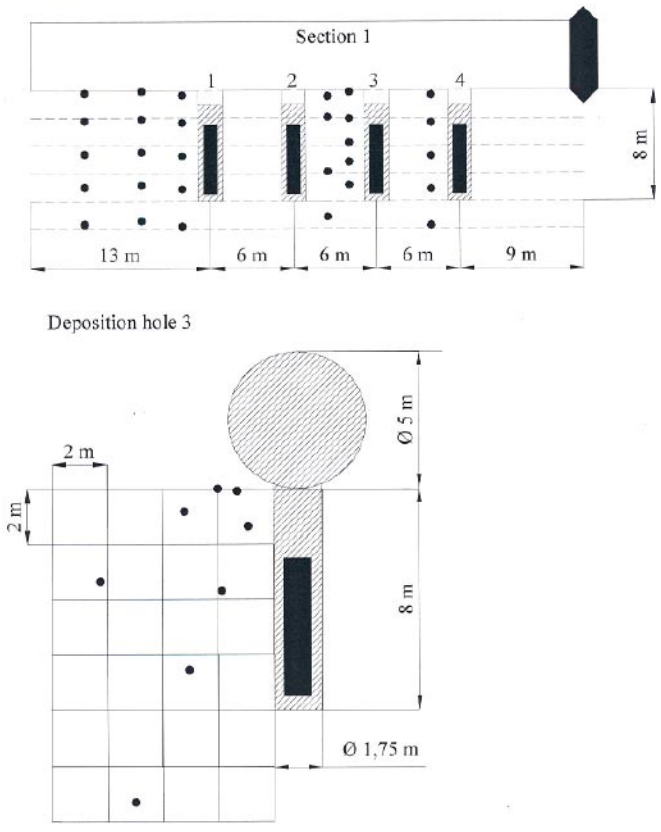

Figure 6-1. *Overview of the temperature sensors in the rock. Length section (upper) and cross section (towards the end of the tunnel) /Goudarzi and Johannesson 2004/.*

6.3 Description of data

Samples for measurements of thermal properties sampled within the Äspö area and rock type classified according to Äspö nomenclature have been reclassified according to Simpevarp nomenclature. The following results were obtained, see Table 6-1.

Table 6-1. Thermal conductivity values and classification of samples with Äspö and Simpevarp nomenclature. Results from laboratory and field measurements /Sundberg and Gabrielsson 1999 (A) (data from prototype tunnel), Sundberg 2002 (B)/.

Sample	Secup-seclow	Äspö nomenclature	Simpevarp nomenclature	Therm cond (W/(m×K))	Reference
KA 3539-1	1.0–1.22	Äspö diorite	Ävrö granite	2.42	(A)
KA 3539-2	5.50–5.68	Alt. Äspö diorite	Quartzmonzodiorite	2.63	(A)
KA 3545	0.83–1.11	Alt. Äspö diorite	Ävrö granite	2.72	(A)
KA 3551	0.95–1.15	Alt. Äspö diorite	Ävrö granite	2.76	(A)
KA 3563	0.88–1.12	Äspö diorite	Ävrö granite*	2.39	(A)
KA 3569	0.87–1.20	Äspö diorite	Ävrö granite	2.42	(A)
KA 3575	1.03–1.27	Äspö diorite	Ävrö granite	2.44	(A)
KA 3581	1.10–1.33	Äspö diorite	Ävrö granite	2.50	(A)
KA 3587	0.97–1.14	Äspö diorite	Ävrö granite	2.33	(A)
KA 3593-1	1.42–1.63	Äspö diorite	Ävrö granite	2.55	(A)
KA 3593-2	4.19–4.43	Xenolite	Quartzmonzodiorite	2.38	(A)
KA2599G01	4.33–4.43	Äspö diorite	Ävrö granite	2.16	(B)
KA2599G01	4.53–4.63	Äspö diorite	Ävrö granite	2.87	(B)
KA2599G01	4.73–4.83	Äspö diorite	Ävrö granite	3.05	(B)
KA2599G01	4.93–5.03	Äspö diorite	Ävrö granite	2.66	(B)
KA2599G01	5.13–5.23	Äspö diorite	Ävrö granite	2.50	(B)
KA2599G01	5.90–5.94	Äspö diorite	Ävrö granite	2.49	(B)
KA2599G01	14.63–14.67	Äspö diorite	Ävrö granite	2.34	(B)
KA2599G01	15.10–15.20	Äspö diorite	Ävrö granite	2.61	(B)
KA2599G01	15.30–15.40	Äspö diorite	Ävrö granite	2.67	(B)
KA2599G01	15.50–15.60	Äspö diorite	Ävrö granite	2.56	(B)
KA2599G01	15.70–15.80	Äspö diorite	Ävrö granite	2.54	(B)
KA2599G01	15.90–16.00	Äspö diorite	Ävrö granite	2.53	(B)
KA2599G01	24.02–24.12	Äspö diorite	Ävrö granite [1)]	2.76	(B)
KA2599G01	24.22–24.32	Äspö diorite	Ävrö granite	2.48	(B)
KA2599G01	24.42–24.52	Äspö diorite	Ävrö granite [2)]	2.57	(B)
KA2599G01	24.62–24.72	Äspö diorite	Ävrö granite [3)]	2.72	(B)
KA2599G01	24.82–24.92	Äspö diorite	Ävrö granite [4)]	3.56	(B)
KA2599G01	25.32–25.36	Äspö diorite	Ävrö granite	2.47	(B)
KA2599G01	44.28–44.32	Ävrö granite	Ävrö granite	2.99	(B)
KA2599G01	50.10–50.14	Fine-grained granite	Fine-grained granite	3.58	(B)
KA2599G01	61.89–61.93	Fine-grained granite	Fine-grained granite	3.68	(B)
KA2599G01	70.60–70.64	Äspö diorite	Ävrö granite	2.84	(B)
KA2599G01	85.10–85.50	Äspö diorite	Ävrö granite	2.69	(B)
KA2599G01	101.85–101.89	Alt. Äspö diorite	Ävrö granite	3.11	(B)

Sample	Secup-seclow	Äspö nomenclature	Simpevarp nomenclature	Therm cond (W/(m×K))	Reference
KA2599G01	120.05–120.09	Ävrö granite	Ävrö granite	3.22	(B)
KA2599G01	126.35–126.39	Ävrö granite	Ävrö granite	3.55	(B)
Section 3535	Meas 1 No 1	Äspö diorite	Ävrö granite *	2.73 [5)]	(A)
Section 3535	Meas 2 No 1	Äspö diorite	Ävrö granite *	2.67 [5)]	(A)
Section 3566	No 1	Äspö diorite	Ävrö granite *	3.16 [5)]	(A)
Section 3583	No 1	Äspö diorite	Ävrö granite *	2.80 [5)]	(A)
Section 3583	No 2	Äspö diorite	Ävrö granite *	2.78 [5)]	(A)

* Not reclassified.
[1)] Strong foliation and epidot filled joints.
[2)] Elements of fine-grained mafic rock type.
[3)] Diffuse elements of red granite.
[4)] Mixed with red granite and elements of fine-grained mafic rock type.
[5)] Field measurement with multi probe method.

Some of the field measurements at the prototype repository were disturbed by water movements. Table 6-2 shows apparent thermal conductivity influenced by water movements. The results are significant higher compared to Table 6-1. Location of samples and field measurements in the prototype tunnel is showed in Figure 6-2.

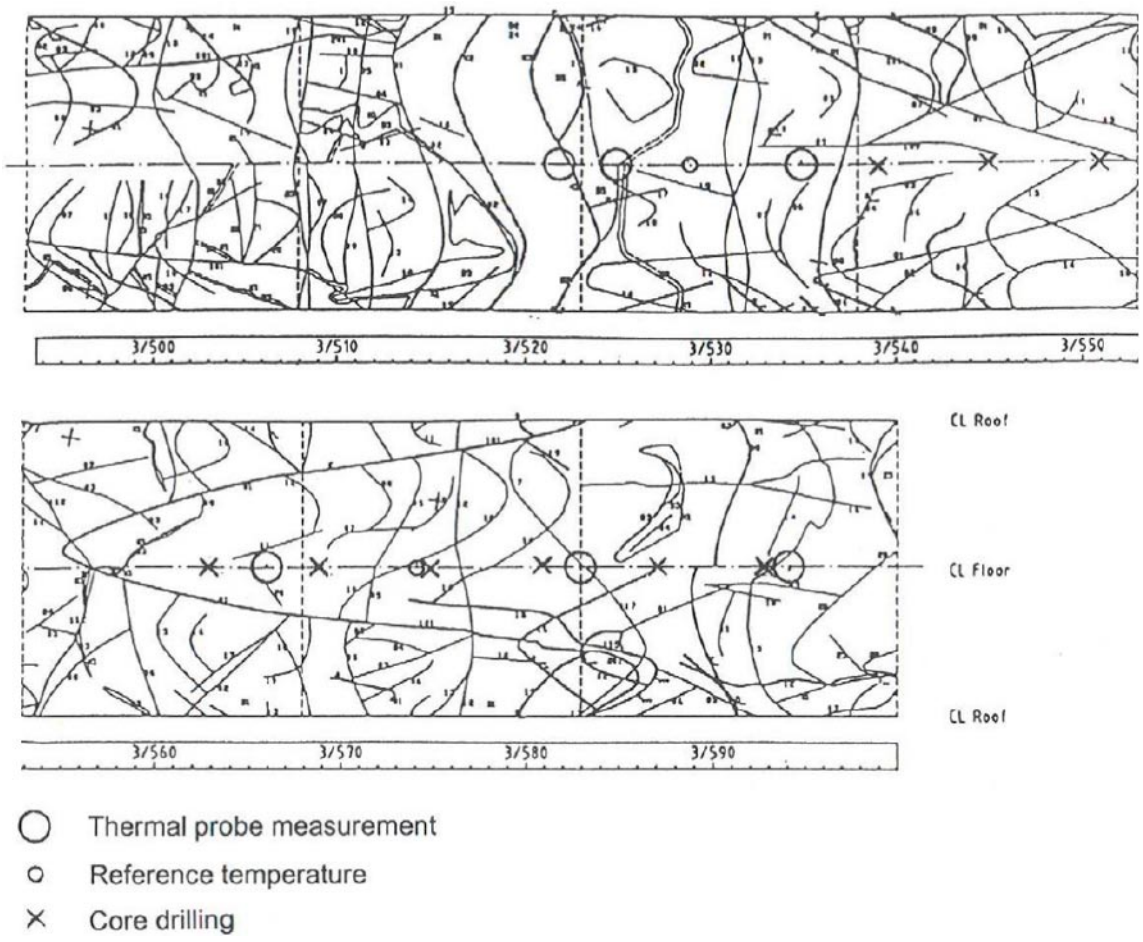

Figure 6-2. *Location of boreholes (samples) and field measurements in the prototype tunnel.*

Table 6-2. Measuring results for field measurements of thermal conductivity influenced by water movements.

Sample	Comment	Äspö nom	Simpevarp nom	Apparent therm cond (W/(m×K))
Section 3535	Meas 1 No 2	Äspö diorite	Ävrö granite	3.49
Section 3535	Meas 2 No 2	Äspö diorite	Ävrö granite	3.76
Section 3594	No 1	Äspö diorite	Ävrö granite	5.98
Section 3594	No 2	Äspö diorite	Ävrö granite	3.64
Mean				4.22
Mean (extreme value excluded				3.63

6.4 Waterbearing fractures and lithology

The prototype tunnel has been mapped due to water bearing fractures and different rock types. In Figure 6-3 to Figure 6-5 water conductive fractures are showed together with observations of moist and water. Sections for location of canisters are also indicated in the figures. Most of the water comes from the inner part of the tunnel, see Figure 6-6.

Lithological and fracture mapping are showed in Figure 6-7. The dominating rock type, according to Äspö nomenclature, is Äspö diorite.

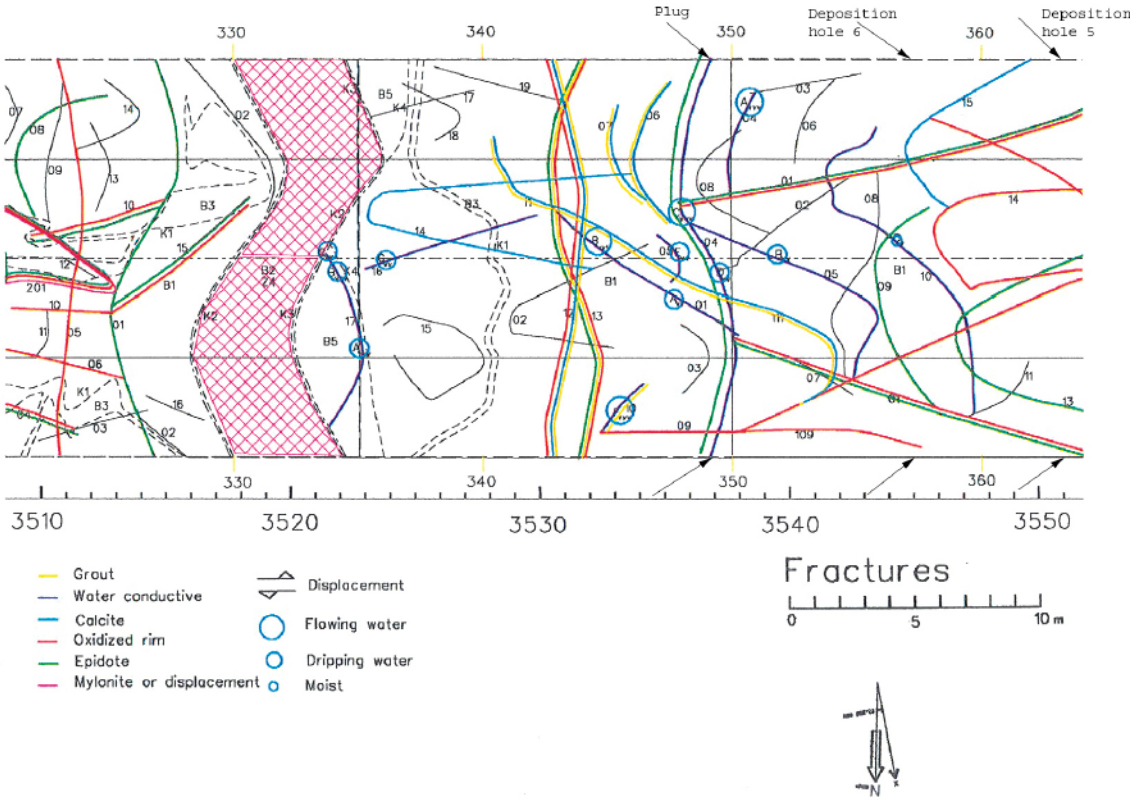

Figure 6-3. *Water conductive fractures with observations of water together with the location of the different canisters in the outer section of the prototype tunnel. Modified from /Patel et al. 1997/.*

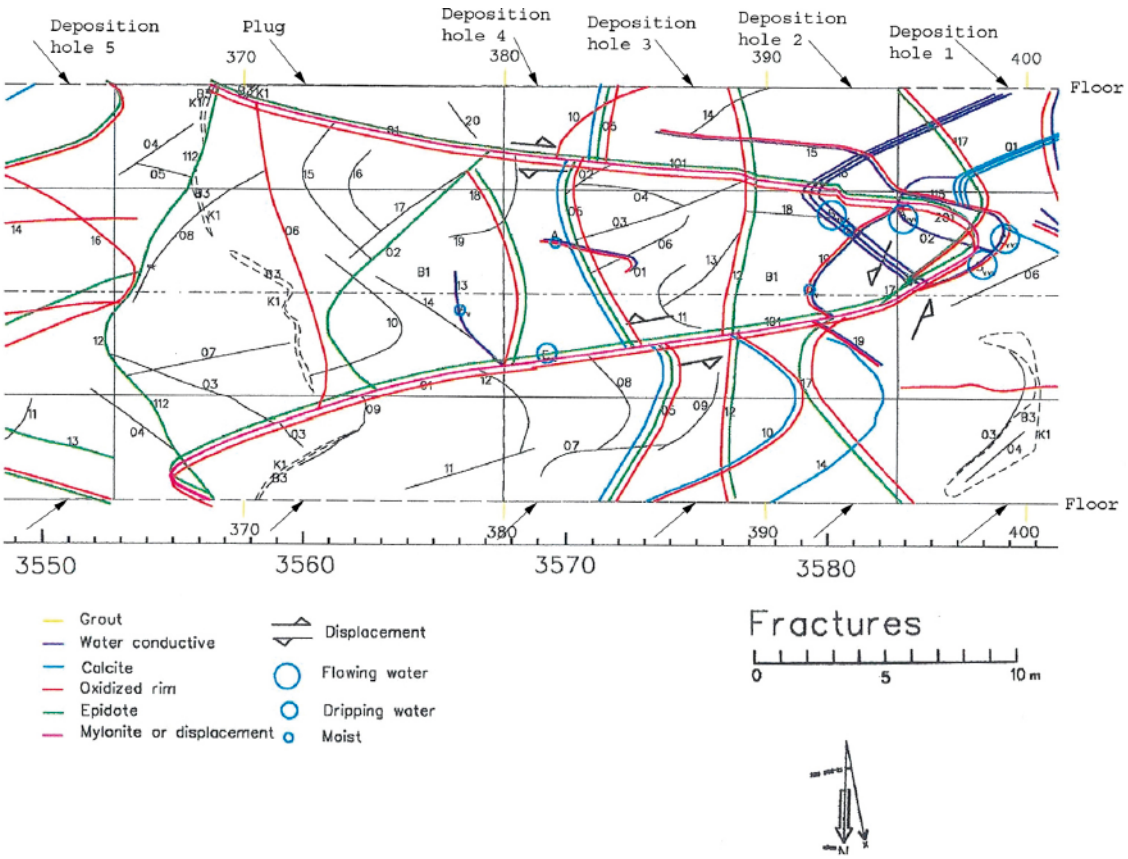

Figure 6-4. *Water conductive fractures with observations of water together with the location of the different canisters in the middle section of the prototype tunnel. Modified from /Patel et al. 1997/.*

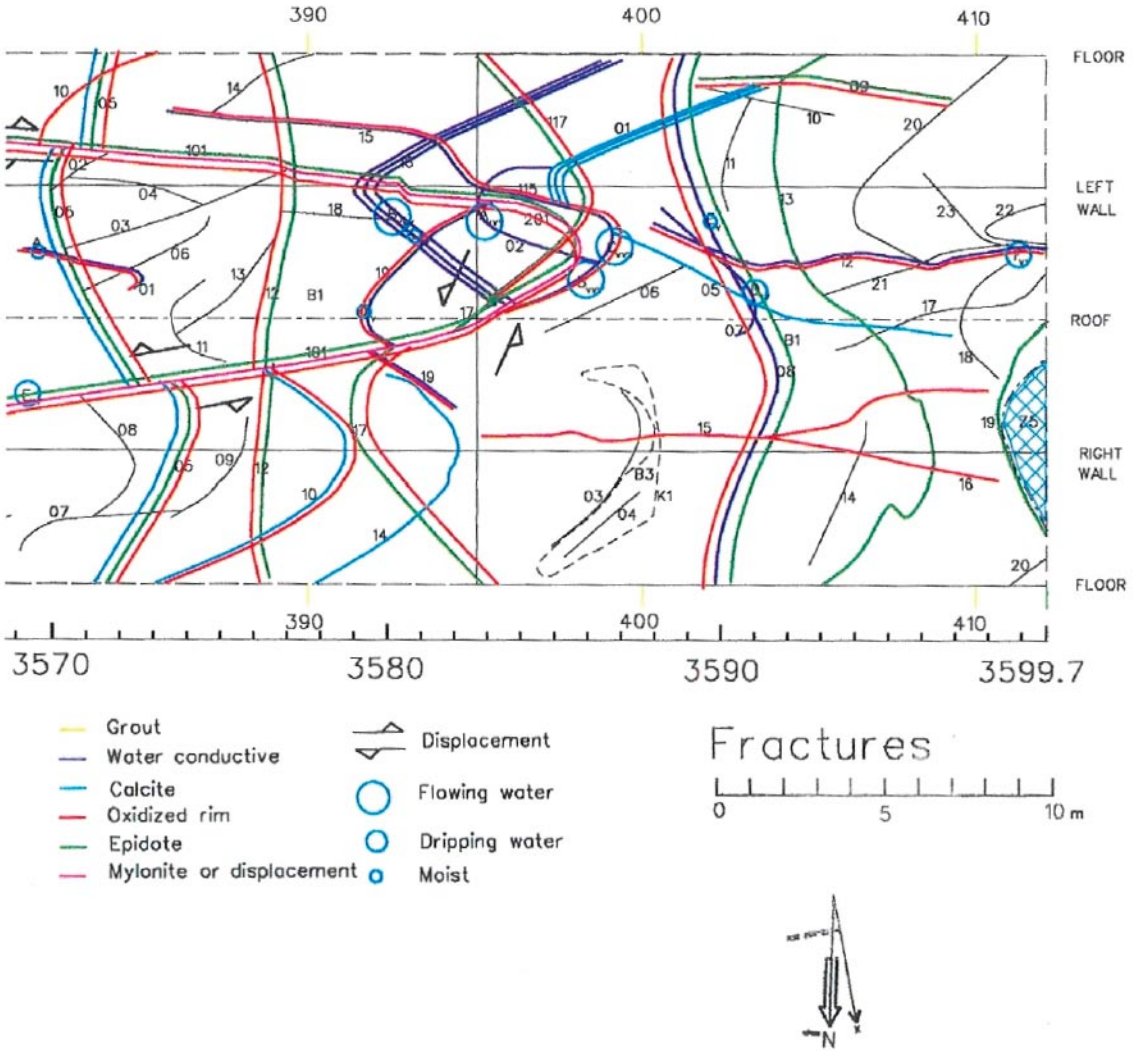

Figure 6-5. *Water conductive fractures with observations of water in the inner section of the prototype tunnel. For location of the different canisters, see previous figure /Patel et al. 1997/.*

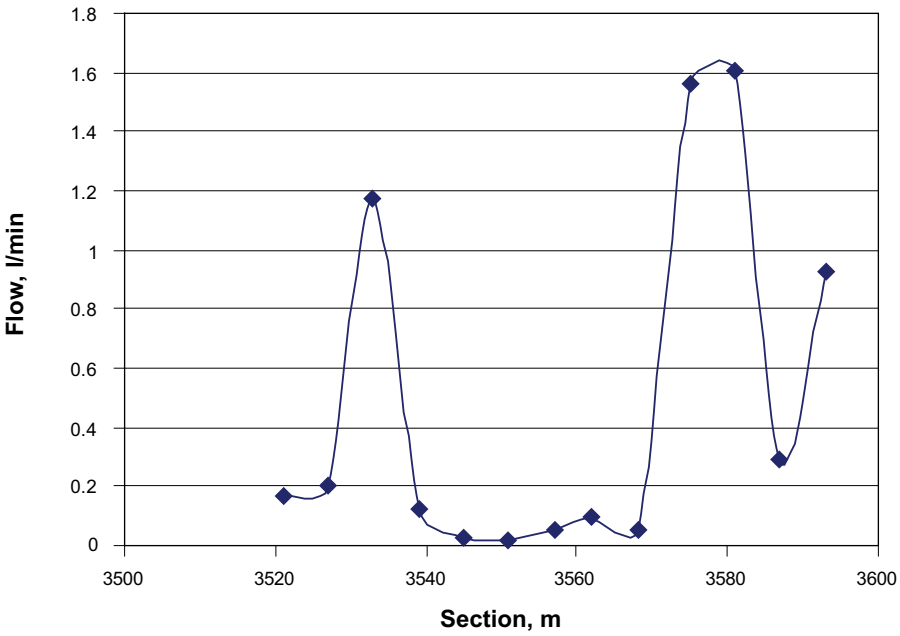

Figure 6-6. *Inflow measurements data from the prototype repository. The total flow was 5.2 l/minute (mean). Data from /Patel et al. 1997/.*

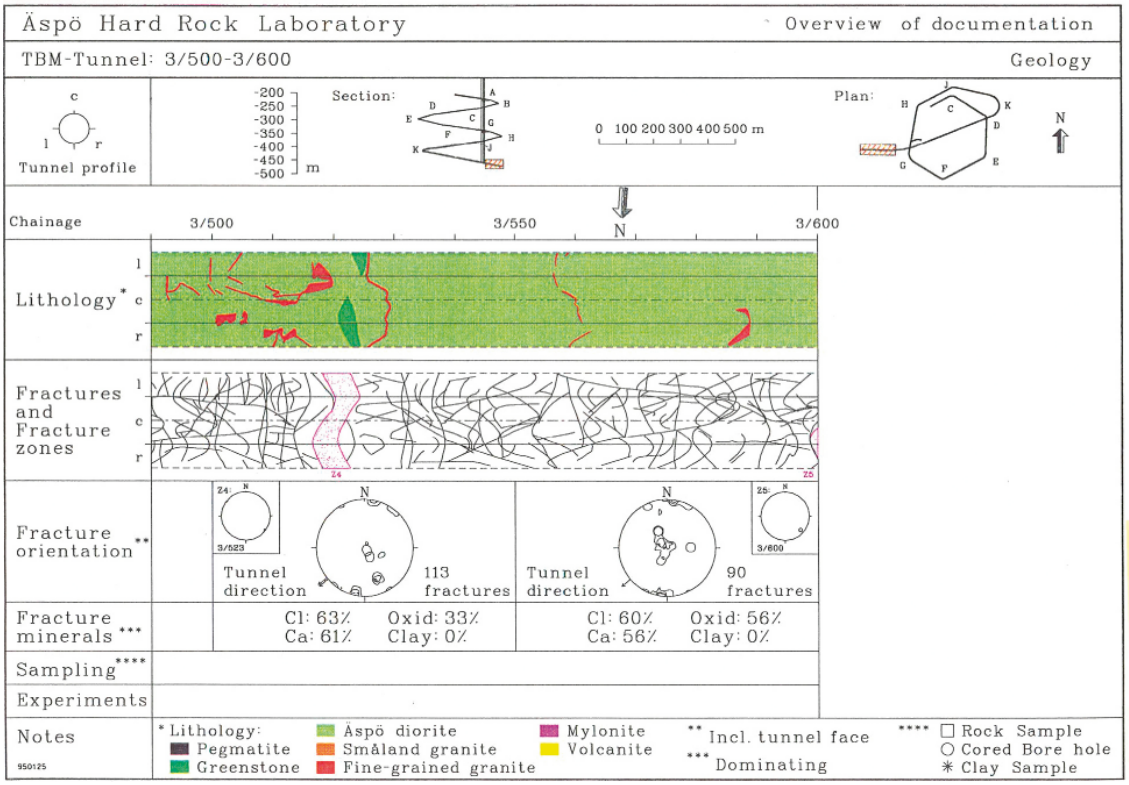

Figure 6-7. *Lithological and fracture mapping of the prototype tunnel /Rhén 1995/.*

6.5 Prognosis of thermal properties

A prognosis of the thermal conductivity has been made based on sample results from laboratory measurements with the TPS method /Sundberg and Gabrielsson 1999, Sundberg 2002/ together with samples measured within this project (see Chapter 4) and field measurements /Sundberg and Gabrielsson 1999/. Different prognosis models have been calculated based on a number of assumptions regarding population and rock type nomenclature.

The following assumptions have been done regarding populations and rock type nomenclature for seven different prognosis models:

1. Prototype repository section 1 (inner), laboratory measurements (6 samples), Äspö diorite.
2. Prototype repository section 2 (outer), laboratory measurements (4 samples), Äspö diorite.
3. Prototype repository section 1 and 2, laboratory measurements (10 samples), Äspö diorite.
4. Prototype repository section 1 and 2, field measurements (5 samples), Äspö diorite.
5. Äspö area, laboratory measurements (31 samples), Äspö diorite.
6. Äspö area, laboratory measurements (32 samples), Ävrö granite.
7. Äspö and Simpevarp, laboratory measurements (37 samples), Ävrö granite.

Äspö nomenclature has been used for all prognoses except for no 6 and 7 for which Simpevarp nomenclature has been used.

Probability plots to evaluate the distribution of data included in the different models have been calculated and the results are presented in Figure 6-8 for models 1–4, in Figure 6-9 for model 5, and in Figure 6-10 for models 6-7. The distribution models with best fit to data consist of both lognormal and extreme value distributions. It is reasonable to assume that a set of representative measurements of thermal conductivity is approximately lognormally distributed. However, when data sets from different populations are combined, as in Figure 6-9 and Figure 6-10, it is not surprising that data no longer follows a lognormal distribution (sampling from mixed populations should be avoided if possible because biases can be introduced, see /Chai 1996/). Empirically, the extreme value distribution exhibit the best fit to these data sets of the limited number of evaluated ones.

Distribution models of the different populations are presented in Figure 6-10. The higher uncertainty in the upper end of the prognosis is possibly due to elements of granite in samples with high thermal conductivity classified as Ävrö granite.

A summary of the prognosis models for the thermal conductivity within the prototype repository is presented in Table 6-3. It is also possible to combine different prognosis models for different purposes.

To illustrate the background data of the seven different prognoses, cumulative histograms are presented in Figure 6-12 and Figure 6-13.

It can be discussed weather data for all prognosis models are representative. The measured samples from Simpevarp have all been taken from a limited, only 1 m long, part of borehole KAV01 (prognosis model 6 and 7). Further, the 15 samples measured in this project are all sampled within an approximately 20 m long section of borehole KA2599G01, see Chapter 4. These 15 samples constitute almost half of the data for the distribution models no 5 to 7.

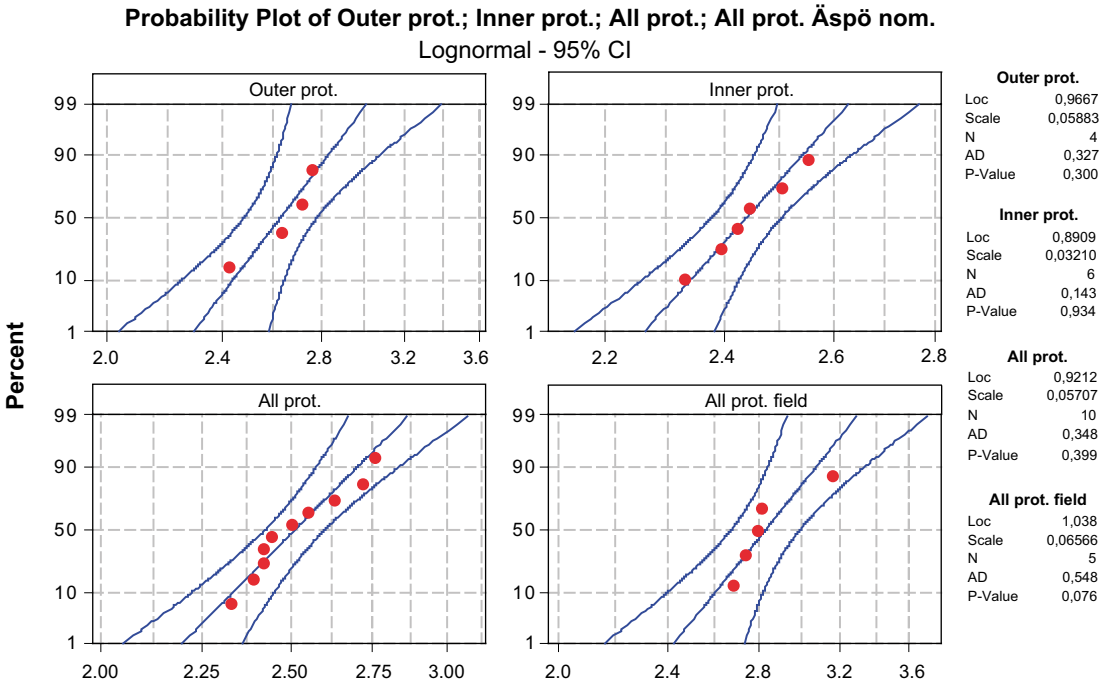

Figure 6-8. *Probability distribution (lognormal distributed) of four thermal conductivity populations (models 1–4) from prototype repository classified as Äspö diorite with Äspö nomenclature.*

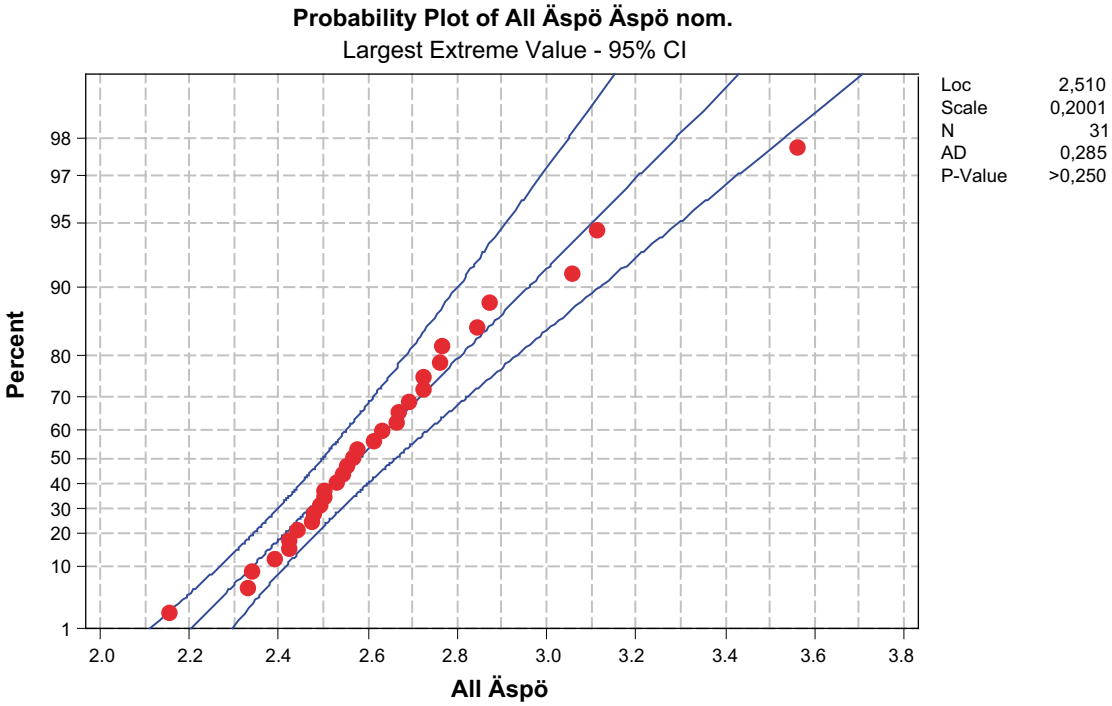

Figure 6-9. *Probability distribution (extreme value distributed) of all thermal conductivity measurements from the Äspö area (model 5) classified as Äspö diorite with Äspö nomenclature.*

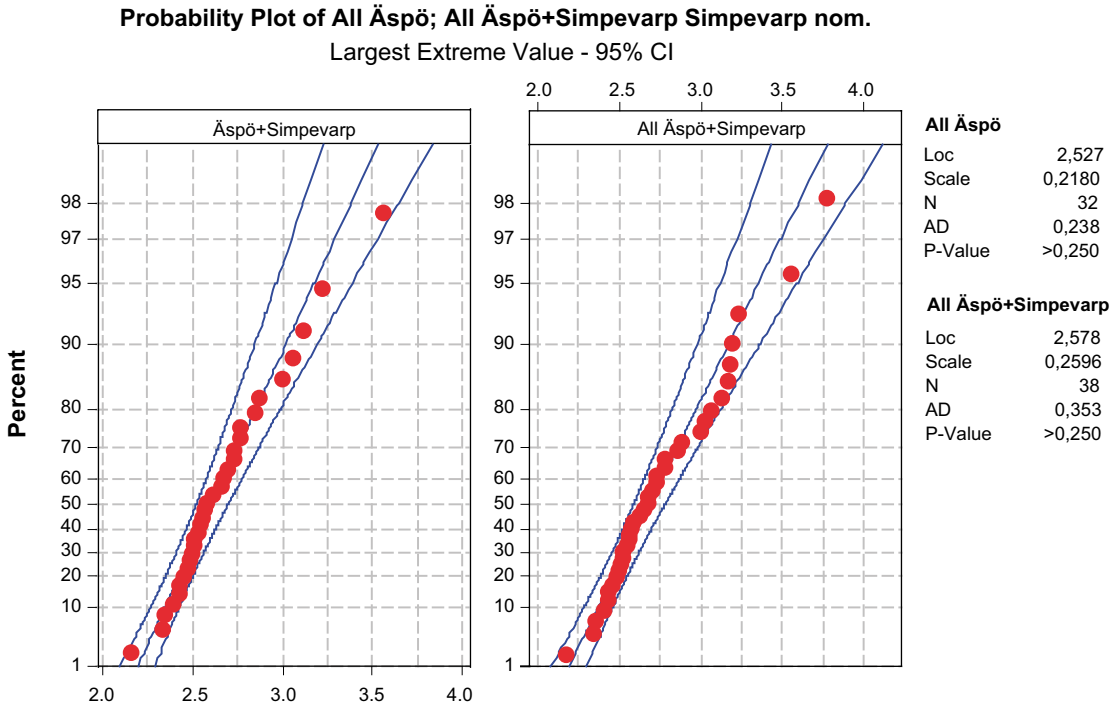

Figure 6-10. *Probability distribution (extreme value distributed) of all thermal conductivity measurements from the Äspö area and the Äspö area together with the Simpevarp data (model 6–7) classified as Ävrö granite with Simpevarp nomenclature.*

Table 6-3. Summary of results from prognosis modelling of thermal properties.

Prognosis	Population	Mean (W/(m×K))	Std.dev (W/(m×K))	Number of samples	Distribution
1	Prototype repository section 1 (inner), laboratory measurements, Äspö diorite.	2.44	0.08	6	Lognormal
2	Prototype repository section 2 (outer), laboratory measurements, Äspö diorite.	2.63	0.15	4	Lognormal
3	Prototype repository section 1+2, laboratory measurements, Äspö diorite.	2.52	0.15	10	Lognormal
4	Prototype repository section 1+2, field measurements, Äspö diorite.	2.83	0.19	5	Lognormal
5	All measurements Äspö area, laboratory measurements, Äspö diorite.	2.62	0.27	31	Largest extreme value
6	All measurements Äspö area, laboratory measurements, Ävrö granite.	2.65	0.29	32	Largest extreme value
7	All measurements Äspö and Simpevarp area, laboratory measurements, Ävrö granite.	2.73	0.35	37	Largest extreme value

According to these presumptions the best prognosis should be number 3, based on all laboratory measurements from the prototype repository, or a combination of no 3 and 4 (the latter based on field measurements). The results for the field measurements (2.86 W/(m×K)) are a bit higher than the laboratory measurements (2.52 W/(m×K)) and are possible influenced by water movements. However, also the results from the temperature measurements at the prototype repository are influenced by water movements, especially in the initial stage after installation of the backfill. The weight mean of these two prognosis model (3 and 4) is 2.62 W/(m×K) and may be a prognosis of the effective thermal conductivity.

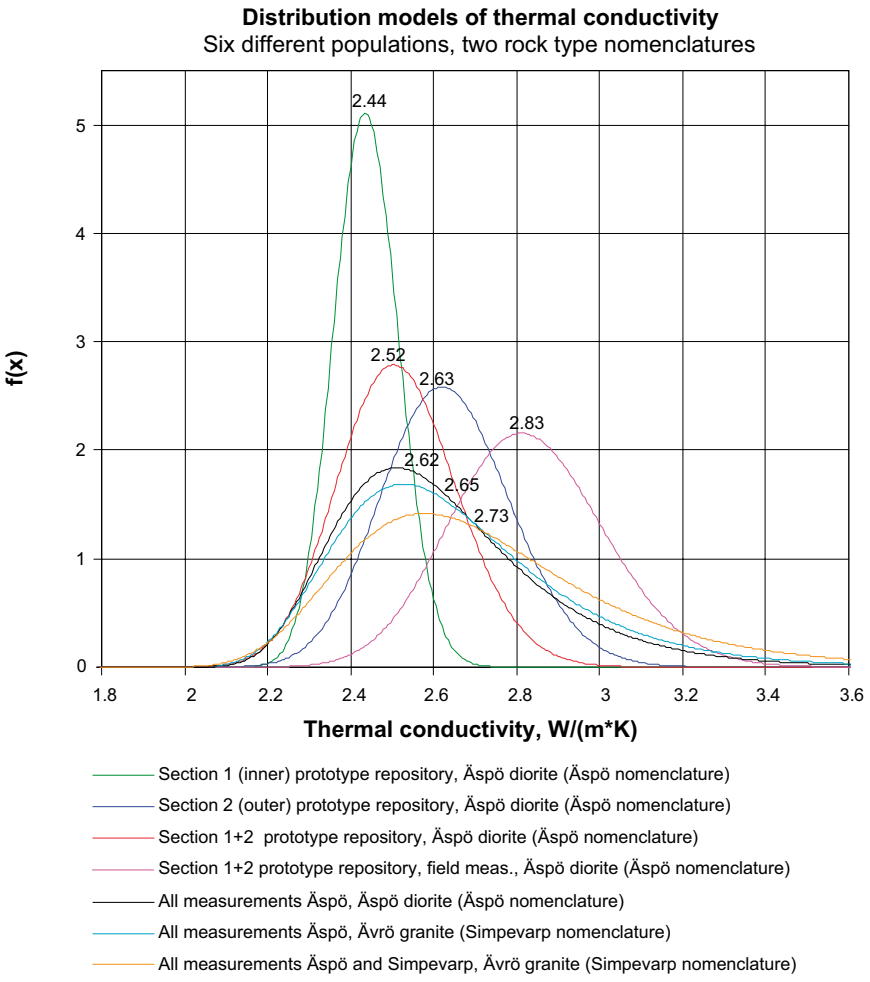

Figure 6-11. *Seven prognosis models based on different populations and rock type nomenclatures.*

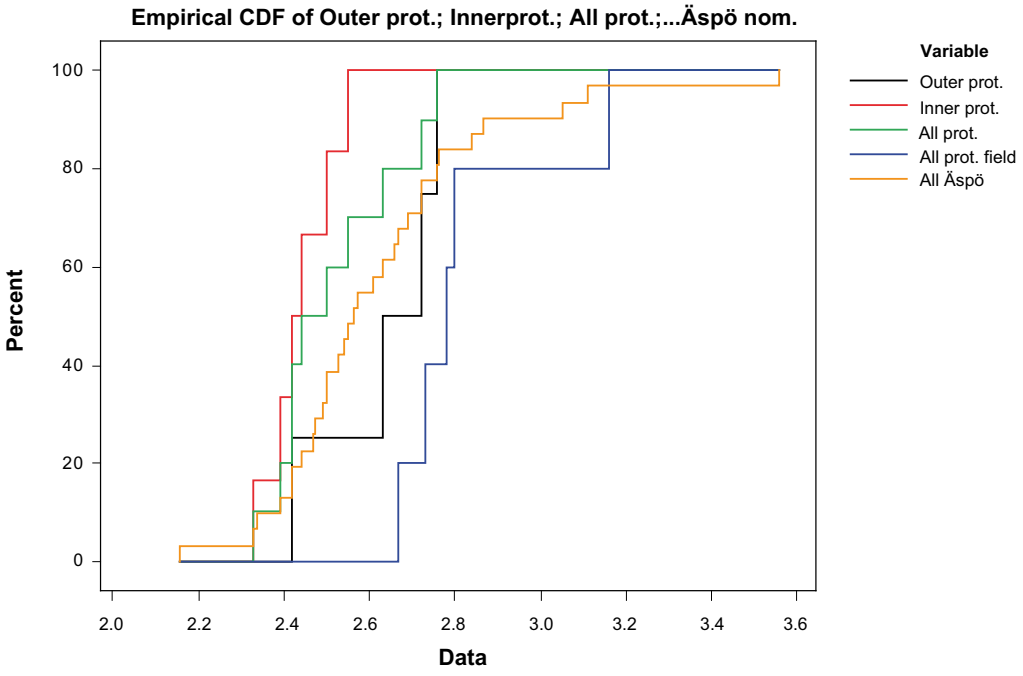

Figure 6-12. *Cumulative histograms of data (measured thermal conductivity) to the five prognosis models based on Äspö nomenclature (models 1–5).*

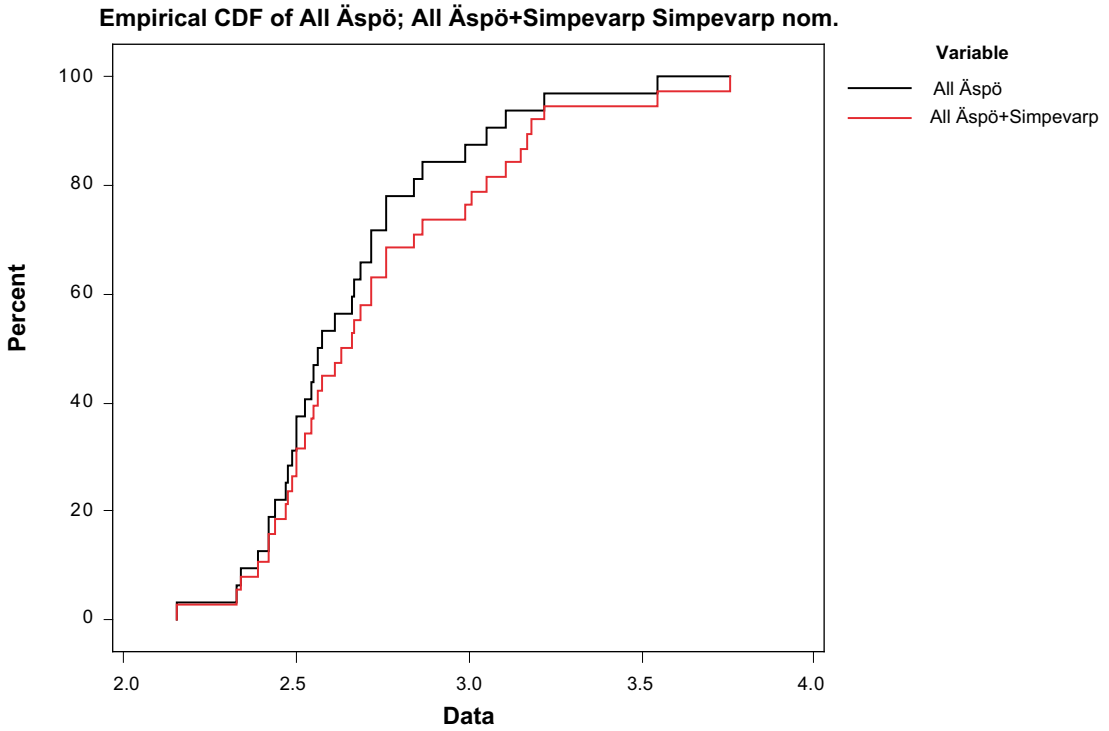

Figure 6-13. *Cumulative histograms of data (measured thermal conductivity) to the two prognosis models based on Simpevarp nomenclature (models 6–7).*

6.6 Inverse numerical modelling

6.6.1 Introduction

Measured data

The material used in this study consists of measured data from thermal test at the prototype repository:

- Canister power rates. The power rates for the six different canisters have been measured, screened and adjusted. The new calculated power rates are available with an average sampling frequency for the six canisters varying from 17 to 24 readings per day.
- Rock temperatures have been measured at 37 temperature sensor locations with roughly an hourly frequency for 527 days.
- Special file with initial temperatures at the 37 sensor locations.
- Sensor locations.
- Temperature on the inside and the outside of the canisters.

The files with canister power rates were merged into one file where every change in power rate for any canister was arranged in chronological order. The massive file containing all rock temperature data was split into 37 different files – one for each sensor. The sensor locations are given in a local grid pertaining to each canister. These coordinates were transformed to the global grid. Initial temperatures screened against the initial readings from the measured rock temperature files. The canister temperature files are not used in this study In Figure 6-14, the heat sources are indicated as blue quadruples and the sensors are indicated as black and grey circles.

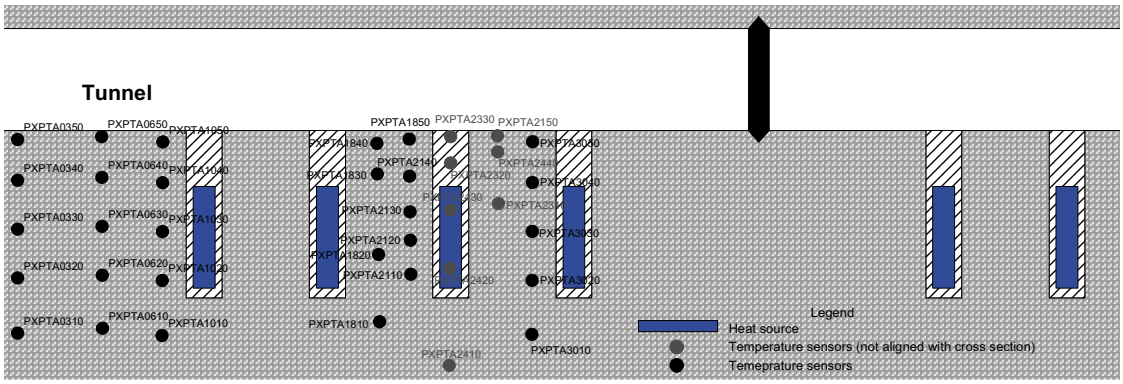

Figure 6-14. *Location of temperature sensors. The inner part of the prototype tunnel to the left. The numbering of canisters is from the left. See also Figure 6-1.*

Idealizations

This study focuses on the thermal conditions in the rock mass. Thus, the conditions at the canister and in the bentonite buffer are not of primary interest in this study. Similar to the thermal response tests carried out for ground-coupled heat pumps it is assumed that these conditions have little influence on the evolution of rock temperatures after a certain initial period. The heat transfer properties of the buffer and the capacities of the involved materials are of course important in the immediate vicinity of the canisters and when the heating is started. Most of the released heat is then absorbed in the canister and buffer. A certain initial period is therefore ignored during the parameter fitting procedure.

The water saturation of the bentonite buffers can be mentioned as an example of the complexity of the boundary conditions close to canister. The bentonite buffers surrounding the canisters are fairly dry when the heating starts, but there is a rapid increase in the water saturation as the experiment starts. Saturation of bentonite buffers around the canisters is predicted to take 2–3 years along the buffer and 5–6 years in the thicker bentonite below and above the canister. The relative humidity of the sensors indicates that the bentonite is close to water saturation after one year of operation although the conditions seem to be fairly heterogeneous.

The tunnels above the deposition holes are backfilled with a mixture of bentonite (30%) and crushed rock.

Comparison with thermal response test

The evaluation method of the inverse modelling has similarities with a thermal response test with a thermal probe, which are a common technique to evaluate the thermal properties of solid materials. The thermal response test is performed by supplying a constant heat rate from a cylindrical probe inserted into the material. The length of the probe is often chosen so that three-dimensional end-effects become negligible during the test period. A temperature sensor in the probe registers the temperature evolution during the period. The thermal properties are determined based on the shape of the measured temperature response.

The left figure in Figure 6-15 shows the measured fluid temperature during a response test for a 175 m borehole (diameter 115 mm) used for ground-source heat pumps. The duration of the test was about 76 hours. A logarithmic time-scale is used. The right figure shows the measured temperature response of a thermal probe at the prototype repository.

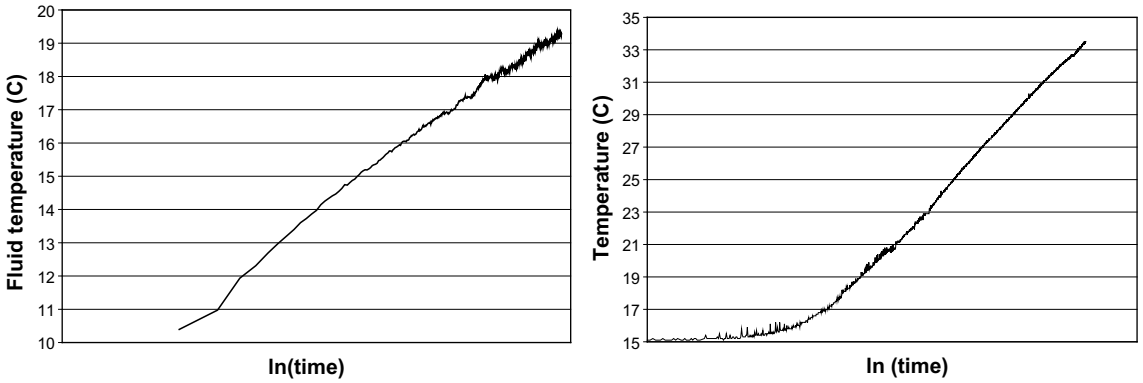

Figure 6-15. *Left: Measured fluid temperature during a response test for a 175 m borehole used for ground-source heat pumps. Right: Measured temperature response of thermal probe PXPTA1020 at the protoype repository.*

The collected data for an initial period of 15 hours is not used during the evaluation in order to minimize the influence of capacitive effects in the borehole, since it is difficult to obtain details of the actual heat transfer properties in the borehole heat exchanger. The thermal conductivity is evaluated from the slope of the curve (see Figure 6-15).

The response curves of temperature sensors in the rock around the deposition holes have a similar character. However, the infinite line-source theory is not applicable to the analyses of prototype repository due to the large diameter of the deposition holes in relation to their vertical extension and distance to other deposition holes. The response curve also has contributions from several heat sources (canisters). The basic idea of the evaluation method used in this report is anyway similar in its focus on the slope of the response curve.

6.6.2 Modelling

Evaluation method

The measured thermal response in the surrounding rock is analyzed by inverse modelling of the thermal properties of the rock mass. In this study, a three-dimensional finite difference model of the prototype repository (canisters, buffers, tunnel, etc) is used to calculate the transient temperature increase due to the heat generation in the canisters. The value of a homogeneous rock thermal conductivity is varied until the best fit with measured data is obtained for each sensor point. The evaluation period for the fitting procedure is varied in order to study sensitivity to different time-scales.

Numerical model

The numerical model of the repository uses an explicit finite difference scheme. The code is based on models previously developed for underground thermal energy storage applications and it has been extended to accommodate the geometry of the repository.

The simulated ground region encompasses a parallelepipedical volume of 120×150×120 m^3 and is described with a grid using 54×197×59 = 627,642 cells for the numerical simulation scheme.

Assumptions

The thermal properties of the different materials involved large-scale thermal process are assumed to be homogeneous. The thermal properties are given in Table 6-4.

Table 6-4. Thermal properties of the materials involved in the thermal process.

	Thermal conductivity (W/(m×K))	Volumetric heat capacity (MJ/(m³×K))
Canister	15.0	4.00
Buffer	1.5	3.40
Tunnel	1.5	2.50
Rock	To be estimated	2.20*

* A value of 2.32 (MJ/(m³×K)) was also used in order to test the sensitivity to this parameter.

All thermal properties are constant, which means that the thermal problem is linear. Different solutions to the heat conduction problem can then be superimposed on each other to form the complete temperature field. Here, this technique is used by superimposing two parts of the thermal response – the initial temperature field and the temperature increase due the heat generation in the canisters. The initial temperature is assumed to be constant although it is apparent from the initial rock temperatures that there is a certain thermal disturbance from the activities in the deposition tunnel. This disturbance will decline with time. The influence of this disturbance will reduced if a certain initial time period is omitted from the fitting procedure. The initial temperature in the calculation of the thermal disturbance is set to zero everywhere.

Fitting procedure

The measured thermal response is used to find the thermal conductivity that result in the best fit with the simulated thermal response. The thermal conductivity of the rock is set to a constant homogeneous value for each calculation of the temperature disturbance due to the heat generation within each canister. The value of thermal conductivity is varied from 1.9 to 3.7 W/(m×K) with an increment of 0.1 W/(m×K). During the simulation for each value of the thermal conductivity, the temperature disturbance (increase) at each temperature sensor location is calculated. The temperatures are stored with a time interval of 12 hours for a total simulation time of 730 days.

In the second step the simulated values are interpolated in time to match the times at which the measured data were collected for each sensor. The third step involves comparison of the measured and simulated temperatures for each point and thermal conductivity during the chosen evaluation interval. The average temperature of the measured temperature and the simulated temperature increase during the evaluation period is first calculated. The difference between these averages is assumed to be the initial temperature for the simulated temperatures, which are then the sum of this initial temperature and the temperature increase. The square of the difference between measured and simulated temperature for each measured time in the evaluation period is summed. This procedure is repeated for each value of thermal conductivity. Finally, we have the square sum for 18 values of thermal conductivity in the range from 1.9 to 3.7 W/(m×K) for each sensor. The thermal conductivity of the best match between measured and simulated values for a given sensor is found by minimizing a polynomial fit to the 18 values.

The choice of evaluation period is guided by three different concerns:

- To minimize the influence of an incomplete description of the local conditions in the canister and bentonite buffer, a certain initial period should not be included in the fitting procedure. For instance, the varying saturation level in the bentonite buffer will influence the local heat transfer characteristics from the canister to the borehole wall. This will affect the temperature increase (capacitive effects) of the canister. Lower heat transfer capacity gives higher canister temperature and thus more energy is stored in the canister and less is released to the surrounding. It is apparent from the measured canister temperature that the temperature rise is most pronounced in the beginning. Later the temperature becomes more stable and the energy absorbed in the canister decreases.
- Local disturbances of the initial temperatures. These disturbances are due to activities and varying temperatures in the deposition holes and the tunnel during construction. The distances from the surfaces to which these temperature changes penetrate depend on the duration of exposure. The variation in measured initial temperature is an indication of this process. After the sealing of the tunnel there will be a decline of the disturbances on a time-scale similar to the exposure duration. The chosen fitting procedure may result in simulated "initial" temperatures being slightly different than the measured ones.
- Another important process may be convective heat transport due to large-scale groundwater flow in the fissures. The basic influence is most pronounced on a long time scale. Using a fitting procedure based on conductive heat transport will lead to increasingly higher "effective" thermal conductivities when longer evaluation periods are considered in order to compensate for the energy transport away from the rock around the canisters.

It should be emphasized that the fitted thermal conductivity values are calculated for each sensor point individually without regard to the thermal response of any other point. However, it is also possible to give a thermal conductivity considering the best fit for all 37 sensor points. The procedure to obtain this overall thermal conductivity value is carried out as follows. For each sensor point, the square sum of the differences between measured and calculated temperatures for the 18 values of thermal conductivity in the range from 1.9 to 3.7 W/(m×K) is normalized through division by the number of temperature observations. Then the normalized values for the 37 sensor points are summed up for each value of the thermal conductivity (1.9 to 3.7 W/(m×K)). The thermal conductivity of the best overall match between measured and simulated values considering all sensors is found by minimizing a polynomial fit to the 18 values.

6.6.3 Result of evaluated thermal conductivity

The influence of the duration of the evaluation period is for two different start values – 30 days and 160 days. The reasons for omitting a certain initial time period have been explained above.

Influence of duration of evaluation period and initial temperatures

The point PXPTA2120 with the largest temperature change is used as a reference. The first comparison for the two cases is made with an end time of 250 days. The fitted simulated thermal responses are given in Figure 6-16 and Figure 6-17.

A comparison for the two cases is made with an end time of 525 days. The fitted simulated thermal responses are given in Figure 6-18 and Figure 6-19.

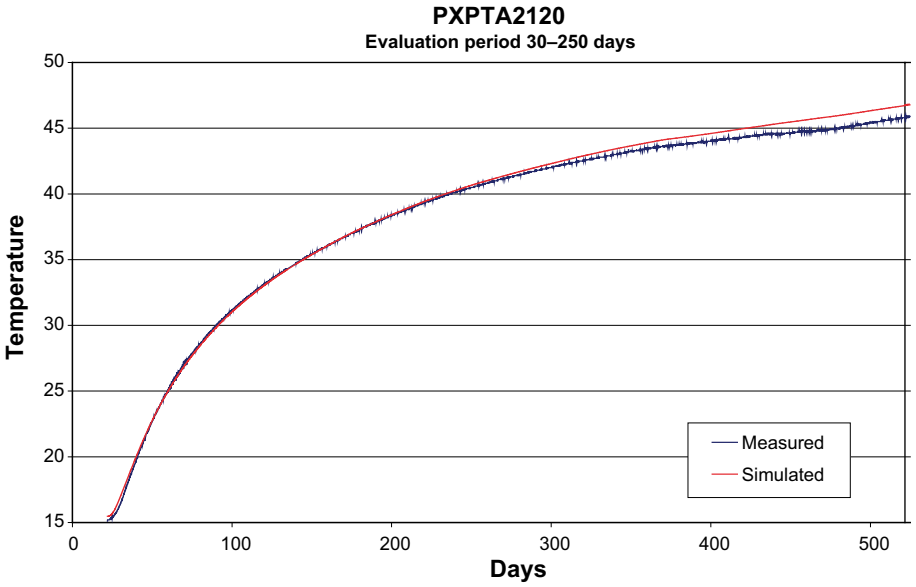

Figure 6-16. *Thermal response of thermal probe PXPTA2120 during 525 days. The period 30–250 days is used for fitting the measured and simulated response.*

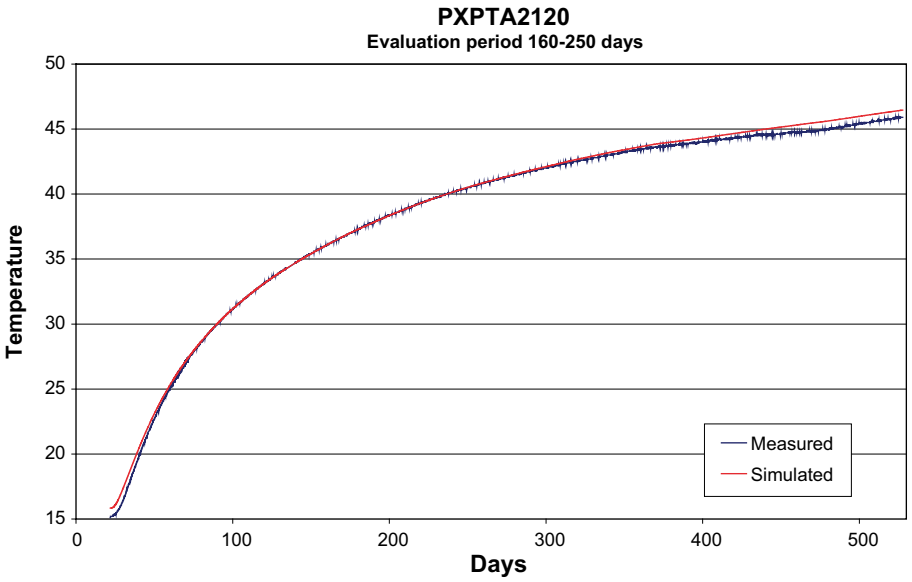

Figure 6-17. *Thermal response of thermal probe PXPTA2120 during 525 days. The period 160–250 days is used for fitting the measured and simulated response.*

A general observation is that setting the start time for the evaluation period at 160 days results in better fit during the chosen evaluation period than the setting the time to 30 days. There is a certain disagreement during the initial period before 160 days. It is of course more difficult to obtain a better fit for the period starting at 30 days since it is considerably longer. In this case, a noticeable deviation occurs at the end of the evaluation period.

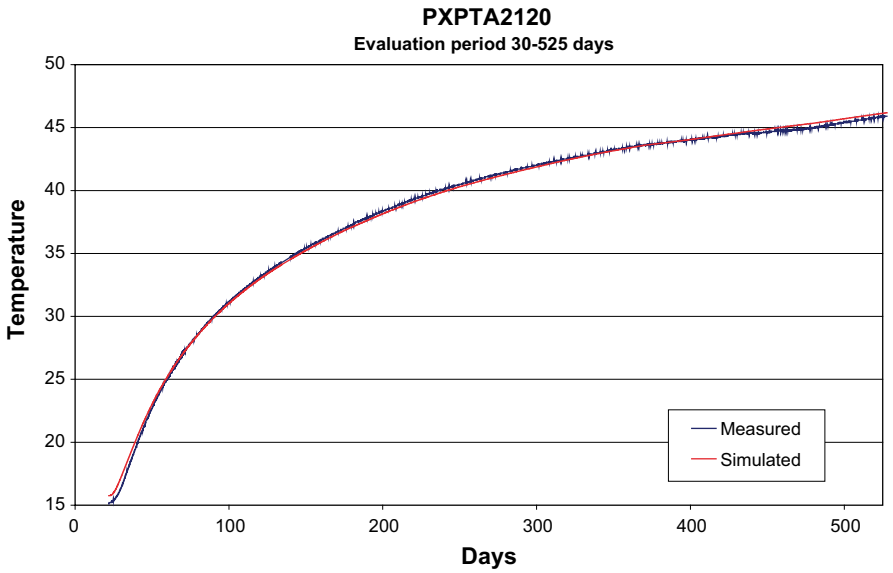

Figure 6-18. *Thermal response of thermal probe PXPTA2120 during 525 days. The period 30–525 days is used for fitting the measured and simulated response.*

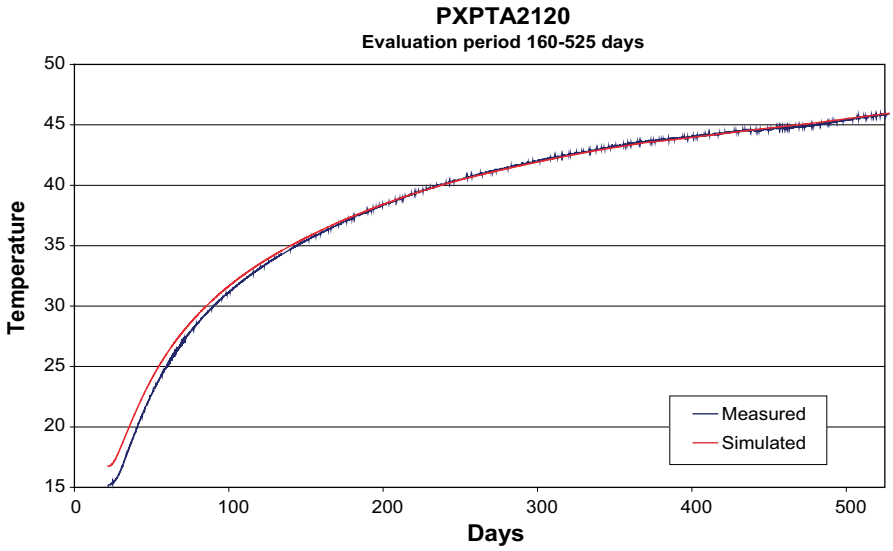

Figure 6-19. *Thermal response of thermal probe PXPTA2120 during 525 days. The period 160–525 days is used for fitting the measured and simulated response.*

Figure 6-20 shows the average measured rock temperature, the average simulated temperature increase and the difference between these values during the evaluation period from 160 to 250 days for all the 37 temperature sensors. The results have been ordered according to magnitude of average simulated temperature increase. This reflects to some degree the temperature sensor's proximity to a canister. The influence of a relative error in the measurements and local deviations in the initial temperatures will be less for such sensors. See Figure 6-22.

The difference between the measured temperature and the simulated temperature increase may be regarded as the "fitted" initial temperature of the simulation. The fitted initial simulation temperature is compared with the measured initial temperature in Figure 6-21.

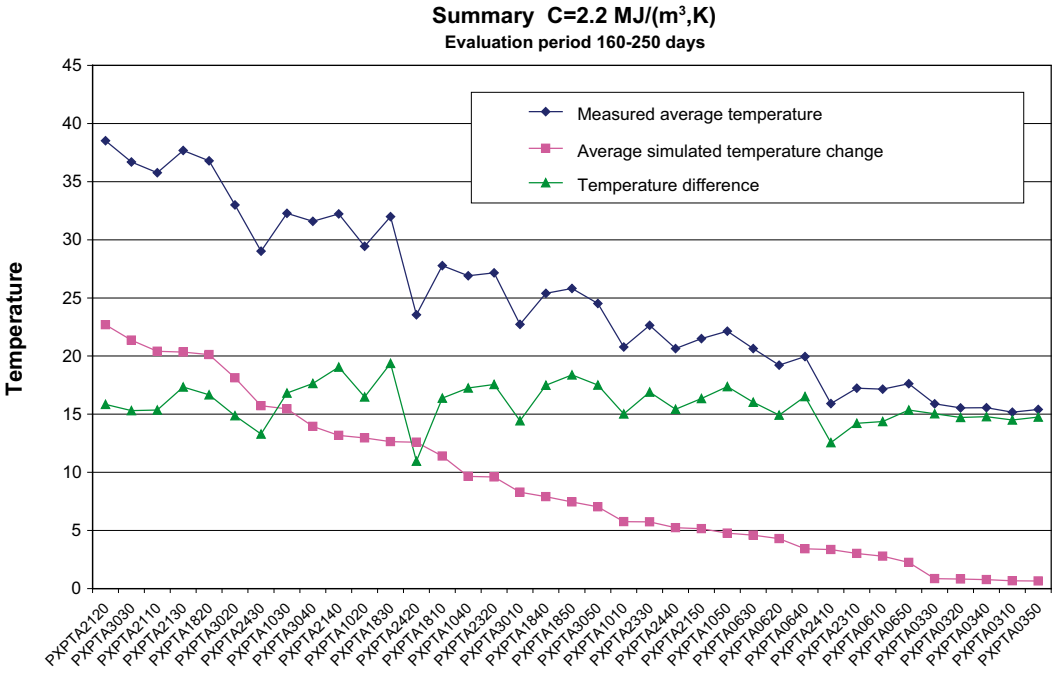

Figure 6-20. *Average measured rock temperature, average simulated temperature increase and difference between these values during the evaluation period 160–250 days for each of the 37 temperature sensors.*

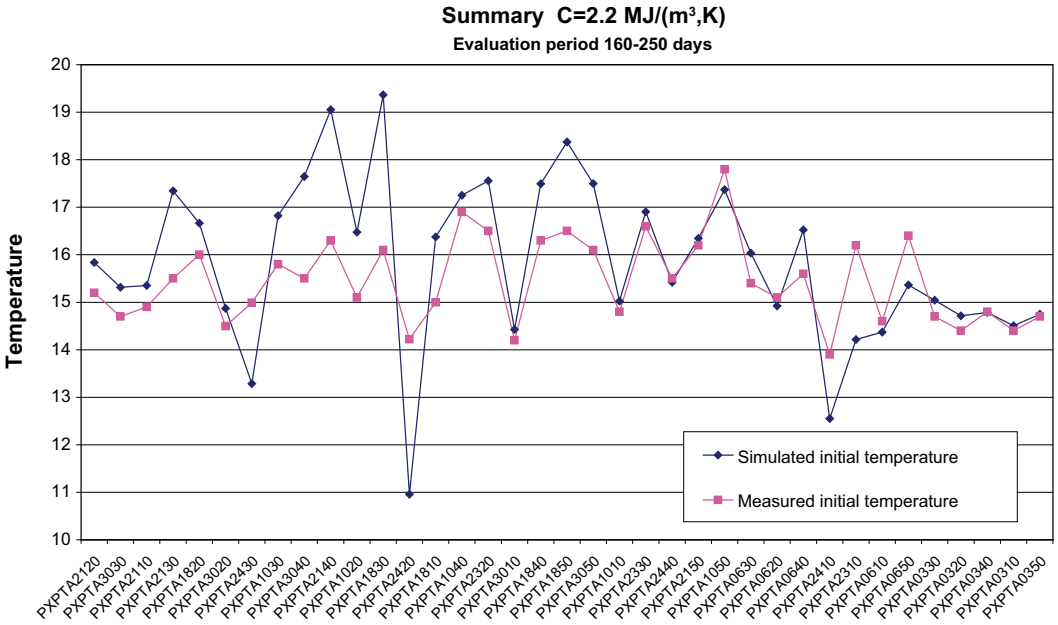

Figure 6-21. *Measured initial temperature and fitted "initial" temperature for each of the 37 temperature sensors. The period 160–250 days is used for fitting the measured and simulated response.*

The measured initial temperatures range between 14°C and 18°C with a tendency to higher values close to the tunnel and the deposition boreholes. The original undisturbed rock temperature is likely to have been much more uniform in the relatively limited region. With a vertical gradient of about 15°C/km, the range of initial temperature at probes would have

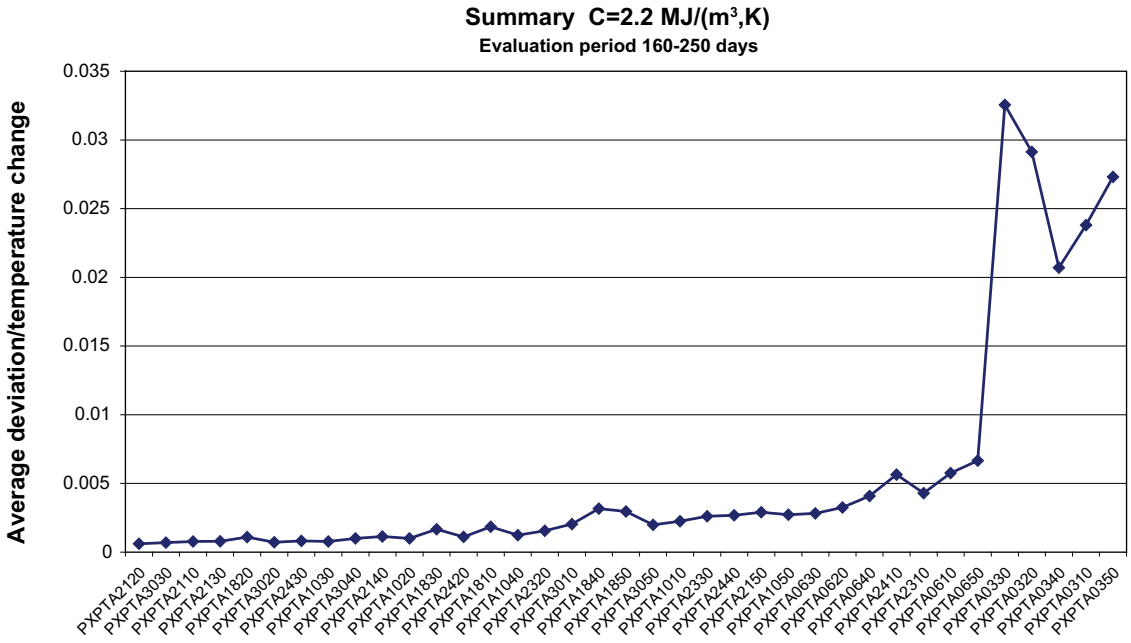

Figure 6-22. *Average deviation between measured and simulated temperatures in relation to simulated temperature increase for each of the 37 temperature sensors. The period 160–250 days is used for fitting the measured and simulated response.*

been within 0.2°C. It is evident from the measurements that there are "residual" temperature disturbances from the local climate in the deposition tunnel. These disturbances, which can be treated as a superimposed thermal process, will decline with time. The examination of the fitting procedure for thermal probe PXPTA2120 (see Figure 6-16 to Figure 6-19) indicates that omitting a longer initial time period from the fitting is likely to result in larger difference between fitted and measured initial temperature. Shifting the evaluation from and early period to a later one tends to give higher fitted thermal conductivities, which may be the result of a general temperature decrease or convective heat transport due to groundwater flow. The largest difference between measured and fitted initial temperatures is found for probes PXPTA2140 and PXPTA1830, which are fairly close on the same vertical level. Also the adjacent probes PXPTA2130 and PXPTA1850 show a large difference.

The corresponding curves for the evaluation periods 160–365 days and 160–525 days are given in Appendix E.

Summary of results for different evaluation periods

The rock thermal conductivity that gives the best fit between measured and simulated temperatures for each of the 37 temperature sensors is presented in Figure 6-23 for the three evaluation periods 160–250 days, 160–365 days, and 160–525 days. The corresponding values for a starting time of 30 days in the evaluation period are shown in Figure 6-24. A definite trend towards higher values of the fitted thermal conductivity can be noted for almost all points when the end time of the evaluation period is extended.

The influence of the start time for the evaluation is compared for a fixed end time of 525 days in Figure 6-25. Changing the start time from 30 to 160 days yields higher values of the fitted thermal conductivities for almost all points.

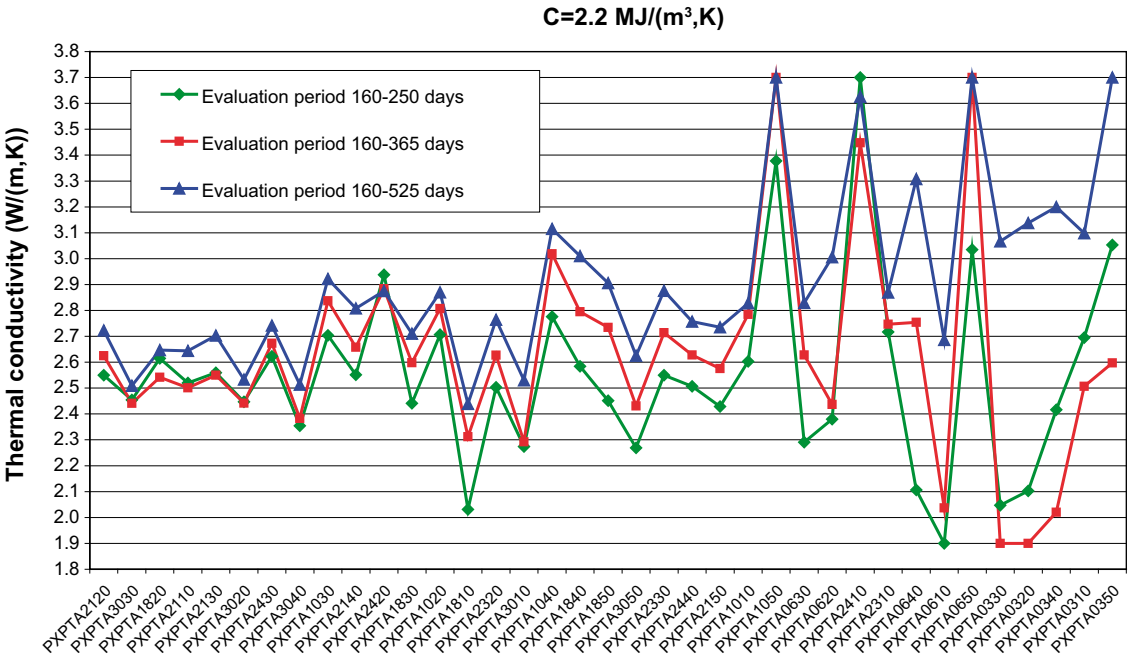

Figure 6-23. *Rock thermal conductivity that gives the best fit between measured and simulated temperatures for each of the 37 temperature sensors. An evaluation period of 160–250 days, 160–365 days, or 160–525 days is used.*

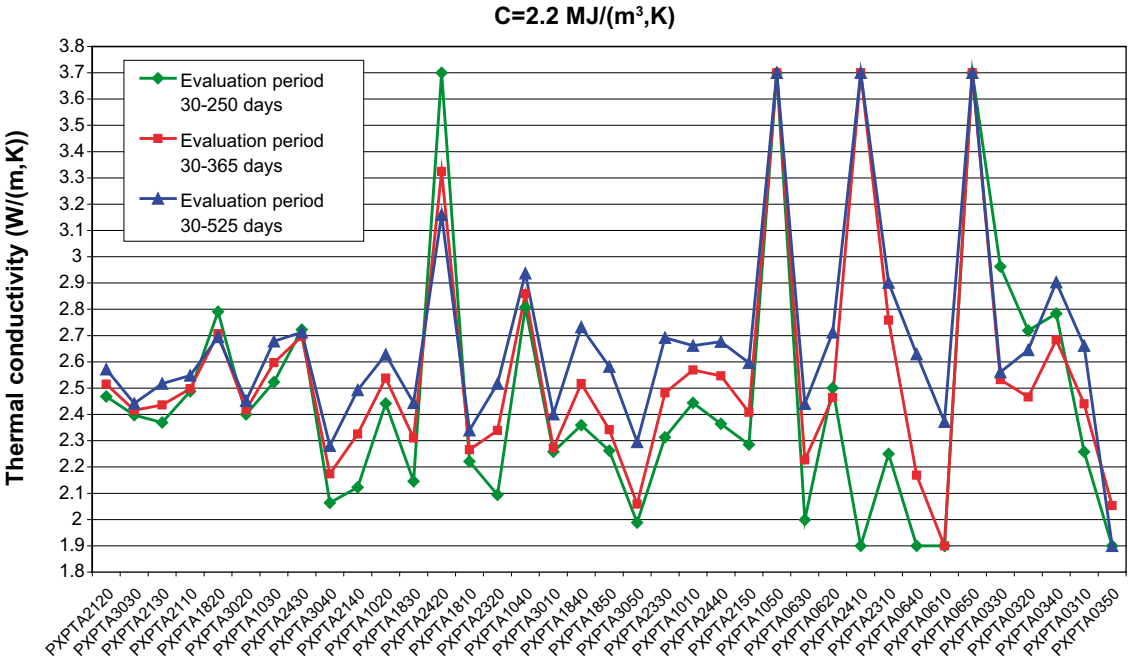

Figure 6-24. *Rock thermal conductivity that gives the best fit between measured and simulated temperatures for each of the 37 temperature sensors. An evaluation period of 30–250 days, 30–365 days, or 30–525 days is used.*

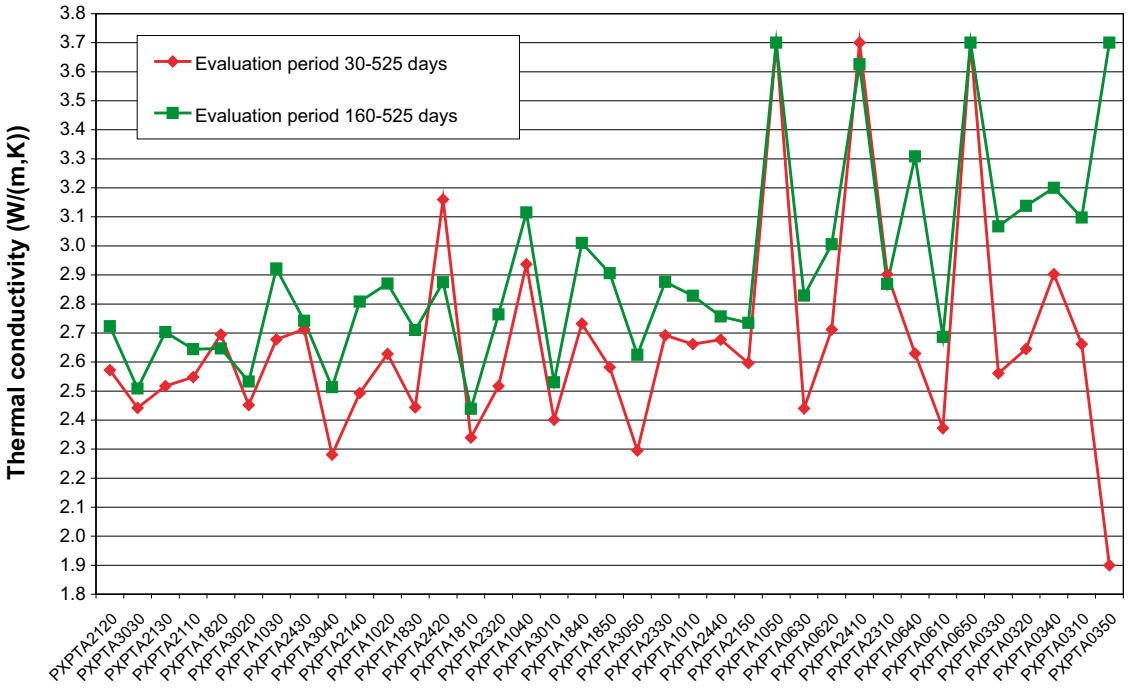

Figure 6-25. *Rock thermal conductivity that gives the best fit between measured and simulated temperatures for each of the 37 temperature sensors. An evaluation period of 30–525 days or 160–525 days is used.*

Influence of volumetric heat capacity

The influence of the volumetric heat capacity of the rock has been assessed by performing a calculation with a 5% higher value than the reference case, see Figure 6-26. The fitted "initial" temperature is given in Figure 6-27. As can be expected, the slope of the response curve is practically determined by the thermal conductivity, whereas the fitted "initial" temperature has to be raised to compensate for the increased capacitive effect of the rock.

Influence of large-scale temperature change

The activities in the tunnels (e.g. ventilation) may disturb the rock temperatures. If the air temperature in the tunnels becomes higher than the initial undisturbed rock temperatures, it will cause a temperature increase in the rock close to the tunnel. The thermally disturbed zone will grow slowly with time until the tunnel is backfilled. It is documented that the air temperature near the prototype repository is changing and has an annual wave form with an amplitude of about 10°C (max/min temp approximately 20/10°C) /Fälth 2005/. The altered geohydrological conditions around the tunnel will also cause groundwater movements and associated convective heat transfer on a large scale.

To check the possible influence of a slow large-scale (global) temperature drift, a general constant temperature change of –0.2°C per year has been superimposed. The simulated temperature increase (slope) will thus become lower for a given thermal conductivity. In order to compensate for this effect, the fitting procedure will find a lower thermal conductivity. See Figure 6-28 and Figure 6-29. The influence is larger for temperature sensors far away from the canisters where the temperature increase is small. Conversely, a constant global temperature increase will require higher thermal conductivities.

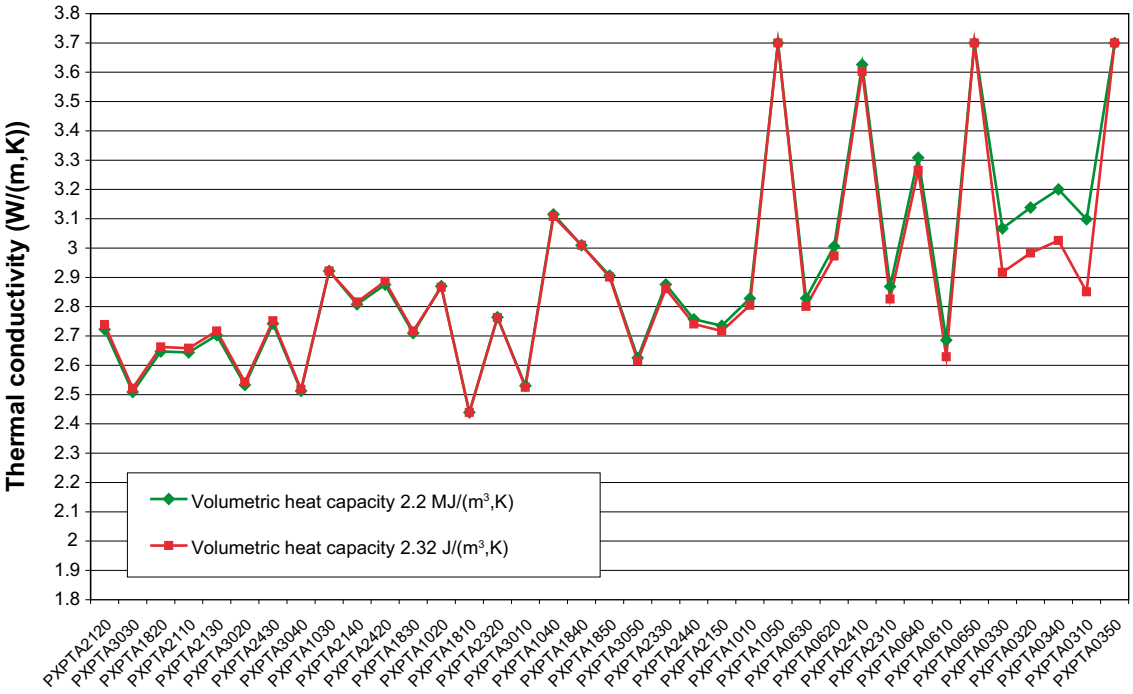

Figure 6-26. *Rock thermal conductivity that gives the best fit between measured and simulated temperatures for each of the 37 temperature sensors for an evaluation period of 160–525 days. The volumetric heat capacity is 2.2 MJ/(m³×K) or 2.32 MJ/(m³×K).*

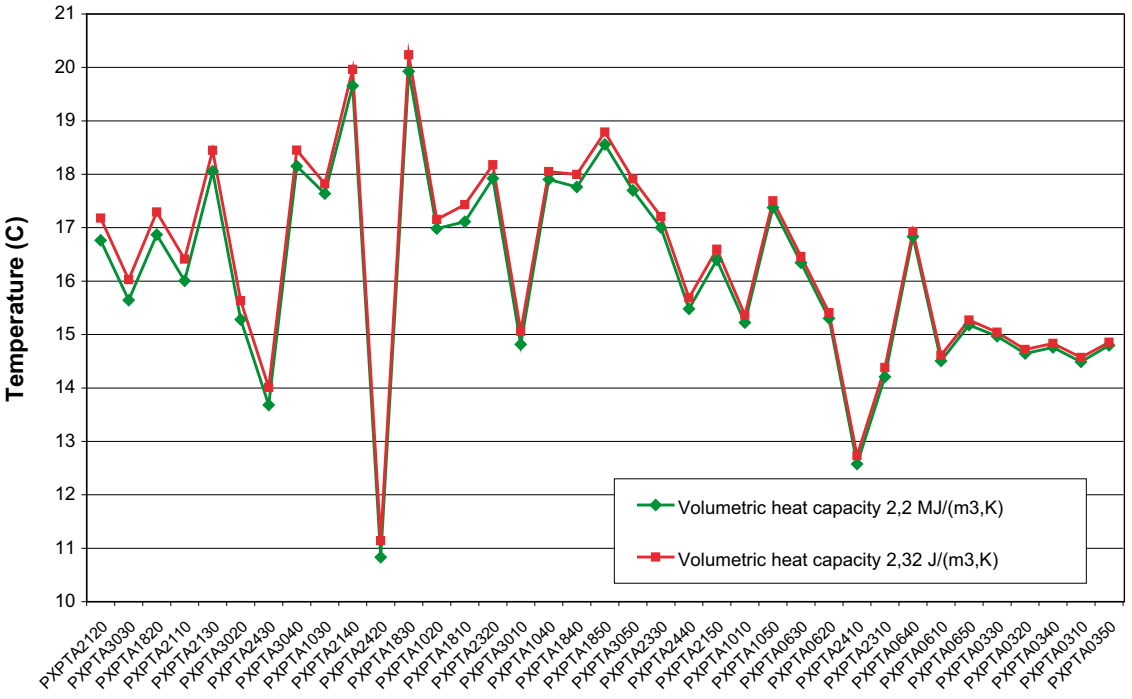

Figure 6-27. *Fitted "initial" temperature for each of the 37 temperature sensors for an evaluation period of 160–525 days. The volumetric heat capacity is 2.2 MJ/(m³×K) or 2.32 MJ/(m³×K).*

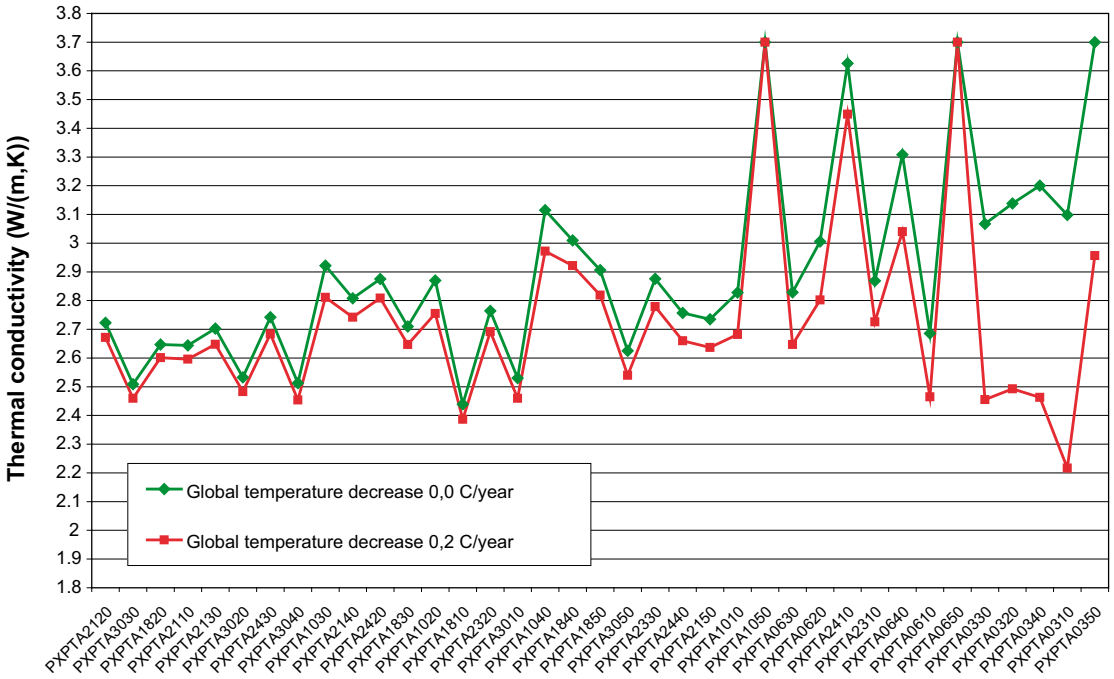

Figure 6-28. *Rock thermal conductivity that gives the best fit between measured and simulated temperatures for each of the 37 temperature sensors for an evaluation period of 160–525 days. The global temperature change is 0°C/year or –0.2°C/year.*

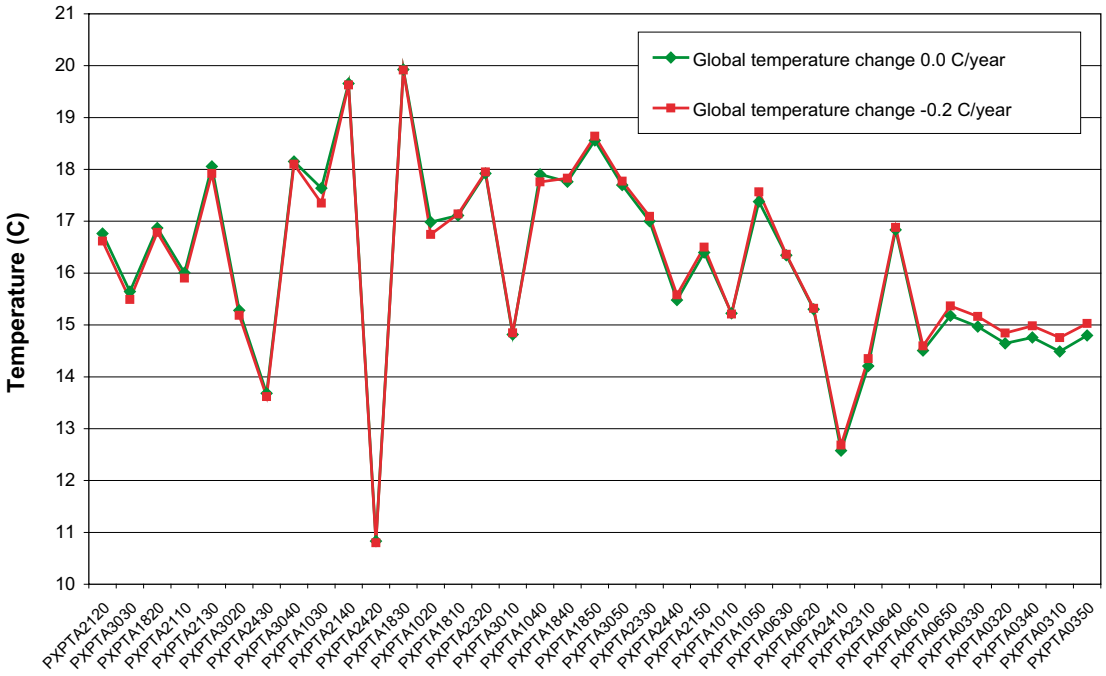

Figure 6-29. *Fitted "initial" temperature for each of the 37 temperature sensors for an evaluation period of 160–525 days. The global temperature change is 0°C/year or –0.2°C/year.*

The rock thermal conductivity that gives the best fit between measured and simulated temperatures for each of the 37 temperature sensors is presented in Figure 6-30 for the three evaluation periods 160–250 days, 160–365 days, and 160–525 days. Compared with the case without global temperature change, there is a trend towards lower values of the fitted thermal conductivity especially for distant sensors with small temperature increase due to canister heating. The relative influence of the global temperature change is larger for these sensors. The fitted thermal conductivity values still become larger with longer duration of the evaluation period.

6.6.4 Results due to location of temperature sensors

Thermal conductivity was assessed through an inverse modelling where measured data was fitted to simulated temperature curves. The simulated curves was for each sensor location calculated for 19 cases assuming a thermal conductivity from 1.9 to 3.7 W/(m×K) with 0.1 increments. During the modelling, a fitting procedure including different time periods of measurements were used. In Figure 6-31 to Figure 6-33, the thermal conductivity achieved from curve fitting using data form different time periods from 160 through 525 days after the initiation of the experiment were used. In Figure 6-14, the identities of individual temperature sensors are shown.

High thermal conductivity values are modelled in the inner parts of the tunnel, especially close to the tunnel surface. These high values may be caused by water movements, which have been reported in the actual parts of the tunnel. Due to the limited period of heating, evaluated thermal conductivity values close to the canister are probably the most reliable.

However, also the simulation of the initial temperatures may be an indication of water movements, see Figure 6-21. The largest difference between measured and fitted initial temperatures is found for probes PXPTA2140 and PXPTA1830, which are fairly close on the same vertical level. Also the adjacent probes PXPTA2130 and PXPTA1850 show a large difference, see Figure 6-34. A convective heat transport is a possible explanation.

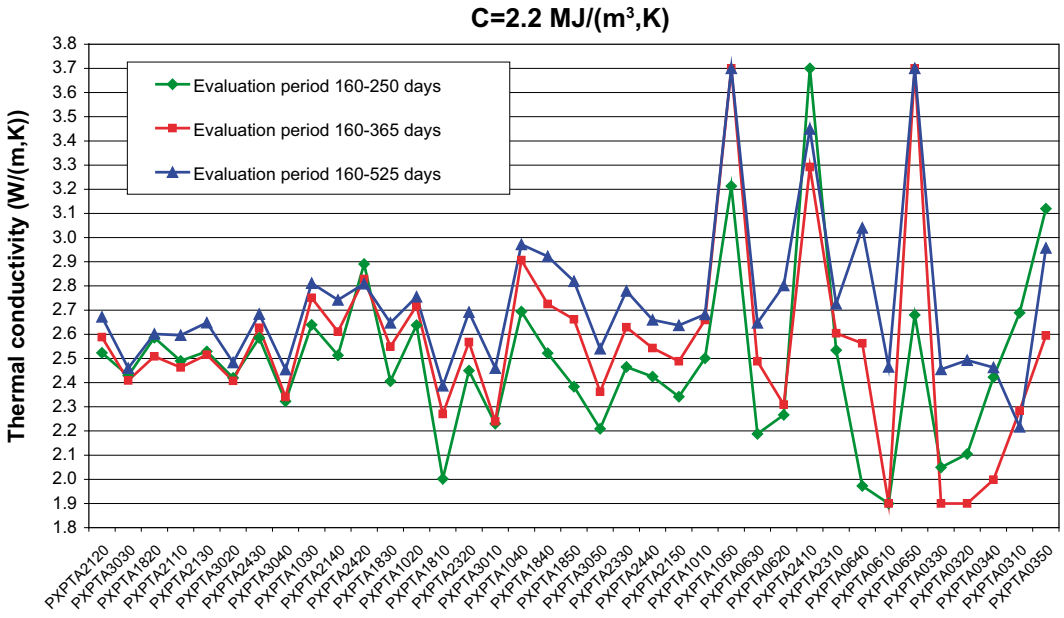

Figure 6-30. *Rock thermal conductivity that gives the best fit between measured and simulated temperatures for each of the 37 temperature sensors. An evaluation period of 160–250 days, 160–365 days, or 160–525 days is used. The global temperature change is –0.2°C/year.*

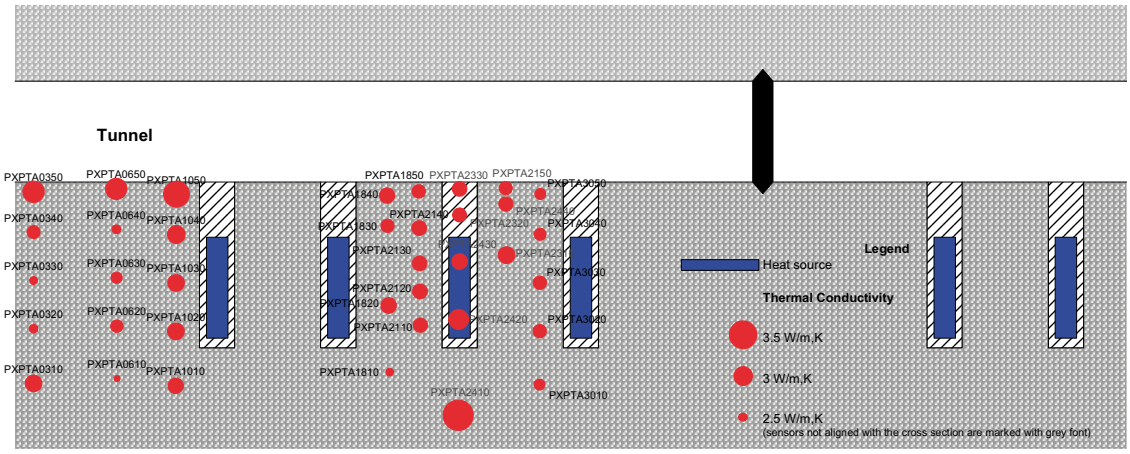

Figure 6-31. *Thermal conductivity from simulation including curve fitting for 160 through 250 days.*

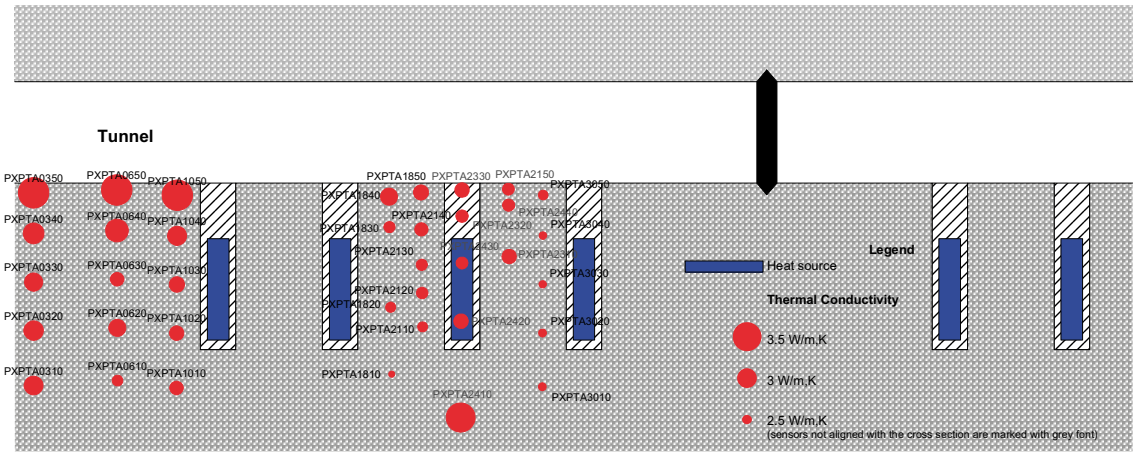

Figure 6-32. *Thermal conductivity from simulation including curve fitting for 160 through 525 days.*

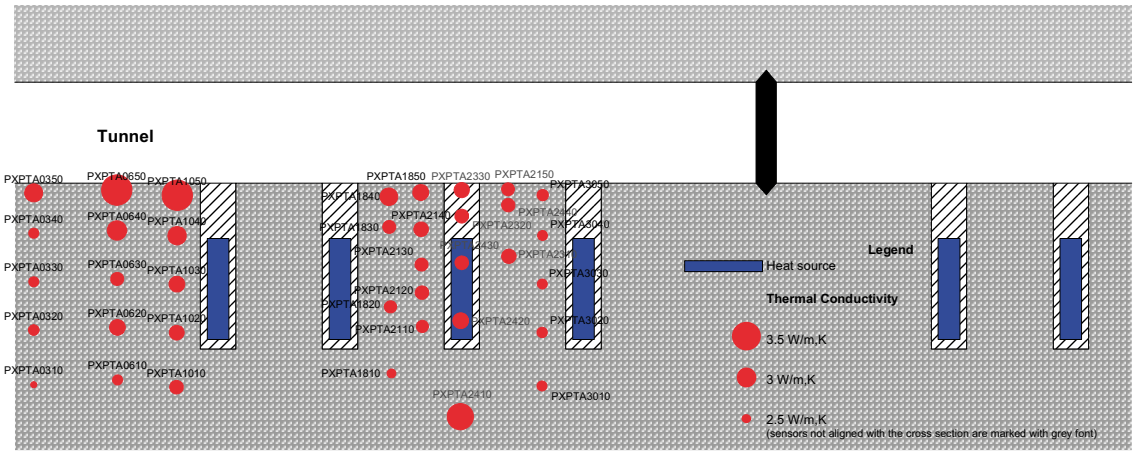

Figure 6-33. *Thermal conductivity from simulation including curve fitting for 160 through 525 days including a correction for thermal drift of 0.2 degrees Celsius annually.*

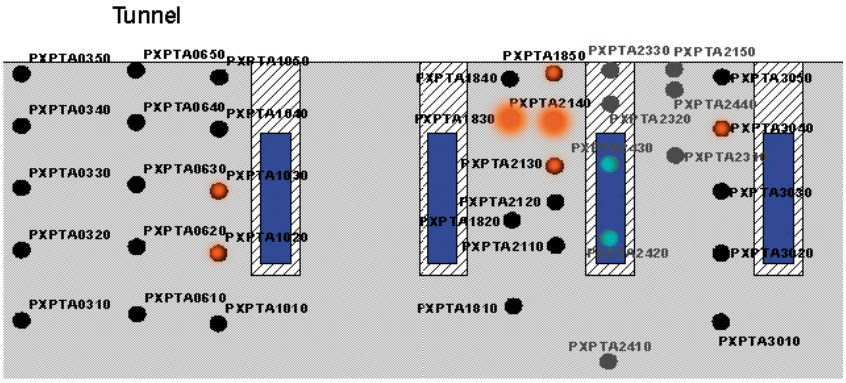

Figure 6-34. *Largest differences between measured and fitted initial temperatures indicated with red (high fitted temperatures) and blue (low fitted temperatures).*

6.7 Verification of prognosis

The measured thermal response has been used to estimate the effective thermal conductivity by finding the best fit with results obtained by a numerical simulation of the thermal process around the repository. A thermal conductivity value is estimated for each of the 37 temperature sensors placed in the surrounding rock by matching the slope of the curve for a given evaluation period. An initial time period was omitted in the fitting procedure to reduce the influence of heat transfer properties and capacitive effects of the deposition holes.

Temperature measurements for 525 days from the start of canister heating were available for the evaluation. The data is evaluated for different time intervals in order to study if the fitted thermal conductivity changes with time.

It is found that the fitted thermal conductivity increases with the duration of the evaluation period. This may be explained by the influence of groundwater flow or a low rate of temperature increase on a large scale. This large-scale increase may be caused by changed thermal conditions due the activities in the tunnels and/or a disturbed geohydrological situation.

Table 6-5 shows the thermal conductivity that gives the best fit considering all temperature sensors. The sensitivity of the fitted thermal conductivity with regards to the volumetric heat capacity is small. The overall influence of a large-scale (global) temperature drift is also fairly small, although it becomes relatively important for temperature sensors with little increase due to canister heating.

Table 6-5. Thermal conductivity that gives the best fit considering all temperature sensors.

Case	Evaluation period (days)	Thermal conductivity (W/(m×K))
Reference	30–250	2.46
Reference	30–365	2.50
Reference	30–525	2.57
Reference	160–250	2.51
Reference	160–365	2.58
Reference	160–525	2.72
Volumetric heat capacity +5%	160–525	2.73
Global temp. change –0.2 C/year	160–250	2.47
Global temp. change –0.2 C/year	160–365	2.53
Global temp. change –0.2 C/year	160–525	2.65

In Table 6-6 comparison are made between best prognosis (2.52 W/(m×K)) and inverse modelling (2.65 W/(m×K)) for all sensors. However, some of the temperature sensors used in the best fit (inverse modelling) is probably influenced by water movements. Therefore it is possible that the best prognosis of the effective thermal conductivity is a combination of laboratory (thermal conductivity) and field measurements (effective thermal conductivity) at the prototype repository.

In Table 6-7 comparison is also made of the prognosis with the best fit of inverse modelling to individual temperature sensors, including standard deviation for both types of distributions. The standard deviation is calculated from the thermal conductivity values based on best fit between measured and simulated temperature for individual temperature sensors. The prognosis no 3 (2.52, std 0.15) are close to the mean of the modelled individual values (2.65, std 0.18). If prognosis no 3 combines with no 4 (field measured values) almost identical results compared to the modelled ones are achieved (2.62 W/(m×K)).

Table 6-6. Modelled thermal conductivity compared with prognosis (mean values). Best fit to all sensors. Most relevant values in bold (judgement). Prognosis numbers refers to Table 6-3.

Case	Modelled thermal conductivity W/(m×K)	Prognosis W/(m×K)	Comment
Inverse modelling (160–525 days)	2.72		
Inverse modelling (160–525 days), including possible global temp change –0.2°C/year	**2.65**		
Laboratory measurements section 1, inner (prognosis 1)		2.44	
Laboratory measurements section 1+2 (prognosis 3)		**2.52**	“Best“ prognosis of thermal conductivity
Field measurements section 1+2, not obvious influenced by water (judgement) (prognosis 4)		2.83	
Laboratory and field measurements, combination of prognosis 3 and 4		**2.62**	“Best“ prognosis of effective thermal conductivity

Table 6-7. Modelled thermal conductivity compared with prognosis (mean values). Best fit to individual sensors. Most relevant values are in bold (judgement). Prognosis numbers refers to Table 6-3. Field measurements disturbed by water movement are only for comparison.

Case	Modelled thermal conductivity W/(m×K)	Std W/(m×K)	Prognosis W/(m×K)	Std W/(m×K)
Inverse modelling (160–525 days)	2.91 (N=37)	0.34		
Inverse modelling (160–525 days), values above 3.4 excluded	2.81 (N=33)	0.22		
Inverse modelling (160–525 days), including possible global temp change –0.2°C/year	2.73 (N=37)	0.32		
Inverse modelling (160–525 days), including possible global temp change –0.2°C/year, values above 3.4 excluded	2.65 (N=34)	0.18		
Laboratory measurements section 1, inner (prognosis1)			2.44	0.08

Case	Modelled thermal conductivity W/(m×K)	Std W/(m×K)	Prognosis W/(m×K)	Std W/(m×K)
Laboratory measurements section 1+2 (prognosis 3)			2.52	0.15
Field measurements section 1+2, not obvious influenced by water (judgement) (prognosis 4)			2.83	0.19
Laboratory and field measurements, combination of prognosis 3 and 4			2.62	
Field measurements, section 1, obvious influenced by water movements, Table 6-2			3.63 (4.22)	

6.8 Discussion

A large scale temperature disturbance is indicated in the modelling. A better and more reliable fit is possible if the first part of the temperature data is excluded or if a constant negative temperature drift is introduced. The temperature appears not to have been stable when the experiment started. This assumption is strengthened by the fact that temperature measurements from 1999 (field measurements of thermal conductivity) indicate a temperature of about 11.5–12.5°C (at 0.6 m below rock surface), which can be compared with a starting temperature of 14–17°C for the experiment, see Figure 6-24. Rather large annual temperature oscillations in the air have also been measured during the last two years near the prototype repository with amplitudes of about 10°C /Fälth 2005/.

The first part of the experiment seems to have larger uncertainties, both due to temperature drift and uncertainties in heating power.

The best prognosis of the thermal conductivity at the prototype repository is judged to be number 3. This prognosis is based on laboratory determinations of thermal conductivity on samples from the prototype repository. The results for the field measurements from the prototype repository (prognosis 4) are a bit higher than the laboratory measurements and are possible influenced by small water movements. However, also some of the results from the temperature measurements at the prototype repository are probably influenced by water movements, especially in the initial stage after installation of the backfill. The combination of these two prognoses (weight mean) may be the best prognosis of the effective thermal conductivity (2.62 W/(m×K)).

The verification of prognosis of thermal conductivity is judged to be good in the perspective best fit of all temperature sensors. However, for some individual sensors there is a large discrepancy between the individual and the overall best fit. The heat transport in the vicinity of these sensors is likely to be influenced by groundwater movements. Evaluated effective thermal conductivities of more than 3.5 are found for sensors near the floor in the inner part of the tunnel. Water bearing fractures are present in this region (Figure 6-4) and local field measurements of thermal conductivity are obviously influenced by water, see Table 6-2 (values) and Figure 6-2 (location).

For some sensors there is a rather bad fit to measured data. The five sensors with the largest square-sum error are situated at the inner end of the tunnel, and are those showing the smallest temperature increase, and are therefore sensitive to disturbances. If the sensors with the largest evaluated conductivity (above 3.4 W/(m×K)) are excluded from the mean, the result is close to the prognosis.

The relatively wide range of measured initial temperature shows that there is a considerable thermal disturbance, which can be explained by the varying air temperature during the construction phase. The accuracy of the evaluation would have been improved if the rock temperature had been allowed to equilibrate after the sealing of the tunnel and verified to be stable before the heating of the canisters began. It may also have made it possible to determine if there was a long-term large-scale drift in temperatures.

The influence that the uncertainty of the initial temperature has on the evaluated effective thermal conductivity can be reduced in the fitting procedure by excluding data from an initial period. Extending the duration of the measurement would allow more initial data to be omitted in order to improve accuracy and would also enhance prediction of groundwater flow effects.

7 Methodology of upscaling in thermal modelling

7.1 Introduction

If the rock is relatively homogeneous, variation in thermal conductivity at a given scale is averaged out at a certain distance (a larger scale). There is a need for upscaling of thermal properties to the scale of interest, in order to decrease the variability due to small scale determinations.

The upscaling process must take into account the spatial variability within a rock type due to mineralogical and chemical changes in the magma. Furthermore, another type of variability is due to the presence of different rock types within a lithological domain. The variability is more pronounced where the difference in thermal conductivity is large between the most common rock types of the domain. A large variability of this type can also be expected in a domain of many different rock types. This type of variability is only reduced significantly when the scale becomes large compared to the spatial occurrence of the rock. This latter type of variability is subsequently referred to as “between rock type”.

7.2 Spatial variability within and between rock types

7.2.1 Types of spatial variability

There are three main causes for the spatial variability of thermal conductivity; (1) small-scale variability between minerals, (2) spatial variability within each rock type, and (3) spatial distribution of different rock types. The first type entails variability in sample data (TPS measurements and modal analysis), where the small-scale variability can be substantial. However, the variability is rapidly reduced when the scale increases. This variability is of limited interest and will not be further discussed.

The second type, spatial variability within a rock type, is a result of the process of rock formation but also of the rock classification system. This variability cannot be reduced but the uncertainty about the variability may be reduced by investigations. This is achieved by analysing large sets of spatial data, so that reliable variograms of thermal conductivity can be created.

The third type of variability, spatial distribution of different rock types, is a result of the rock forming processes and cannot be reduced. It can be analysed deterministically or by indicator variograms.

7.2.2 Spatial variability within rock types

The relationship between density and thermal conductivity offers excellent possibilities to analyse the spatial variability and scale effects in boreholes because more or less continuous sets of density data are available from the boreholes. From these large data sets, stable variograms can be constructed. This can be compared to the uncertain variogram in Figure 4-6 construct by limited amount of TPS data.

Variograms can be used for at least two types of analyses: (1) analysis of the spatial variation of thermal conductivity within a specific rock type, and (2) analysis of the spatial distribution of different rock types.

Examples of variograms of spatial variability within rock type Ävrö granite are presented in Figure 7-1. About 50% of the variance occurs at scales larger than a few meters. However, it is important to realise that the variance in the figure is not only an effect of the spatial variability but also of the random measurement errors resulting from the density logging technique. In reality, a larger part of the total variance may be attributed to large-scale spatial variability.

Several different scales can be identified in Figure 7-1. Rapid changes in correlation occur regularly, almost in a stepwise manner. These changes are believed to result from rapid changes in the composition of the Ävrö granite, i.e. as a result of the rock forming processes. There is a strong correlation up to a few meters and a weaker, large-scale correlation up to about 100 m. This is believed to be general conclusions, but somewhat different results can be expected for other boreholes depending on the composition of Ävrö granite in the specific borehole.

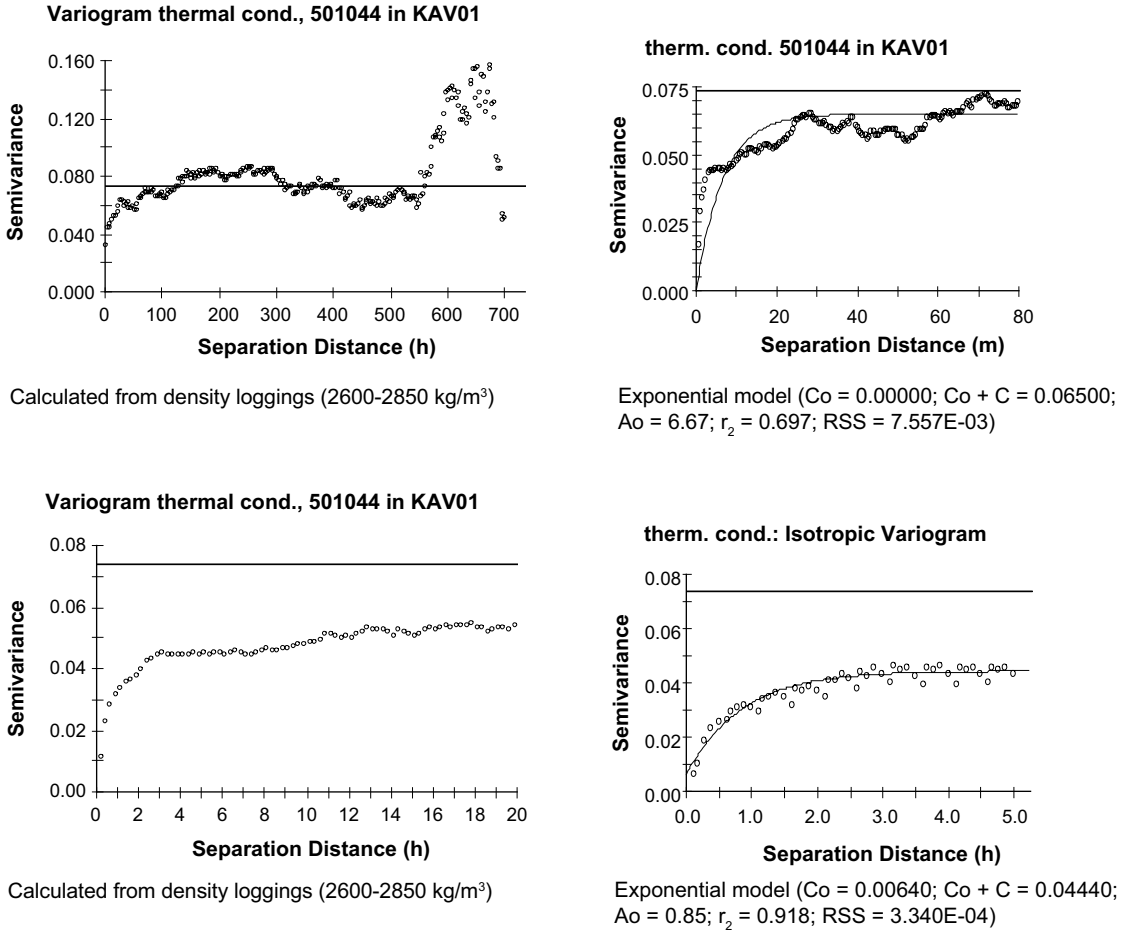

Calculated from density loggings (2600-2850 kg/m^3)

Exponential model (Co = 0.00000; Co + C = 0.06500; Ao = 6.67; r_2 = 0.697; RSS = 7.557E-03)

Calculated from density loggings (2600-2850 kg/m^3)

Exponential model (Co = 0.00640; Co + C = 0.04440; Ao = 0.85; r_2 = 0.918; RSS = 3.340E-04)

Figure 7-1. *Variogram of thermal conductivity for Ävrö granite (501044) in borehole KAV01, estimated from density logging data. The variograms are plotted in four scales: 0–700 m, 0–80 m, 0–20 m, and 0–5 m separation distance. The straight line indicates the total variance in data.*

7.2.3 Spatial variability between different rock types

The spatial distribution of different rock types contributes to the spatial variability of thermal conductivity in the rock mass because different rock types have different thermal properties. In this report, this type of spatial variability of thermal conductivity is referred to as variability between rock types. In this section, the focus is on the spatial distribution of different rock types.

The spatial distribution of different rock types can be described deterministically or visualised and modelled by indicator variograms. Examples of indicator variograms for Ävrö granite is presented for two boreholes in Figure 7-2. The variance in such a variogram is calculated from indicators of "0" and "1", where "0" indicates absence of the rock of interest and "1" indicates presences /Isaacs and Srivastava 1989/. In Figure 7-2, indicator "1" indicates presence of Ävrö granite and "0" symbolises presence of a different rock type, i.e. the rock mass is classified in two categories. The variance on the y-axis is a measure of transition frequency between the two classes /Goovaerts 1999/. In other words, if two locations (A and B) in the borehole are selected, the indicator variance is the probability that either A or B, not both, is located in Ävrö granite. The relatively low probability in Figure 7-2 (~ 0.15) is because Ävrö granite dominates in the two boreholes, and therefore it is much more likely that both A and B are located in Ävrö granite.

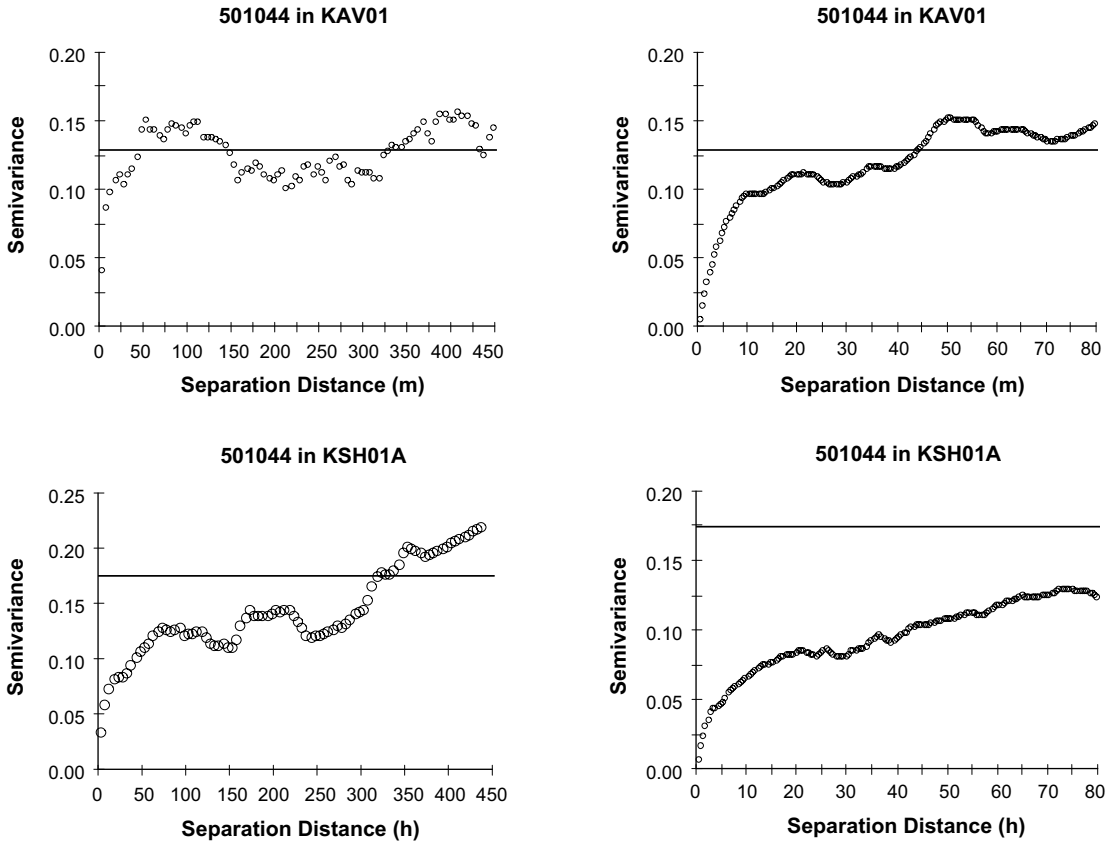

Figure 7-2. *Indicator variogram of the occurrence of Ävrö granite (501044) in borehole KAV01 (upper) and KSH01A (lower) for two different scales: 0–450 m and 0–80 m separation distance. The diagrams are constructed based on lithological classification (boremap).*

The difference between the two boreholes is relatively large, illustrating that this type of variability can be quite different from one borehole to the other. However, some general conclusions can be drawn. There is a strong correlation of the occurrence of Ävrö granite up to about 5–15 m. A less pronounced correlation can be traced up to distances of more than 50 m. At larger distances, there are large differences between the two boreholes. Similar variograms could also be developed to describe the occurrence of other rock types in the boreholes.

Obviously, the spatial distribution of different rock types results in a spatial variability of thermal conductivity if the rock types have different thermal properties. This variability is more pronounced where the difference in thermal conductivity is large between the most dominating rock types. Large variability can also be expected in a rock domain with many different rock types. It is believed that the variability of thermal conductivity between rock types is important for most rock domains. Of special importance is that this variability is only reduced significantly when the scale of thermal conductivity is large compared to the occurrence of rock types.

7.3 Approaches to thermal modelling

A methodology for lithological domain modelling and modelling of scale dependency has been developed. Different approaches are used in the modelling work where all of them use a lithological model of the considered area as a geometrical base. The geological Boremap log of the boreholes, showing the distribution of dominant and subordinate rock types, is used as input jointly with a lithological domain classification of borehole intervals. Two criteria need to be fulfilled for the boreholes to be included in the domain modelling:

- Lithological data with complete rock classification of the borehole (both dominant and subordinate rock types must be available.
- Density logging of good quality must be available.

However, if only rock types without known relationship between density and thermal conductivity occurs in the borehole (see Section 5.1), only the first criteria need to be fulfilled.

Modelling of the mean thermal conductivity of the domain is performed according to the main approach, including both approach A and C in Figure 7-3 (depending on the demand for density loggings to be used). Spatial variability for the domain can be estimated as the sum of variance due to different rock types and the variance due to spatial variability within the dominating rock types:

$$V_{tot} = V_{between\ rock\ type} + V_{within\ rock\ type} \qquad \text{Equation 7-1}$$

The “between rock type” variability is qualitatively different from, and therefore likely to be independent of, the “within rock type” variability. Therefore, the addition of variances is reasonable.

The spatial variability between rock types is handled the same way for all approaches by assigning rock type models (PDF:s) to borehole sections and performing stochastic simulation. In addition to variability between rock types, the spatial variability within rock types needs to be considered. This is performed in one of the following ways, where capital letters refer to Figure 7-3:

A. Spatial variability within rock types is taken into account based on density loggings.

B. Spatial variability within rock types is taken into account based on density loggings, but is adjusted upwards (extrapolated) to account for lack of spatial data for some sections of the boreholes (subordinate rock types etc).

C. Spatial variability within rock types is ignored.

D. Spatial variability within rock types is estimated from stochastic simulation (difference between A and C) and is added to the calculated variance between rock types.

E. Spatial variability within rock types is estimated from TPS data of the dominating rock types and is added to the calculated variance between rock types.

F. Spatial variability within rock types is estimated from variograms of the dominating rock types and is subtracted from the rock type model.

A schematic description of the different thermal conductivity modelling approaches is illustrated in Figure 7-3. The figure also illustrates how the different approaches are related to each other and what kind of result the approaches provide.

Of importance at the domain level is the scale representative for the canister, i.e. the scale at which the thermal conductivity is important for the heat transfer from the canister. At present knowledge, this scale is assumed to be 1–10 m and therefore the approach in the lithological domain modelling is to use different scales to study the scale effect, and to draw conclusions of representative thermal conductivity values from that.

In the following sections, each and one of the different modelling approaches will be described more in detail.

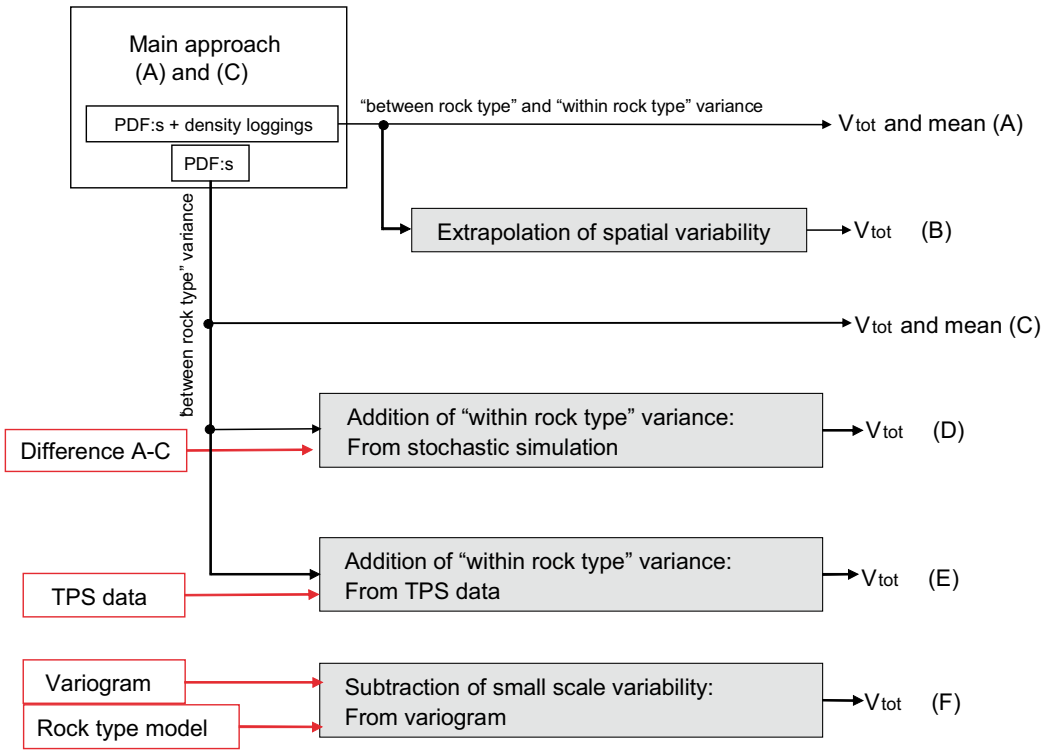

Figure 7-3. *Schematic description of the different thermal conductivity modelling approaches, how they are related to each other and the results they provide. V_{tot} is the total variance for the considered scale.*

7.4 Main approach (A) and (C)

7.4.1 Procedure

The main modelling approach for different lithological domains is illustrated in Figure 7-4 and Figure 7-5.

Figure 7-4 illustrates the main modelling approach in cases where borehole density loggings are possible to use and Figure 7-5 in cases where they are not.

The modelling according to the main approach is performed as follows:

Thermal conductivity values, both measured and calculated from modal analysis, are used to produce PDF:s (Probability Density Functions) for rock types present in the domains. These PDF:s are referred to as rock type models. Density loggings are transformed into thermal conductivity estimates according to the model described in Section 5.1.

The total length of boreholes, or parts of boreholes, belonging to a domain is assumed to be a representative realisation of the domain. Each borehole belonging to a domain is divided into 0.1 m long sections and each section is assigned a thermal conductivity value according to the lithological classification of that section. Both dominating and subordinate rock types are considered in this context. The principle for assignment of thermal properties is

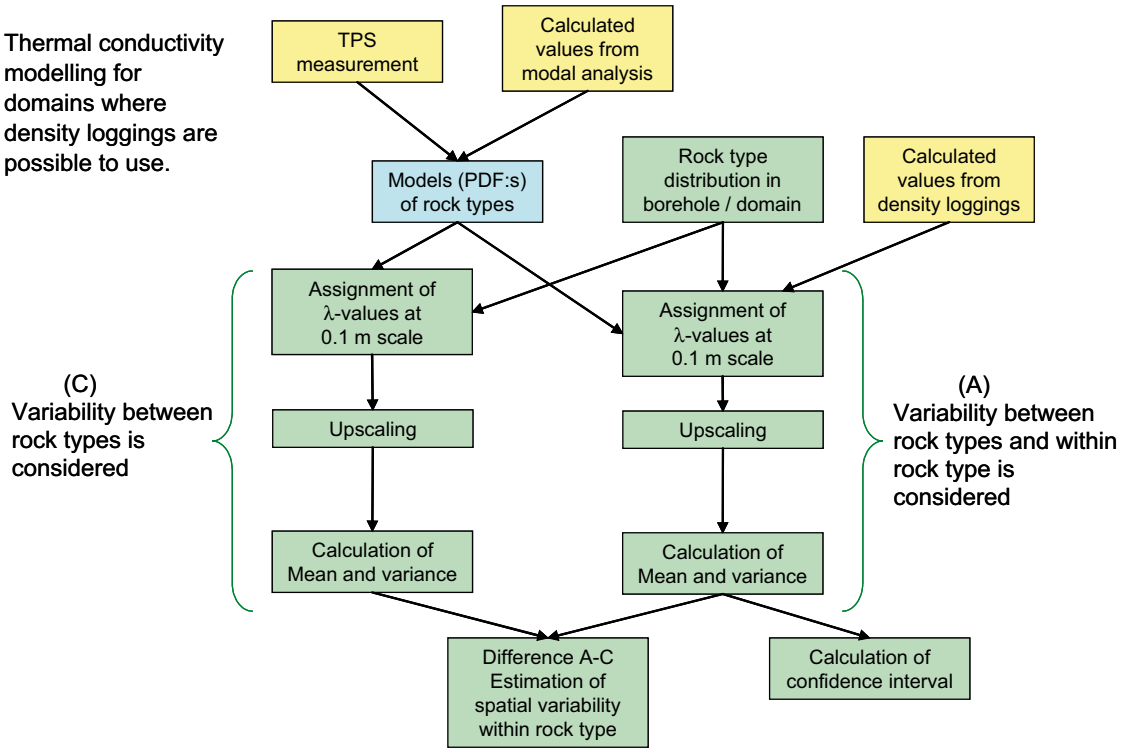

Figure 7-4. *Main approach (A) and (C) for modelling of thermal conductivity for domains where density loggings are applicable. The purpose of approach C is to estimate the spatial variability within rock types. This variability is required in approach D. Yellow colour indicates the data level, blue the rock type level, and green the domain level.*

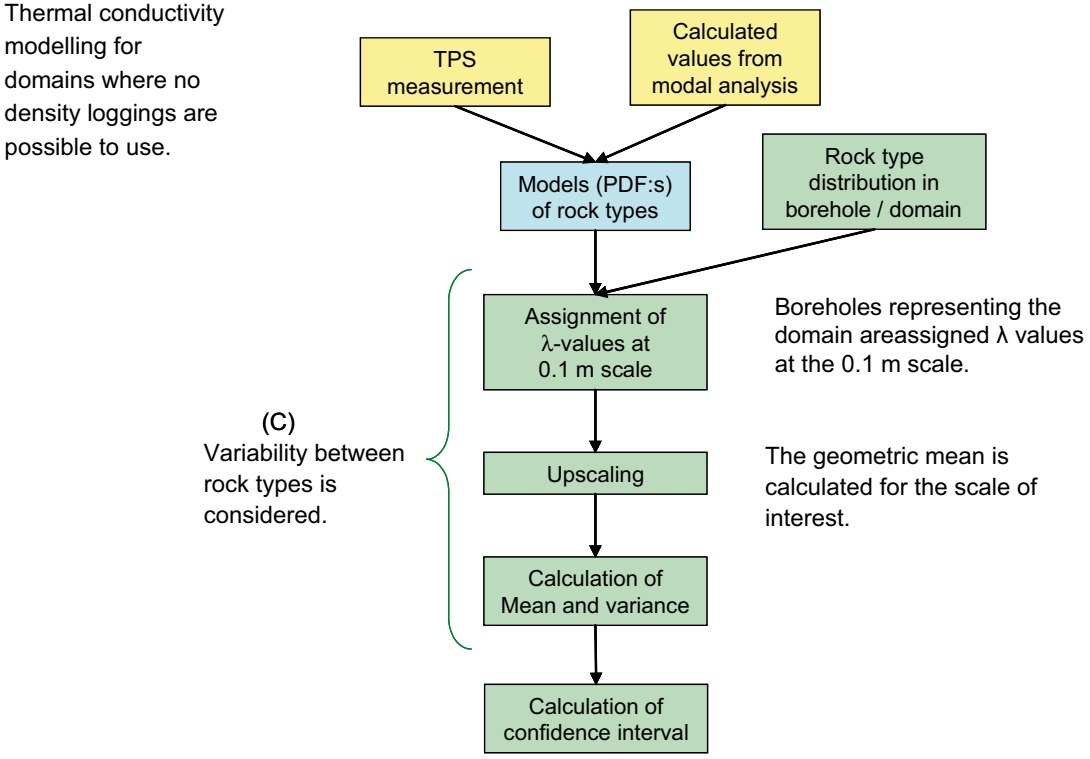

Figure 7-5. *Main approach (C) for modelling of thermal conductivity for domains where no density loggings are applicable. Yellow colour indicates the data level, blue the rock type level, and green the domain level.*

illustrated in Figure 7-6. For rock types where a relationship between density and thermal conductivity has been found the principles are:

- Primarily, the thermal conductivity values calculated from density loggings are used. This implies that spatial variability within the rock type is considered.
- If the density value is outside the valid density range, as stipulated by the relationship between density and thermal conductivity, a value of the thermal conductivity is randomly selected from the rock type model (PDF).

Other dominating and subordinate rock types are assigned thermal properties according to:

- A value of thermal conductivity is randomly selected according to the rock type model (PDF). This implies that only the spatial variability between rock types is considered.
- For rock types where no rock type model is available (due to lack of data), no value is assigned to that 0.1 m section (section is ignored in the calculations). For rock types with a low degree of occurrence in the domain, the influence on the result will be insignificant.

The next step is the upscaling from the 0.1 m scale to an appropriate scale. The upscaling is performed on a range of scales, from 0.1 m up to approximately 60 m. The upscaling is performed in the following way, illustrated both in Figure 7-6 and Figure 7-7:

1. The boreholes representing the domain are divided into a number of sections with a length according to the desired scale.
2. Thermal conductivity is calculated for each section as the geometric mean of the values at the 0.1 m scale. This gives the effective thermal conductivity at the desired scale, see Section 7.4.2.

3. The mean and the variance of all sections at the desired scale are calculated. For each scale, the calculations are repeated n times with different assignment of thermal conductivity values at the 0.1 m scale (stochastic simulation). This produces representative values of the mean and the standard deviation for the desired scale. The required number of calculations (n) depends on the length of the boreholes, the desired scale, the percentage of density data used, and the required precision of the result. For applications in Simpevarp, 10 realisations were sufficient in the Monte Carlo simulation /Sundberg et al. 2005/.
4. The calculations are repeated for the next scale.

In Figure 7-6, 25 sections are indicated, each with a length of 0.1 m. For the scale 0.5 m, the thermal conductivity $\lambda_{0.5-1}$ is estimated as the geometric mean of five 0.1 m sections, $\lambda_{0.5-2}$ as the geometric mean for the next five 0.1 m sections, and so on. The mean and variance is then easily computed for the 0.5 m scale. This sequence is repeated for the other scales of interest. The effect of upscaling is illustrated in Figure 7-7.

Confidence intervals can be derived directly from the result of the stochastic simulation. No assumption of the type of statistical distribution of the thermal conductivity values is required in this approach. It must be stressed that these confidence intervals mainly includes uncertainty due to natural variability in the rock mass. Uncertainties resulting from lack of knowledge of the true variability and representativeness etc are not included explicitly in the domain modelling. An approach for including lack-of-knowledge uncertainty is presented in Chapter 9.

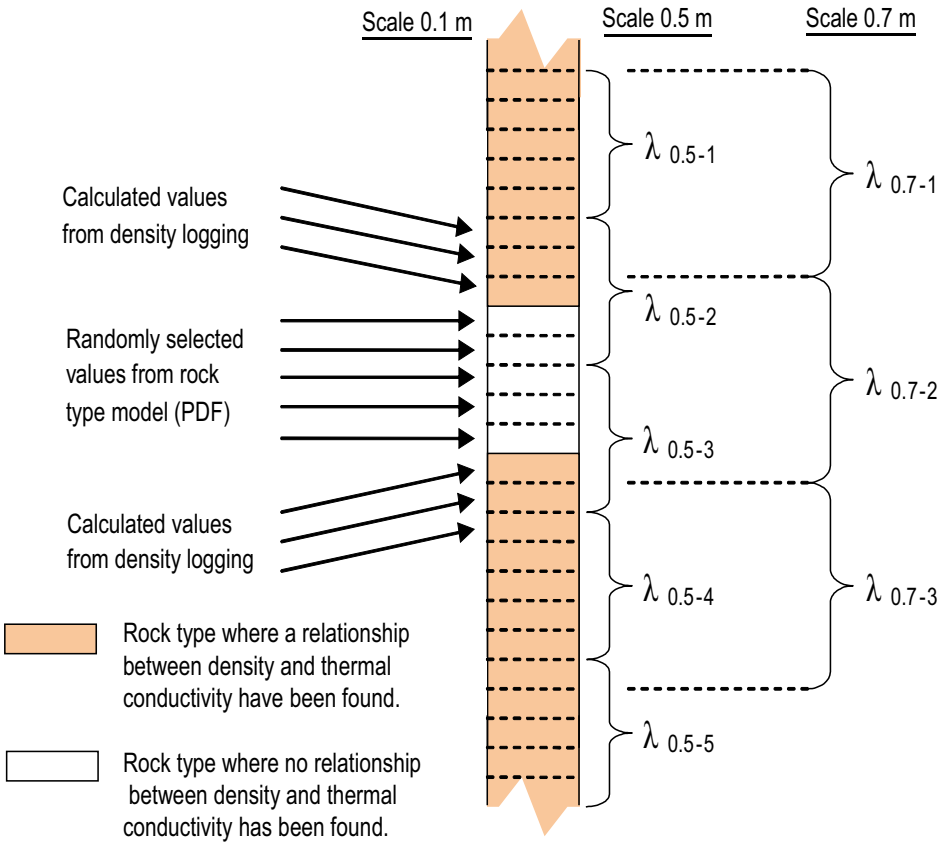

Figure 7-6. *Thermal conductivity is assigned to 0.1 m sections by calculation from density loggings or randomly selected from the rock type models. Upscaling is performed by calculating geometric means for different scales, for example 0.5 and 0.7 m.*

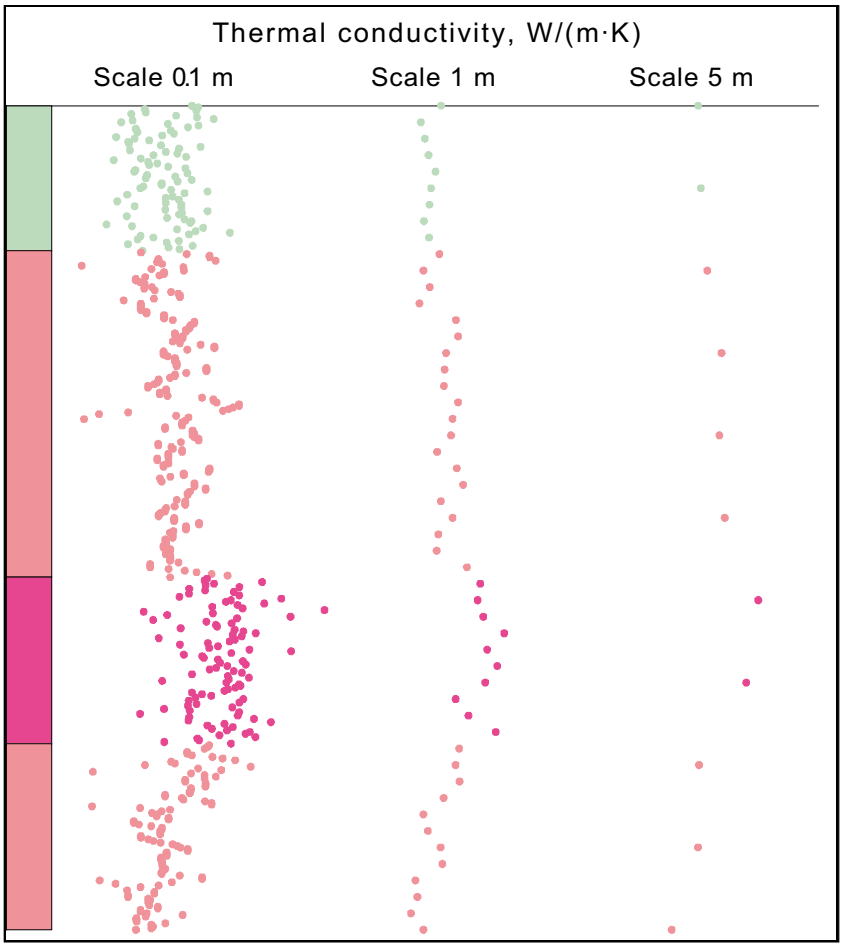

Figure 7-7. *Effects of applying the principle for upscaling of thermal conductivity, as given in Figure 7-6. As can be seen, the spatial variability within the rock types is levelled out due to the modelling concept.*

As illustrated in Figure 7-4 and Figure 7-5, the main approach (A) and (C) is slightly different between domains where density loggings can or cannot be used. Domains where density loggings can be used also take into account the spatial correlation within the dominating rock type. This is not possible for domains where no reliable relationship between density and thermal conductivity is presently available. Therefore, the variance for the latter domains is grossly underestimated. This is the main disadvantage of this modelling approach.

7.4.2 Theory of upscaling

Above, the geometrical mean equation is used to produce an effective thermal conductivity in an appropriate scale from small scale determinations. The geometric mean equation is simple to use and is often applied for estimation of effective transport properties /Dagan 1979, Sundberg 1988/. However, the effective transport properties are influenced by the variance, which is not considered when the geometric mean is calculated. According to /Gutjahr et al. 1978/ and /Dagan 1979/, the effective hydraulic conductivity is slightly different due to the dimensionality of the problem. /Dagan 1979/ derived the following general solution to the effective mean hydraulic conductivity (transformed to thermal conductivity):

$$\lambda_e = -(m-1) \times \lambda_x + \left(\int f(\lambda)\, d\lambda / (m-1) \times \lambda_x + \lambda\right)^{-1} \qquad \text{Equation 7-2}$$

Where m is the dimensionality of the problem and f(λ) the frequency function. If λ_x is substituted with λ_{max} and λ_{min}, the result is Hashin's and Shtrikman's well known upper and lower bounds for an isotropic material /Hashin and Shtrikman 1962/. If λ_x is substituted with λ_e, the self consistent approximation (SCA) is obtained as follows:

$$\lambda_e = 1/m \times (\int f(\lambda)\, d\lambda / (m-1) \times \lambda_e + \lambda)^{-1} \qquad \text{Equation 7-3}$$

For a lognormal distribution, the effective conductivity according to Equation 7-3 for two dimensions (m=2) coincides with the geometric mean. For tree dimensions (m=3) the effective conductivity is slightly higher. Equation 7-3 is used to calculate the thermal conductivity from the mineral distribution of rocks /Sundberg 1988/.

If the standard deviation (σ) of the $\log_{10}$ (λ) is small, the effective thermal conductivity can be approximated as follows for a lognormal conductivity distribution:

$$2D: \lambda_e = \lambda_G \qquad \text{Equation 7-4}$$

$$3D: \lambda_e = \lambda_G [1 + \sigma^2/6] \qquad \text{Equation 7-5}$$

where λ_G is the geometric mean thermal conductivity. However, in this thermal application the variance is low and therefore the geometric mean is a sufficient approximation, see example Table 7-1.

Table 7-1. Comparison between geometric mean and SCA (3D) for samples from KA2599G01.

Sample	Secup-seclow m	Therm. cond. (W/(m×K))	Therm. cond. (W/(m×K)), values above 3.5 excluded
KA2599G01	5.90–5.94	2.49	2.49
KA2599G01	14.63–14.67	2.34	2.34
KA2599G01	25.32–25.36	2.47	2.47
KA2599G01	44.28–44.32	2.99	2.99
KA2599G01	50.10–50.14	3.58	–
KA2599G01	61.89–61.93	3.68	–
KA2599G01	70.60–70.64	2.84	2.84
KA2599G01	85.10–85.50	2.69	2.69
KA2599G01	101.85–101.89	3.11	3.11
KA2599G01	120.05–120.09	3.22	3.22
KA2599G01	126.35–126.39	3.55	–
Geometric mean		**2.96**	**2.75**
Std		0.475	0.323
N		11	8
SCA		**2.97**	**2.76**

7.5 Extrapolation of spatial variability (B)

When modelling a domain according to the main approach the spatial variability "within rock types" may not be fully considered. The reason is that density loggings cannot be used for all rock types. In addition, some density logging data may be outside the range of validity of the relationship. These sections get randomly assigned thermal conductivity values from the rock type models, resulting in that the variability "within rock types" will not be fully considered. In this approach, an attempt is made to correct for this.

It is assumed that all rock types have the same spatial variability. By replacing thermal conductivity values estimated from density logging with random PDF values it is possible to study the effect of ignoring the spatial variability "within rock type" for some parts of the borehole. By removing more and more values calculated from density loggings, and replacing them with random values from PDF:s, it is possible to construct a graph of how the variance is affected, see Figure 7-7. Extrapolation of the variance or standard deviation (for the selected scale) as a function of the percentage of spatial data used in the modelling of the domain can then be performed.

It is reasonable to assume that the total variance estimated with this approach deviates from the true variance. The reason is that the spatial variation of other rock types than Ävrö granite probably is different, which is not considered in the correction. In most cases, an overestimation of the variance can be expected because the heterogeneity of Ävrö granite is expected to be larger than for other rock types.

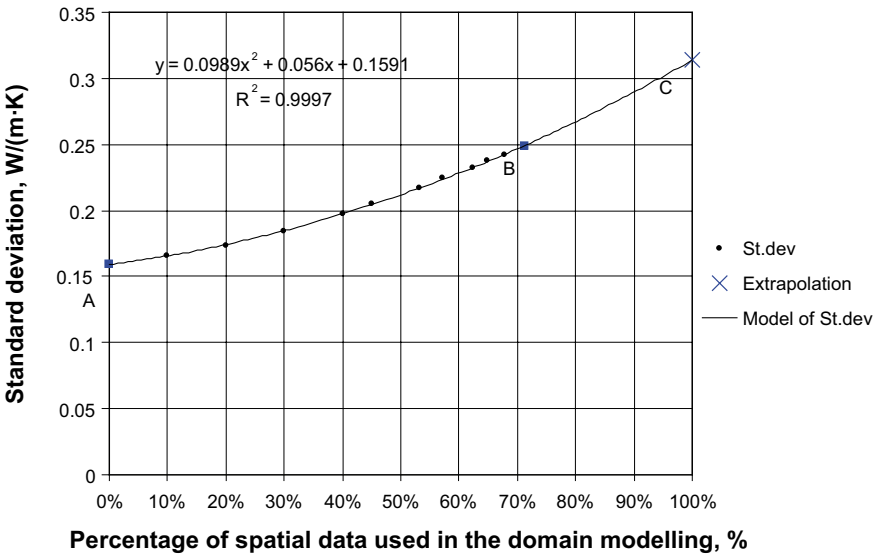

Figure 7-8. *Example of extrapolation of standard deviation for thermal conductivity at scale 0.8 m for domain RSMA01 in Simpevarp. At point A, all data are randomly assigned without consideration of spatial variability within the Ävrö granite. Point B corresponds to 71.3% of the values estimated from density loggings. Point C is extrapolated and corresponds to 100% spatial data, assuming the same spatial variability as in Ävrö granite for the remaining 28.7% of data.*

7.6 Addition of ”within rock type” variance: From stochastic simulation (D)

One possible way of adding the spatial variability within rock types is the following:

1. For domains where the thermal conductivity of one or several rock types can be calculated from density loggings, both simulation (A) and (C) is performed, according to Figure 7-4. For simulation (A), the thermal conductivities are calculated both from PDF models and density loggings resulting in both “between rock type” and “within rock type” variability. For simulation (C), all thermal conductivity values are randomly selected from the rock type PDF models and no data from density loggings are used, resulting in only “between rock type” variability. The variance contributed by spatial correlation within rock types is assumed to be the difference between simulation (A) and (C), see Figure 7-4.
2. For domains where the thermal conductivity of the rock types cannot be calculated from density loggings only simulation (C) is performed. It is then assumed that the variance caused by spatial variability within the rock types is identical to that of the domains where both simulation (A) and (C) can be performed. The total variability is estimated by addition of the two types of variances.

The addition of variances is assumed valid, according to Equation 7-1 (see text in Section 7.3). According to this approach the total variance at domain level may be over- or underestimated depending on the relation of the properties for the different rock types.

7.7 Addition of “within rock type” variance: From TPS data (E)

In this approach, the spatial variability within the dominating rock type is estimated based on TPS measurements. Analysis of TPS data can provide a rough estimation of the spatial variability within the rock type. TPS measurements are classified in spatial groups depending on their location and the geometric mean is calculated for each group. This gives a set of data in the desired scale (based on the spatial groups). The variance for this data set is a rough estimate of the variance for the desired scale. This procedure can be repeated for different scales and the resulting variances can be plotted against the scale in a graph (see example in Figure 7-9. The variance for the desired scale can be estimated from the graph and this “within rock type” variance is then added to the “between rock type” variance calculated in the main approach (C).

For domains with several dominating rock types the concluding “within rock type” variance is estimated slightly differently. In such cases, the variance is estimated as a weighted sum of the spatial variances for the dominating rock types, where the weighting factors are the fractions of each rock type in the domain. Although this approach only provides a rough estimate of the total variability it encompasses all the major types of variability within the domain.

It is not easy to assess whether this approach under- or overestimates the total variance for the domain. There are several factors that may influence this, such as the spatial variability in subordinate rock types compared to dominating rock types. Still, it is believed that this approach gives a quite reasonable estimate of the variability compared to the other approaches but a prerequisite is that a sufficient number of TPS measurements are available.

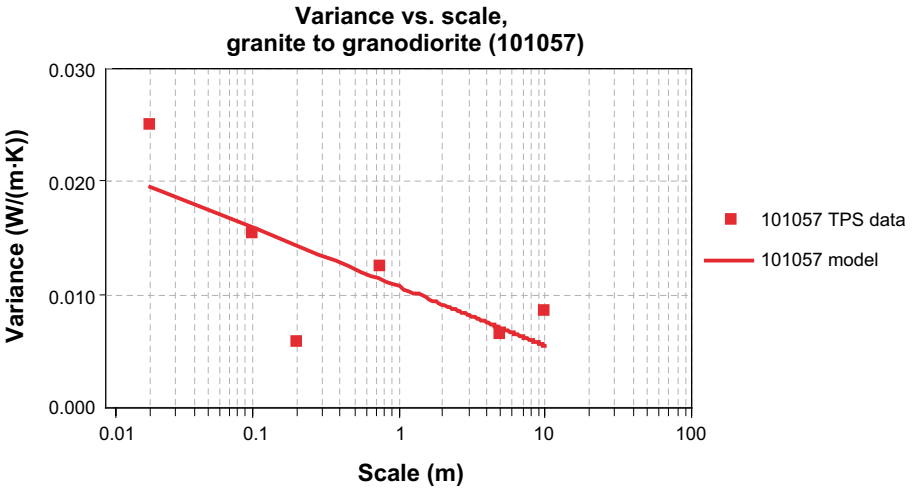

Figure 7-9. *Example of a graph of the "within rock type" variance estimated from TPS data.*

7.8 Subtraction of small scale variability: From variogram (F)

In this approach, variograms for the dominating rock type of the domain is used to estimate the small scale variance that is rapidly reduced when the scale increases. The variograms are based on data from boreholes representing the domain. The data may be both TPS data (see Figure 4-6) and calculated thermal conductivity values from density loggings (see Section 5.1).

The small-scale variability for the scale of interest is determined from the variogram for the dominating rock type. It is subtracted from the total variability of the same rock type (variance of the rock type model, PDF). This residual variability is assumed to be the variance after upscaling to the desired scale. The basis for the approach is that variability in scales smaller than the desired is evened out.

Variograms of different boreholes within the same domain may indicate that there is a difference between the boreholes regarding spatial correlation. This can be a problem when only a few boreholes are available. It emphasises the question of representativeness of the boreholes for the domain modelling.

There is reason to believe that this approach underestimates the variance because only the dominating rock type is considered and the others are ignored, i.e. the "between rock type" variance is not considered. This is a major disadvantage of the approach if the domain is heterogeneous.

7.9 Evaluation

The main approach (A) for upscaling results in a data set of thermal conductivity values at the desired scale. This data set can be visualised by statistical plots and any statistical parameter of the domain can be estimated; the mean, standard deviation, percentiles etc. However, for domains not composed of Ävrö granite no such reliable data set can be produced. The reason is that there are not enough measurements available for reliable modelling of spatial variability within other rock types than Ävrö granite. Therefore, indirect

techniques have been used to estimate statistical parameters of such domain. These statistical parameters do not describe the domain satisfactory because the statistical distribution of data at the desired scale is not known. This may result in non-reliable estimates of the low tail of thermal conductivity values, which is problematic for the design of the repository.

The discussion above indicates that the approach needs to be developed to take spatial variability in all dominating rock types into account, so that data sets can be produced for any desired scale and for all relevant domains. This requires stochastic modelling in 3D. For modelling of spatial variability, variograms can be used, see examples in Section 7.2. Reliable variograms require that enough data are available for the rock types.

8 Uncertainty in thermal data

8.1 Uncertainty model

All thermal data are associated with some uncertainty. Uncertainty occurs at three different levels: (1) data level, (2) rock type level, and (3) domain level. Uncertainty at the data level includes uncertainties about the true value of a sample or measurement. At the rock type level, uncertainties in the rock type models are addressed. Uncertainty at domain level refers to thermal conductivity at canister scale for the domain of interest.

Qualitative estimates of the various types of uncertainties are given in Table 8-1, Table 8-2, and Table 8-3 for the three different levels. Of major interest is the total uncertainty at the canister scale at domain level, because this affects the design of the repository. This is discussed in the next section.

Table 8-1. Uncertainty in thermal conductivity data at data level. Each uncertainty consists of a random and a systematic part. Subjective qualitative estimates are given in three classes; small, medium, and large uncertainty.

Uncertainty in:	Random uncertainty (expected random variation)	Systematic uncertainty (expected bias)
TPS data		
Measurement technique	Small	Small
Measurement scale vs sample	Medium	Small
SCA data		
Determination volume fraction of minerals	Small	Medium
Alteration of minerals	Medium	Large
Thermal conductivity of minerals	–	Medium
Method of calculation	Small	Small
Modal analysis scale vs sample	Large	Small
Density logging data		
Measurement technique	Medium	Medium
Filtering and recalibration	Small	Small
Measurement scale	Small	Small
Statistical relationship between thermal conductivity and density, including scale representativeness, laboratory density measurements, rock type classification, natural variability, and selection of regression model.	Medium	Medium
All data		
Database errors (Sicada. Remaining after quality control)	Small	Small

Table 8-2. Uncertainty in thermal conductivity data at rock type level. Each uncertainty consists of a random and a systematic part. Subjective qualitative estimates are given in three classes; small, medium, and large uncertainty.

Uncertainty in:	Random uncertainty (expected random variation)	Systematic uncertainty (expected bias)
All thermal data		
Boremap logging and classification of rock samples	Small	Small – medium
Temperature and pressure effects	Small	Small
Representativeness of data	–	Large
Method of correction, SCA data	–	Medium
Spatial variability within rock type	Natural (large)	–
Statistical model, PDF (assumptions)	Small	Small

Table 8-3. Uncertainty in thermal conductivity data at domain level. Each uncertainty consists of a random and a systematic part. Subjective qualitative estimates are given in three classes; small, medium, and large uncertainty.

Uncertainty in:	Random uncertainty (expected random variation)	Systematic uncertainty (expected bias)
Canister scale		
Geological model (boremap logging, rock type occurrence, extension of domains)	Large	–
Deformation zones, fractures etc.	Medium	Medium
Water flow	Small	Large
Representativeness of boreholes	–	Large
Spatial variability within domain	Natural (large)	–
Anisotropy	Small	Small
Upscaling methodology	Medium	Small
Significant scale for the canister	Small	Medium
Statistical model (assumptions of distribution, confidence intervals etc)	Small	Small

8.2 Evaluation of uncertainty at canister scale

All of the uncertainties listed in Table 8-1, Table 8-2, and Table 8-3 more or less contribute to the total uncertainty of the thermal conductivity at canister scale. However, only a minor part of them are believed to significantly affect the result at canister scale. The uncertainties at canister scale are of two types: (1) a potential random error, and (2) a potential systematic error (bias).

The representativeness of the boreholes is believed to be the most important uncertainty of all. Boreholes that do not represent the rock mass of interest will lead to biased results, and highly unrepresentative boreholes may give false indications of the thermal properties. A highly sophisticated modelling cannot combat this. Comparison of different boreholes may give indications if there is a potential for large bias due to bad representativeness.

In addition to this major uncertainty there are some other important ones. These differ, depending on if Ävrö granite dominates or not. This is because different upscaling approaches are applied for domains where Ävrö granite dominates and domains dominated by other rock types (Chapter 7).

When Ävrö granite is the dominating rock type, data from density loggings is used in the upscaling model. It is believed that uncertainties associated with the density loggings dominate for such rock domains. The major uncertainties are uncertainty in:

- the noise in the density logging data (measurements),
- the statistical relationship between density and thermal conductivity.

Both a potential random error and a bias are believed to affect the results. The noise in density loggings can be reduced by improving the density logging technique. The statistical relationship between density and thermal conductivity can be improved by performing a large number of measurements (density and thermal conductivity) on rock samples of Ävrö granite.

For rock domains where density loggings do not constitute an important part in the modelling there are other uncertainties that dominate. These are mainly uncertainties associated with the rock type models (PDF:s). The most important are:

- spatial variability within the dominating rock types,
- representativeness of rock samples (SCA and TPS data),
- uncertainty in thermal conductivity estimates from modal analysis (SCA data).

The spatial variability within rock types is uncertain when the data set is scarce. Reduction of this uncertainty requires extensive sampling.

The representativeness of rock samples is a major uncertainty. So far, samples have been selected with different purposes, not only based on probabilistic principles. Non-probabilistic sampling always results in biased data and it is not possible to determine the size of the bias. Therefore, a switch to probabilistic sample selection is desired.

The uncertainty in SCA data is important for rock types where the rock type model is based on such data. It results from a range of uncertain factors, such as the determination of the volume fraction of different minerals in a sample, alteration of minerals, correct values of thermal conductivity of minerals, and the scale issue. If possible, it is recommended that TPS data are used instead of SCA data because of the large uncertainties involved

9 Value of information analysis of thermal investigations

9.1 Introduction

The value of different investigation programs can be estimated by so called Value of Information Analysis (VOIA). In the field of hydrogeology the term Data Worth Analysis is also used for this type of analysis by some authors /Freeze et al. 1992/. The basic idea in VOIA is to estimate the value of additional information by studying how the new information reduces uncertainty, usually in relation to the cost of obtaining it. This is performed by analysing the uncertainty with present knowledge and comparing it with the reduced uncertainty that is expected when new information becomes available. Thereby, the value of an investigation program can be assessed.

The origin of VOIA is decision theory. Some examples of applications in engineering and hydrology are from the 1970's /Davis and Dvoranchik 1971, Maddock 1973/. Several applications in hydrogeology were carried out in the 1990's, introduced by /Freeze et al. 1990/ in a series of papers.

Today, VOIA is used in e.g. information technology and economics but there are also examples of VOIA for geoenvironmental problems /Back 2003, IT Corporation 1997, James et al. 1996, McNulty et al. 1997/. As far as known, formal applications of VOIA for problems related to thermal properties of rock are lacking.

The purpose of this chapter is to present a methodology for VOIA for investigation programs of thermal properties of rock at potential repository sites for spent nuclear fuel in Sweden. An application of the methodology is presented for the prototype repository at Äspö HRL. The aim is to demonstrate how the methodology can be applied on a practical problem to identify efficient investigation programs. Other possible applications of the methodology are discussed, aiming at the on-going site-investigations performed by SKB.

9.2 Methodology

9.2.1 Objective of investigations

In this example it is assumed that the objective is to reduce the uncertainty about the mean thermal conductivity (design-parameter λ_d, see below) for the prototype repository and the adjacent rock mass. It is important to point out that the estimated value of information is only valid for this particular objective. Changing the objective to a different one, such as to reduce the uncertainty about the spatial variability in the rock mass, will result in different estimates of the value of information.

9.2.2 The value of information

There are several ways to measure the value of an investigation program. It is often desirable to assess the economic value of the investigation. With a risk-cost-benefit approach, both investment cost and probabilistic cost are considered. This is the highest level of complexity in Figure 9-1 (approach 3).

A somewhat simplified approach is to only include the investigation cost in the analysis. In such a case, the measure of value can be uncertainty reduction per invested amount of money (approach 2 in Figure 9-1).

In cases were it is not practical to assess the value in monetary terms, some surrogate is often used /Dawdy 1979/. One such surrogate of value is reduction of uncertainty. The presumption is that an investigation program leading to a large uncertainty reduction has a larger value than a program with less reduction. This approach more or less resembles a traditional uncertainty analysis (approach 1 in Figure 9-1).

Here, two alternative measures of value will be used; (1) the uncertainty reduction, and (2) the uncertainty reduction per invested amount of money. The uncertainty reduction is associated with a design-parameter λ_d. The design-parameter is to be used for design purposes of the repository, such as to determine the distance between canisters etc. The design-parameter is a statistical parameter and the random uncertainty of λ_d is quantified as a confidence interval of λ_d. When an investigation program is carried out, the confidence interval of λ_d will be reduced and this reduction of uncertainty is a measure of the value of information (approach 1).

As approach 2, the Expected Value of Information (EVI) is estimated. It is the expected reduction in the confidence interval per invested amount of money. By comparing the EVI for different investigation programs, the one with the largest value can be identified.

The design-parameter λ_d can be a confidence limit, a percentile, the mean, or some other statistical parameter. The presented model can handle different design-parameters but in this presentation the mean thermal conductivity is used as a design-parameter. The random uncertainty is defined as the two-sided 95% confidence interval of the mean. The length of that confidence interval (CI) is referred to as CI_{95}.

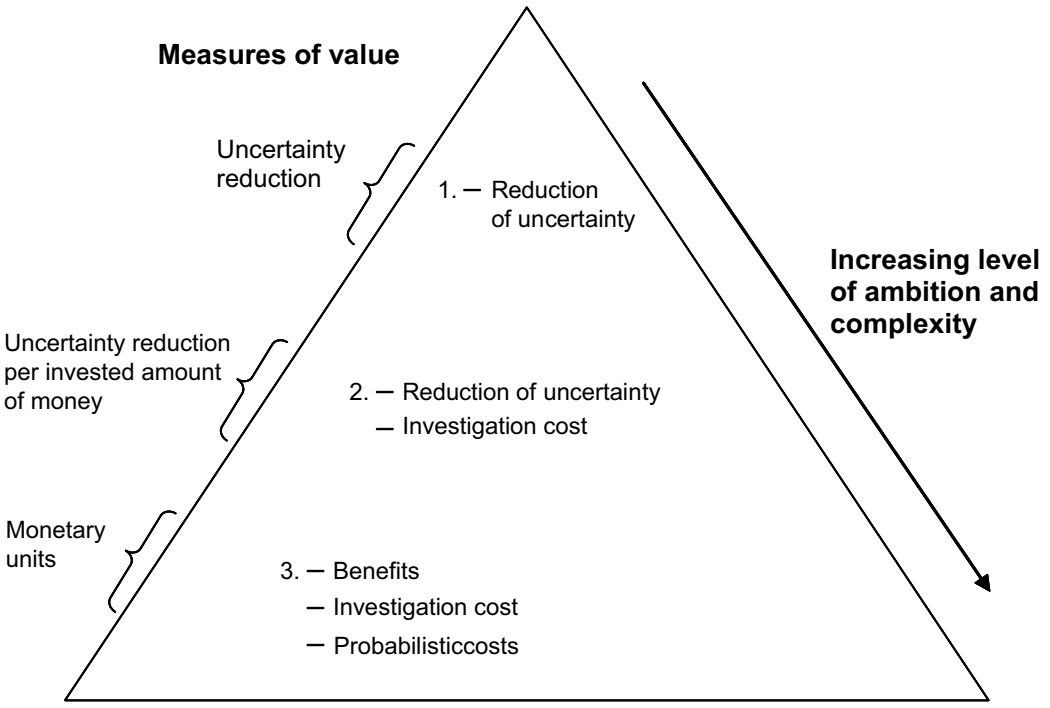

Figure 9-1. *Three approaches for value of information analysis for geo-environmental problems. Approach 1 and 2 are applied in this chapter, whereas approach 3 corresponds to the risk-cost-benefit approach demonstrated by /Freeze et al. 1992/. Approach 2 has been demonstrated by /McNulty et al. 1997/ and /IT Corporation 1997/.*

9.2.3 Modelling of uncertainty and upscaling

Thermal conductivity data are available on a scale smaller than the significant scale for the canister. The significant scale is the scale at which thermal conductivity significantly affects the heat transfer from the repository canisters. A model has been developed for upscaling of thermal conductivity λ to the significant scale, in accordance with Chapter 7 (see Figure 7-6). The relevant uncertainties are quantified, either by statistical techniques (hard data) or by expert opinion (soft data). Uncertainty is propagated through the model by stochastic simulation (Monte Carlo method). The result is a set of λ-values at the scale of interest.

Spatial variability includes variability due to the presence of different rock types as well as spatial variability within the dominating rock type. These are considered by including Boremap (lithology) and density loggings of boreholes in the simulation model. A statistical relationship (empirical) between density data and thermal conductivity is used to calculate thermal conductivity from density loggings. Thus, both variability between different rock types and variability within the dominating rock type is implicitly considered.

For sections of the boreholes where no valid statistical relationship exists, thermal conductivity is modelled by probability density functions (PDF:s) for each rock type. Such rock type models are based on thermal conductivity measurements (TPS method) and calculated values based on modal analyses (SCA method). All subordinate rock sections with an extension of at least 5 cm in the boreholes are considered in the modelling.

In addition to this inherent or natural variability (aleatory uncertainty) there are so-called "lack of knowledge" (epistemic) uncertainties /Lacasse and Nadim 1996/. Five such are considered in the model:

A. Lithological uncertain, expressed as uncertainty in the relative occurrence of different rock types.

B. Uncertain rock type model (PDF) for the dominating rock type Ävrö granite due to unknown representativeness of TPS and SCA data (potential bias).

C. Random prediction uncertainty in the statistical relationship between density and thermal conductivity.

D. Systematic prediction uncertainty (bias) in the statistical relationship between density and thermal conductivity.

E. Scale-dependency of variability of data at the significant scale.

Inclusion of the "lack of knowledge" uncertainties is indicated by capital letters and red arrows in Figure 9-2. How each type of uncertainty is modelled is described below.

Lithological uncertainty (A)

Uncertainty in lithology is considered by defining the percentages of the two dominating rock types as stochastic variables. It is assumed that the contribution to the total uncertainty by the occurrence of subordinate rock types only is of minor importance.

Uncertain rock type model for the dominating rock type (B)

There is a potential for bias in the TPS and SCA data, most importantly for the dominating rock type Ävrö granite. Therefore, the rock type model (PDF) for Ävrö granite is uncertain. This is taken into account by assigning the mean of the PDF as a stochastic variable, see Table 9-4.

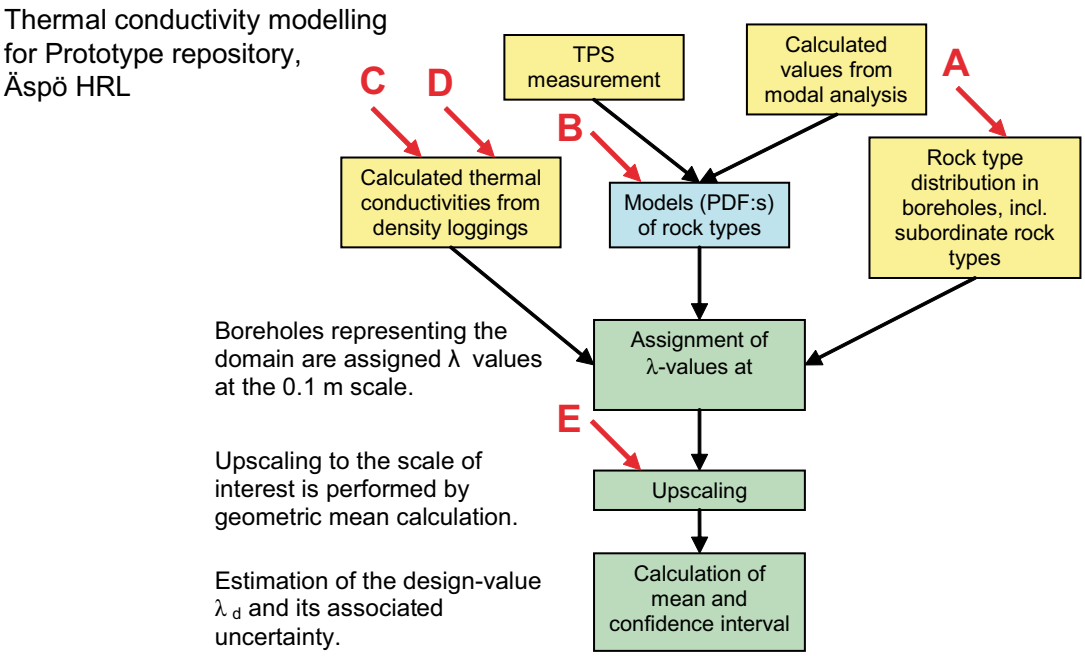

Figure 9-2. *Principle for the upscaling model (simulation model). The five "lack of knowledge" uncertainties are indicated by red arrows and capital letters (see text).*

Random prediction uncertainty (C)

The following relationship is used for calculation of thermal conductivity λ [W/(m×K)] from logged values of density ρ [g/cm^3] /Sundberg et al. 2005/:

$$\lambda = 22.326 - 7.1668 \times \rho \qquad \text{Equation 9-1}$$

The valid range for ρ is 2.6 – 2.85 g/cm^3 and the equation is only applied within this range. Due to uncertainty in the regression equation, prediction of λ from density loggings is associated with prediction uncertainty. To account for this, a random component of prediction uncertainty is added to the calculated thermal conductivity. The stochastic thermal conductivity, denoted λ_{PU}, is estimated as /after Körner and Wahlgren 2000/:

$$\lambda_{PU} = \lambda + t_{p;n-2} \cdot \sqrt{MSE\left[1 + \frac{1}{n} + \frac{(\rho_0 - \bar{\rho})^2}{\sum(\rho_i - \bar{\rho})^2}\right]} \qquad \text{Equation 9-2}$$

for each density value ρ_0. Density ρ_i represents each value in the regression and $\bar{\rho}$ is the mean of the density values. Variable t represents a randomised value from Student's t-distribution as a function of probability p and n-2 degrees of freedom, and MSE is the mean square error of the regression. Equation 9-2 is simply a reformulation of how a prediction interval is calculated.

The approach of adding a random prediction error according to Equation 9-2 is a correct way of modelling the uncertainty if the prediction errors are independent. In the case of spatially correlated prediction errors this approach will lead to an underestimation of the total variability after upscaling (too large variance reduction).

Systematic prediction uncertainty (D)

Comparison of calculated thermal conductivity from density and measurements indicates that there is a potential bias in the statistical relationship. Therefore, a correction is applied. Because the size of the bias is not fully known, the correction is modelled as a stochastic variable, according to Table 9-4.

Scale-dependency of variability (E)

Because the variability in data is scale dependant, simulation of thermal conductivity is performed at a scale that does not underestimate the variability. The scale 0.7 m is selected but it is believed that the significant scale for heat transfer from the repository canisters is somewhat larger.

9.2.4 Value of Information Analysis (VOIA)

The VOIA is performed in three steps:

1. Prior analysis: The design-value λ_d and its associated uncertainty are estimated, based on present information.
2. Preposterior analysis: The design-value λ_d and its associated uncertainty are estimated for each investigation program, but before any investigations are carried out.
3. The value of information is estimated for each investigation program.

The value of investigation program i is estimated in two alternative ways.

Approach 1 – reduction of uncertainty

In this alternative, the value of information is estimated as the reduction of uncertainty in design-parameter λ_d. It is quantified as the percentage reduction of the length of the confidence interval of the mean from the prior to the preposterior stage:

$$\Delta CI_{95,i} = \frac{CI_{95-prior} - CI_{95-preposterior,i}}{CI_{95-prior}} \cdot 100 \qquad \text{Equation 9-3}$$

where $\Delta CI_{95,\,i,}$ [%] is the value of investigation program i, $CI_{95\text{-prior}}$ is the confidence interval of the mean based on present information, and $CI_{95\text{-preposterior}}$ is the confidence interval of the mean that is expected when investigation program i has been carried out.

Approach 2 – reduction of CI per invested amount of money (EVI)

In this alternative, the reduction of the confidence interval is normalised with the investigation cost C_i for program i:

$$EVI_i = \frac{\Delta CI_{95,i}}{C_i} \qquad \text{Equation 9-4}$$

where EVI_i is the expected value of information for investigation program i.

Whether the reduction of uncertainty (approach 1) or the EVI (approach 2) should be used as a measure of value depends on the perspective of the decision-maker. If investigation cost is of importance, approach 2 is the one to prefer. The different investigation programs can be classified according to their value and priority given to the most valuable ones.

9.3 Application

9.3.1 Objective and investigation programs

The model for VOIA was applied for the prototype repository at ÄSPÖ HRL. The objective was to estimate the value of four different investigation and modelling programs. The mean thermal conductivity is used as a design parameter for the prototype repository and the adjacent rock mass. The four evaluated programs are:

- Representative sampling of the rock mass, followed by laboratory measurements
- Modelling of the significant scale for heat transfer from the canister
- Large-scale measurements of thermal conductivity (canister scale)
- Improved statistical relationship between density and thermal conductivity

The purpose of "Representative sampling" is to eliminate possible bias in the thermal conductivity data, especially for the dominating rock type Ävrö granite. For "Significant scale modelling", the purpose is to determine the scale that is significant for the heat transfer from the canister. "Large-scale measurements" is an investigation program with the aim to measure the thermal conductivity at the significant scale for the canister. The fourth evaluated investigation program is additional data collection to improve the statistical relationship between density and thermal conductivity. This relationship (Equation 5-2) is used for estimation of thermal conductivity from density loggings.

9.3.2 Data

Nomenclature

Rock types will be referred to by the nomenclature used in the Simpevarp area, south of Äspö. This is because the rock type models (probability density functions, PDFs) and other relationships of thermal conductivity are based on this nomenclature /Sundberg et al. 2005/.

Lithology

Rock types in the prototype tunnel have been determined from rock cores and geological mapping of the tunnel wall. Rock types in the boreholes include Ävrö granite (including Äspö diorite), fine-grained granite (including aplite), pegmatite, and small amounts of breccia. The distribution of rock types in section 1 (inner section) of the prototype repository was determined to 98% Ävrö granite and 2% Fine-grained granite, based on rock cores from 43 boreholes. The distribution of rock types in section 2 (outer section) was determined to 100% Ävrö granite based on rock cores from 52 boreholes. For the whole tunnel, the distribution was 99% Ävrö granite and 1% fine-grained granite, based on 95 boreholes. The length of the boreholes varies between 3 and 30 m.

The geological mapping of the tunnel wall gives similar results. For section 1, about 98% Ävrö granite and 2% fine-grained granite was noted /Rhén 1995/. The distribution for the whole tunnel is about 99% Ävrö granite and 1% Fine-grained granite.

Rock cores from three boreholes in the adjacent rock mass give a somewhat different picture, see Table 9-1. The total length of these boreholes is approximately 195 m.

Table 9-1. The percentage of rock types in three boreholes (KF0066A01, KF0069A01, and KA3386A01) outside the prototype repository, including subordinate rock types.

Rock type	Percentage	Comment
Äspö diorite and Ävrö granite	82.2	Mainly mapped as Äspö diorite
Fine-grained granite	10.9	Mainly mapped as Aplite
Hybrid rock	4.1	
Amphibolite	2.6	
Other rock types	0.2	

Thermal conductivity

The data of thermal conductivity applied in the modelling are of three types: (1) TPS measurements, (2) calculated values from modal analyses, and (3) calculated values from density loggings.

Table 9-2. Different data sets of thermal conductivity of Ävrö granite.

Data, Ävrö granite	Mean W/(m×K)	St dev W/(m×K)	N
TPS meaurements:			
Prototype repository, section 1	2.44	0.08	6
Prototype repository, section 2	2.63	0.15	4
Section 1 + section 2	2.52	0.15	10
All measurements Äspö (Simpevarp nom.)	2.65	0.29	32
All meas. Äspö+Simp. (Simpevarp nom.)	2.73	0.35	37
Calculations from modal analyses (SCA):			
All samples Äspö+Simp. (Simpevarp nom.)	2.72	0.33	39
Calculations from density loggings:			
Three boreholes outside prototype repos.	2.90	0.31	1,488
Two boreholes Simpevarp	2.96	0.36	13,037

The most important rock type model of thermal conductivity is the one for Ävrö granite since it is the dominating rock type. However, available thermal conductivity data are not easily interpreted. Table 9-2 summarises the different data sets available for Ävrö granite. Based on this data, a model (PDF) is selected. A normal PDF with standard deviation of 0.3 W/(m×K) and an uncertain mean is believed to give a reasonable representation of Ävrö granite for the repository. The mean is uncertain due to potential bias and is therefore modelled as a stochastic variable with 2.70 W/(m×K) as the most likely value and a standard deviation of 0.116 W/(m×K), see Table 9-4. This implies that the true mean is within the range 2.40–3.00 W/(m×K) with a probability of 99%. These values are estimates based on the variations in the different data sets summarised in Table 9-2. The applied rock type models are listed in Table 9-3.

9.3.3 Simulation model

The simulation model illustrated in Figure 9-2 is applied for the prior and preposterior analysis. It is assumed that there is a relationship between density and thermal conductivity. Three boreholes outside the prototype repository are assumed to be representative for the spatial distribution of thermal conductivity values in the Ävrö granite in the prototype repository and the adjacent rock mass. The locations of the boreholes are illustrated in /Staub et al. 2003/. Applied rock type models (PDF:s) are based on data from the prototype repository, other parts of Äspö HRL, from the Simpevarp area south of Äspö, and from literature (see Table 9-3).

Table 9-3. Rock type models (PDF:s) applied in the modelling.

Rock type	Mean W/(m×K)	St dev W/(m×K)	Distribution
Ävrö granite[1]	See text and Table 9-4	0.30	Normal PDF
Fine-grained granite[2]	3.33	0.34	Normal PDF
Amphibolite[3]	3.31	0.48	Normal PDF
Hybrid rock	Ignored	Ignored	
Other rock types	Ignored	Ignored	

[1] Model based on Table 9-2.
[2] Model based on /Sundberg et al. 2005/.
[3] Model based on /Sundberg 1988/.

9.3.4 Prior analysis

The prior analysis is based on present information. Uncertainties are quantified and implemented in the simulation model. A summary of the quantified "lack of knowledge" uncertainties is presented in Table 9-4. The scale 0.7 m is selected as the significant scale in the upscaling, in order not to underestimate the variability.

Table 9-4. Modelling of "lack of knowledge" uncertainties of thermal conductivity λ for the prior analysis at the prototype repository, Äspö HRL.

Type of uncertainty	Modelling approach	Properties
A. Lithological uncertainty: Percentage of Ävrö granite	Percentage of other rock types as a 3-parameter[1] lognormal PDF.	Parameters: Min = 1%, mode = 4%, UCL99 = 17.8%
B. Uncertain rock type model of Ävrö granite	Mean of λ as a normal (gaussian) PDF.	Mean is between 2.40 and 3.00 W/(m×K) with 99% confidence
C. Random prediction uncertainty	Addition of random prediction error component.	See text and Equations 9-1 and 9-2.
D. Systematic prediction uncertainty	Correction for bias as a normal (gaussian) PDF.	Mean 0.20 and st dev 0.04 W/(m×K).
E. Scale-dependancy of variability	Significant scale is assumed to be relatively small not to underestimate the variability.	The scale 0.7 m is selected.

[1] The 3rd parameter of a 3-parameter lognormal probability density function defines the offset of the distribution from zero.

9.3.5 Preposterior analysis

Principles for reduction of uncertainty

In the preposterior analysis, the uncertainty is evaluated based on the investigation programs and their expected outcomes. The presumption is that the uncertainty is reduced when an investigation is performed. The simulation model has different principles of uncertainty reduction for each investigation program. The principles are compiled in Table 9-5 and described below.

Table 9-5. Uncertainty reduction principles for preposterior analysis of four different investigation programs at the prototype repository, Äspö HRL.

Investigation program	Uncertainty reduction principle	Assumptions
Representative sampling and laboratory measurements	Stochastic simulation	Uncertainty B (bias) is reduced by 75%.
Significant scale modelling	Expert opinion + stochastic simulation	Significant scale is assumed to be 2.5 m.
Large-scale measurements	Stochastic simulation + analytical estimation	Uncertainties B, C, and D is eliminated. Standard dev. of the mean is estimated analytically.
Improved statistical relationship between density and therm cond	Expert opinion + stochastic simulation	Uncertainty D (bias) is reduced by 75%.

For each stochastic simulation, 5,000 simulation steps where performed. According to /Alén 1998/ this is a reasonable number for estimation of the 2-percentile and should be well enough for estimation of the two-sided 95% confidence interval of the mean.

Representative sampling and laboratory measurements

The investigation program “Representative sampling” aims at collecting rock samples that are representative for the rock mass and to perform laboratory measurements of thermal conductivity on the samples. This program will reduce the potential bias in the rock type model (PDF) for Ävrö granite. The reduction is simulated by reducing the standard deviation of the stochastic variable (uncertainty B) by 75%, from 0.116 W/(m×K) to 0.029 W/(m×K). This requires that the rock samples are selected in a probabilistic manner from the target population, i.e. the 3-dimesional rock volume.

Significant scale modelling

The “Significant scale modelling” aims at finding the most relevant scale for the design-parameter λ_d. The expected significant scale is believed to be in the range of 1 m to 10 m with a most likely value of 2.5 m, based on expert opinion. Therefore, 2.5 m is used in the preposterior analysis for this investigation program, compared to 0.7 m in the prior analysis. Because of the geometric mean calculation during upscaling, the uncertainty will be reduced.

Large-scale measurements

An investigation program of "Large-scale measurements" will reduce many of the uncertainties included in the upscaling model. In fact, there is little need for an upscaling model when measurements are performed at a large scale. The remaining variability in data will consist of spatial variability at the measurement scale, measurement uncertainty, and questions of representativeness. It is assumed that there are no measurement errors and no bias due to problems of representativeness.

The uncertainty in the mean can be estimated if we know the natural large-scale variability, and given that data follows a normal distribution. Under these assumptions the standard deviation of the mean, s_d, is:

$$s_d = \frac{s}{\sqrt{n}} \qquad \text{Equation 9-5}$$

where s is the standard deviation of the data at the measurement scale and n is the number of measurements. However, simulation results indicate that data are not normally distributed at the 2.5 m scale. Therefore, a modified approach is used:

The simulated standard deviation of the mean is not a reliable estimate of s_d because much more data is used in the simulation than the expected number of large-scale measurements in the investigation program. If we assume that the standard deviation of the mean is directly proportional to the square root of n, as in Equation 9-5, we have:

$$s_d \approx s_{sim} \cdot \sqrt{\frac{n_{sim}}{n}} \qquad \text{Equation 9-6}$$

where s_{sim} is the standard deviation of the mean from the simulation model, n_{sim} is the number of simulated data values at the scale 2.5 m, and n is the number of measurements in the investigation program. The mean is approximately normally distributed and consequently the length of the confidence interval of the mean is:

$$CI_{95} = 2 \times t_{n-1} \times S_d \qquad \text{Equation 9-7}$$

where t_{n-1} is the Student's t-statistic for a two-sided 95% confidence interval. It is assumed that a total of about 30 large-scale measurements are performed.

This approach provides an upper limit of the value of information because measurement uncertainty and possible questions of representativeness are ignored.

Improved statistical relationship between density and thermal conductivity

The investigation program "Improved statistical relationship" aims at reducing the prediction uncertainty and the potential bias in the relationship between density and thermal conductivity. This is achieved by collecting additional rock samples and performing laboratory measurements of density and thermal conductivity. Due to natural variability, only a minor reduction of random prediction uncertainty is expected when more data are collected (n increases in Equation 9-2). This small reduction is not considered in the simulation. However, the potential bias in the statistical relationship is reduced significantly when more data is collected. The reduction is simulated by reducing the standard deviation of the corresponding stochastic variable (uncertainty D) by 75%, from 0.04 W/(m×K) down to 0.01 W/(m×K).

Investigation costs

The investigation costs are required for estimation of the variance reduction per invested amount of money. Rough estimates of the investigation costs are given in Table 9-6. The actual costs can be larger or lower depending on the exact design of the investigations and the level of ambition.

Table 9-6. Rough estimates of the investigation costs for the four evaluated investigation programs.

Investigation program	Cost estimate (SEK)
Representative sampling and laboratory measurements	500,000
Significant scale modelling for the canister	100,000
Large-scale measurements	1,000,000
Improved statistical relationship between density and thermal cond.	300,000

9.4 Results

The results of the simulations for the prior and preposterior stages are summarised in Table 9-6 and Figure 9-3, together with the estimated reduction of uncertainty. It is quite clear which investigation programs supply the most value when cost is not considered (approach 1). The investigation programs "Improved relationship density vs λ" and "Large-scale measurements" supply information of much higher value than do the "Representative sampling" program and the "Significant scale modelling". "Large-scale measurements" is the investigation program of preference, supplying up to 51% reduction of uncertainty of the mean thermal conductivity. This can be compared to a perfect investigation program that completely removes the uncertainty, i.e. 100% reduction of uncertainty.

Table 9-7. Prior and preposterior estimation of the mean thermal conductivity and its associated uncertainty. The value of information is quantified as the percentage reduction of the 95% confidence interval of the mean λd.

Analysis	λ_d W/(m×K)	CI_{95} (W/(m×K))^2	ΔCI_{95}	Approach
Prior analysis				
Present state of knowledge	2.72	0.155	–	Simulation
Preposterior analysis				
1. Representative sampling	2.72	0.137	11%	Simulation
2. Significant scale modelling	2.71	0.153	1%	Exp opinion + sim
3. Large-scale measurements	2.72	0.076	51%	Sim + analytical
4. Improved statistical relationship	2.72	0.091	41%	Exp opinion + sim
A perfect investigation program	–	–	100%	EVPI

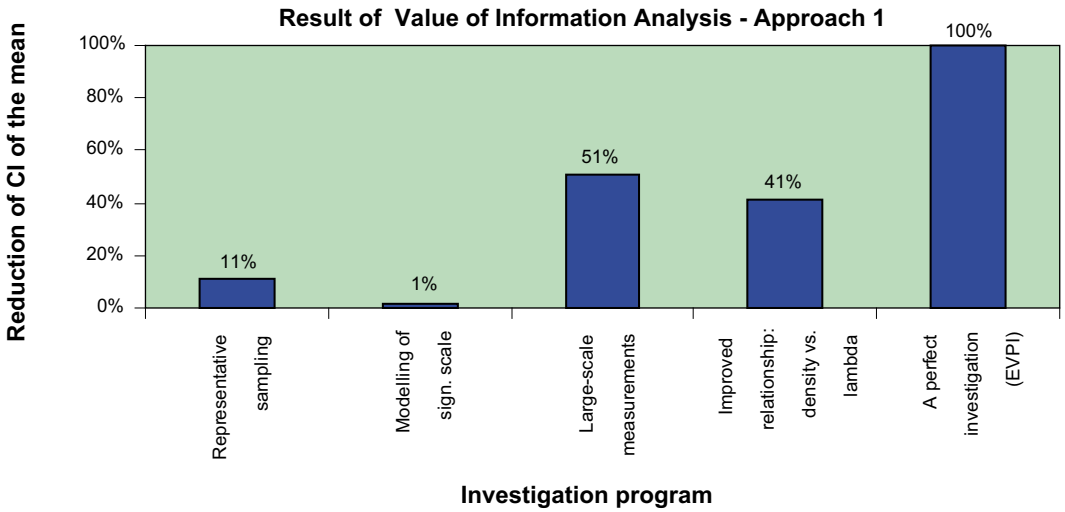

Figure 9-3. *The value of information estimated as the percentage reduction of the confidence interval of the mean λd.*

If investigation cost is included in the VOIA (approach 2), the value of information can be defined as the percentage reduction of the confidence interval (CI) of the mean per invested 100 kSEK. This results in a somewhat different picture compared to approach 1, as illustrated in Figure 9-4 (note that estimated costs are only rough estimates illustrating the order of magnitude). With this definition of EVI the investigation program "Improved statistical relationship" supplies the most value per invested amount of money, and it is consequently the most cost-efficient alternative of the four evaluated ones.

Figure 9-5 illustrates how the reduction of CI varies with the invested amount of money. There is a trend of increasing cost for larger reduction of uncertainty.

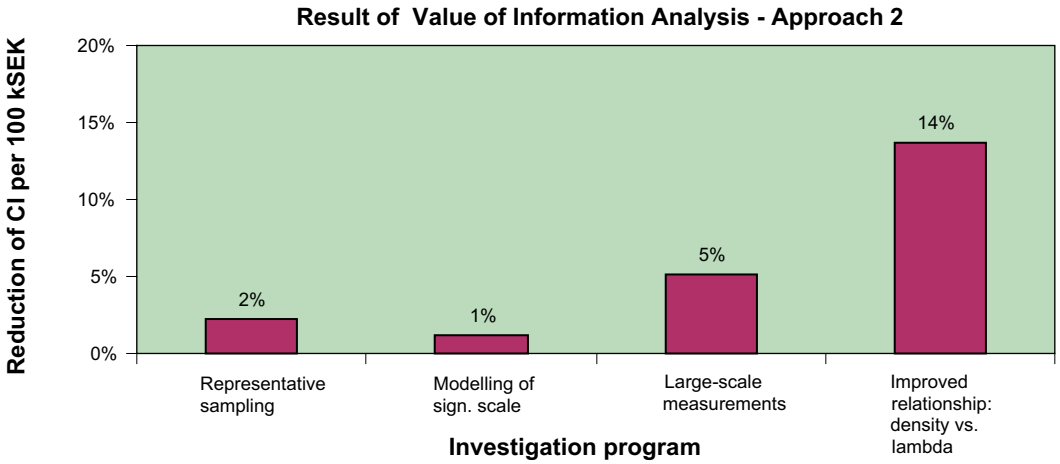

Figure 9-4. *The Expected Value of Information, EVI, calculated as the percentage reduction of CI of the mean per invested 100 kSEK.*

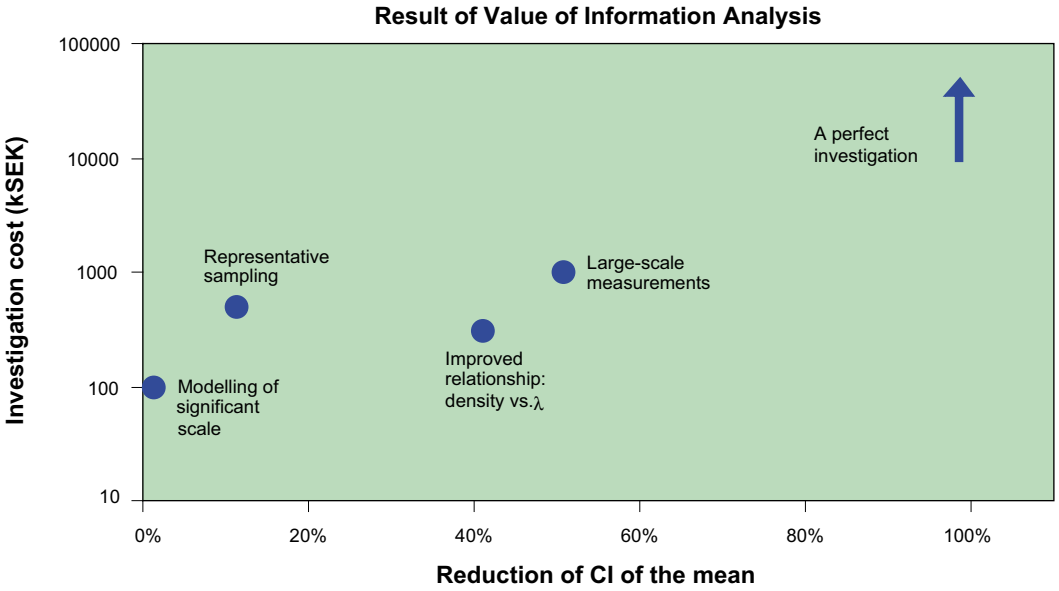

Figure 9-5. *Result of the Value of Information Analysis for the prototype repository. The cost of a perfect investigation is not quantified, only indicated.*

9.5 Discussion

9.5.1 The application at Äspö HRL

The presented results are not self-evident and could not easily have been predicted without a formal VOIA since the problem is quite complex. By performing a formalised but relatively simple VOIA the most valuable investigation programs were successfully identified. as discussed below, the result depend to some extend how the value of an investigation program is defined, i.e. approach 1 and 2, respectively.

Approach 1

Of the four evaluated investigation programs, “Large-scale measurements” is expected to supply the most value, although the value is slightly overestimated because measurements errors are ignored. The program “Improved statistical relationship” is also of high value, significantly larger than “Representative sampling” and “Significant scale modelling”.

Somewhat surprisingly, “Significant scale modelling” is of almost no value. The reason is that the reduction in CI is small when the scale increases, compared to the other involved uncertainties. This is because the mean thermal conductivity is relatively insensitive to changes in scale.

Approach 2

Including investigation cost in the analysis makes it possible to determine the cost-efficiency of different investigation programs (approach 2). This is of help when a limited amount of money is available and the objective is to reduce uncertainty as much as possible given a certain amount of money. A matrix like Figure 9-5 is helpful when both uncertainty reduction and investigation cost should be considered. Programs occurring to the lower right in the matrix are most cost-efficient, whereas programs in the upper left should be avoided.

When investigation cost is considered it is obvious that the most cost-efficient investigation strategy is to improve the statistical relationship between density and thermal conductivity. The value per invested amount of money (EVI) is lower for the program "Large-scale measurements" because of the relatively high investigation costs.

Limitations and sensitivity

It is important to note that general conclusions of the value of information cannot be drawn from the results presented in this chapter. The reason is that value of information is use specific /Dawdy 1979/. Of course, the results depend on the assumptions made about the input parameters to the simulation model but most important is the objective of the investigation. It must be stressed that the presented results are limited to the objective to estimate the mean thermal conductivity in the rock mass and its associated uncertainty. Estimation of the spatial distribution of thermal conductivity is an example of a different objective and this problem would lead to different estimates of the value of information.

The impact of different assumptions in input parameters can easily be assessed by changing the assumptions and studying the results (sensitivity analysis). Such an analysis indicates that the assumption regarding the prediction bias (uncertainty D) has a large influence on the result. However, increasing the potential bias by a factor of 2.5 (standard deviation 0.1 instead of 0.04) does not change the relative order of the investigation programs although the absolute value of information changes.

9.5.2 Other possible applications for SKB

There are several possible applications of VOIA for SKB:s on-going site investigations. At least three types of applications can be identified:

1. A tool for comparing different data acquisition programs against one another, with the purpose to identify the program that supplies the most information for a given problem.
2. A tool for determining when data acquisition should stop, i.e. when additional data do not supply enough new information.
3. A methodology for identification of uncertainties and how they relate. This improves the understanding of the problem and facilitates model building.

The first type has been demonstrated in this chapter for the problem of thermal conductivity in rock. Similar analyses can be performed on thermal problems in SKB:s site investigations, for example to compare different field investigation techniques for determination of thermal conductivity. This can be achieved by comparing precision, accuracy, and cost-efficiency. There are also numerous other possible applications in other fields of the site investigations, such as hydrogeology, rock mechanics, geochemistry etc.

Application of VOIA to determine when data acquisition should stop requires some type of criterion to compare the expected value against. In its simplest form, such a criterion could be a defined variance or variance reduction. When the uncertainty is lower than the criterion, investigation can be terminated.

When a VOIA is performed it is necessary to identify and quantify the various uncertainties, resulting in a better understanding of the problem. This implies that such an analysis has a value even if no formal decision will be taken based on the results. Analysis can be performed at different levels of complexity. In situation where mathematical models are not available, expert opinion can be applied, as illustrated by for example /McNulty et al. 1997/.

9.5.3 Possible developments of the methodology

The analysis can be taken an additional step further by including probabilistic costs, i.e. costs that evolve from an uncertain event (approach 3 in Figure 9-1). The design cost of the repository is a function of λ_d and its uncertainty, and an investment cost-function can be coupled to λ_d and its associated uncertainty. An investigation program will result in a decrease in the expected total cost for the repository because the uncertainties will be reduced. The cost of an investigation program can be compared to the reduction in expected total cost, and thus the ENV of investigation programs can be estimated in monetary terms, and the most cost-efficient one be identified.

Investigation programs may have several different objectives. The methodology presented in this chapter is capable of handling one single objective, such as estimation of the mean thermal conductivity. The methodology can be developed to take several objectives into account in the analysis. Thus, a more complete picture of the value of a multi-objective investigation program could be presented.

10 Conclusions and recommendations

10.1 Conclusions

10.1.1 Scale and methods

- The variation of the maximum canister/buffer temperature, for a large number of canisters, is dependent on the scale at which the thermal conductivity variation occurs. This variation is different in different rock types. However, in all rock types there is a small-scale variation.
- When modelling the temperature distribution for a large number of canisters the result depends on the method of modelling in combination with the thermal conductivity variation at different scales. The appropriate scale for thermal conductivity data therefore depends on the intended method of temperature modelling.
- The scale at which variations of thermal conductivity is significant for the temperature on the canister has been investigated. Below a scale of approximately 1–2 m variation in thermal conductivities is mainly levelled out due to the size of the canister. Consequently it is possible to upscale the small-scale thermal conductivity to at least the 1–2 m scale when assessing the maximum temperature based on an effective thermal conductivity value.
- At the modelling of the significant scale the variation (standard deviation) of temperature increases linearly up to about 10 m. However, this result is based on simulations with the same standard deviation of thermal conductivity for all scales. If the variance reduction due to upscaling had been considered and adjusted for, the increase in variability would have been smaller and the shape different.
- The scale dependence for laboratory measurements of thermal conductivity with different sensor size seems to be small. Furthermore, thermal conductivity measurements are more reliable than the values calculated from mineral distribution and values estimated from density loggings.
- Density logging can be used to estimate thermal conductivity. A physical explanation of the relationship between density and thermal conductivity has been determined for granitic rock and tested for Ävrö granite. The method gives good possibilities to investigate the spatial distribution of thermal conductivity. However, there are uncertainties in the relationship.

10.1.2 Prototype repository – inverse modelling

- There is good agreement between prognosis of thermal conductivity in the prototype repository and the result from inverse modelling based on 37 different temperature sensors, and the rather low thermal conductivity is verified. Some of the temperature measurements seem to be influenced by ground water movements. The evaluated thermal conductivity is therefore an effective value (including convection) and is probably overestimating the real thermal conductivity. The variability in thermal conductivities from best fit of individual sensors seems to be the same as the variability in the prognosis, based on measurements. However, the analysis is simplified and more work is needed to analyse the scale dependence in a better way.

- There is a large discrepancy between the individual fit for some sensors and the overall best fit. The heat transport in the vicinity of these sensors is likely to be influenced by groundwater movements and thus the thermal conductivity is overestimated.
- The relatively wide range of measured initial temperature shows that there is a considerable thermal disturbance, which can be explained by the varying air temperature during the construction phase. The accuracy of the evaluation would have been improved if the rock temperature had been allowed to equilibrate after the sealing of the tunnel and verified to be stable before the heating of the canisters began.

10.1.3 Methodology for upscaling

- Different types of variograms can be used to analyse the spatial distribution of conductivities, preferably calculated from density loggings (semi variograms of thermal conductivity), and the spatial distribution of rock types (indicator variograms). The main challenge is to determine the spatial variability in rock domains where Ävrö granite is absent or subordinate. In order to model the spatial variability for these domains in a reliable way more measurements are required, especially for the dominating rock types.
- A methodology for upscaling of thermal conductivity from measurement scale to a significant scale for the canister has been developed. The variance is reduced when the scale increases but for some rock types the decrease in variance is low, mainly because of the high large-scale spatial variability.

10.1.4 Uncertainties and value of information

- Uncertainties in the whole process have been analysed. The largest uncertainty is the representativity of the boreholes. Another major uncertainty is the statistical relationship between density and thermal conductivity for Ävrö granite.
- A value of Information Analysis (VOIA) has been performed in order to estimate the value of additional investigations by studying how the new information reduces uncertainty in the mean thermal conductivity. Field measurements in a relevant scale supply the highest value, while an improved relationship between density and thermal conductivity is the most cost-efficient alternative of the four investigated ones.
- Small-scale measurements and the following upscaling are affected by uncertainties due to small-scale variability and the upscaling methodology. Measurements at larger scale reduce these uncertainties. Independent of the method of temperature modelling for design, measurements could be performed at a scale of at least about 2 m. However, the most appropriate scale depends on the method of temperature modelling for design of a repository.

10.2 Recommendations

- The modelling approach of thermal properties needs to be improved to take spatial variability fully into account, so that data sets can be produced for any desired scale and for all relevant domains. This will probably require stochastic simulation.
- Field measurements in relevant scale decrease uncertainty in the thermal conductivity. It is recommended that a method for measurements at a larger scale is developed.

- The results of the inverse modelling at the prototype repository indicate that data is influenced by a temperature drift in the rock mass and by water movements. These "errors" are probably most significant in early data. It is recommended that data from a longer period of time are evaluated. Extending the duration of the measurement would also allow more initial data to be omitted in order to improve accuracy. This would also enhance prediction of groundwater flow effects. Furthermore, the evaluation of upscaling effects on the thermal conductivity distribution from the inverse modelling could be improved if a longer period is evaluated.
- The simulation of "significant scale" shows that the statistical deviation of the maximum temperature increases until the scale of the heterogeneities is in the order of 8–10 m. However, this is partly a result of that the same standard deviation of thermal conductivity has been used for all scales. In reality, the variability will decrease at larger scales and this would result in different scale dependence. It is recommended that this is investigated further.
- At design of a repository the influence on the temperature distribution of the thermal conductivity variation is scale dependent. It is recommended that the result from the thermal site descriptive models is coupled to the modelling approach for the design, and vice versa.

There are several possible applications of VOIA for SKB:s on-going site investigations. At least three types of applications can be identified:

1. A tool for comparing different data acquisition programs against one another, with the purpose to identify the program that supplies the most information for a given problem.
2. A tool for determining when data acquisition should stop, i.e. when additional data do not supply enough new information.
3. A methodology for identification of uncertainties and how they relate. This improves the understanding of the problem and facilitates model building.

References

Alén C, 1998. On Probability in Geotechnics. Random Calculation Models Exemplified on Slope Stability Analysis and Ground-Superstructure Interaction, Volume 1. Dissertation Thesis, Chalmers University of Technology, Göteborg, 242 pp.

Back P-E, 2003. On Uncertainty and Data Worth in Decision Analysis for Contaminated Land. Licentiate of Engineering Thesis, Chalmers University of Technology, Göteborg, Sweden, 129 pp.

Blom G, 1970. Statistikteori med tillämpningar. (Statistical Theory with Applications). Studentlitteratur, Lund, Sweden. ISBN 91-44-05591-9.

Chai E Y, 1996. A Systematic Approach to Representative Sampling in the Environment. In: J H Morgan (Editor), Sampling Environmental Media. American Society for Testing and Materials, ASTM, West Conchohocken, pp. 33–44.

Dagan G, 1979. Models of groundwater flow in statistically homogeneous porous formations, Water Resour. Res, 15(1), p 47–63, 1979.

Dawdy D R, 1979. The Worth of Hydrologic Data. Water Resources Research, 15(6): 1726–1732.

Davis D R, Dvoranchik W M, 1971. Evaluation of the Worth of Additional Data. Water Resources Bulletin, 7(4): 700–707.

Eftring B, 1990. Numerisk beräkning av temperaturförlopp. Ett fysikaliskt betraktelsesätt. (Numerical Calculation of Thermal Processes. A Physical Approach, in Swedish). Ph.D. thesis, Dept. of Building Science, Lund University.

Freeze R A, Massman J, Smith L, Sperling T, James B, 1990. Hydrogeological Decision Analysis: 1. A Framework. Ground Water, 28(5): 738–766.

Freeze R A, Bruce J, Massman J, Sperling T, Smith L, 1992. Hydrogeological Decision Analysis: 4. The Concept of Data Worth and Its Use in the Development of Site Investigation Strategies. Ground Water, 30(4): 574–588.

Fälth B, 2005. Personal communication. Clay Technology AB, Lund.

Goovaerts P, 1999. Geostatistics in soil science: state-of-the-art and perspectives. Geoderma, 89(1999): 1–45.

Goudarzi R, Johannesson L, 2004. Äspö HRL, prototype Repository, Sensors data report (Period 010917-040301) Report No:9, SKB IPR-04-24, Svensk Kärnbränslehantering AB.

Gustafsson S, 1991. Transient plane source techniques for thermal conductivity and thermal diffusivity measurements of solid materials. Rev. Sci. Instrum. 62, p 797–804. American Institute of Physics, USA.

Gutjahr AL, Gelhar LW, Bakr AA, MacMillan JR, 1978. Stochastic analysis of spatial variability in subsurface flows. 2. Evaluation and application. Wat. resorces res, vol. 14, no. 5. p 953–959.

Hashin Z, Shtrikman S, 1962. A variational approach to the theory of the effective magnetic permeability of multiphase materials, J. Appl. Phys. 33, 3125.

Horai K, 1971. Thermal conductivity of rock-forming minerals. J. Geophys. Res. 76, p 1278–1308.

HotDisk, 2004. www.hotdisk.se, access 2004-09-22.

Hökmark H, Fälth B, 2003. Thermal Dimensioning of the Deep Repository, SKB TR-03-09, December 2003. Svensk Kärnbränslehantering AB.

Isaaks E H, Srivastava R M, 1989. An Introduction to Applied Geostatistics. Oxford University Press, New York, 561 pp.

IT Corporation, 1997. Value of Information Analysis for Corrective Action Unit no. 98; Frenchman Flat. DOE/NV/13052-T1, U.S. Department of Energy, USA.

James B R, Huff D D, Trabalka J R, Ketelle R H, Rightmire C T, 1996. Allocation of Environmental Remediation Funds Using Economic Risk-Cost-Benefit Analysis: A Case Study. Groundwater Monitoring & Remediation, (Fall 1996): 95–105.

Körner S, Wahlgren L, 2000. Statistisk dataanalys. Studentlitteratur, Lund, 408 pp.

Lacasse S, Nadim F, 1996. Uncertainties in characterising soil properties. In: C.D. Schackelford, P.P. Nelson and M.J.S. Roth (Editors), Uncertainty in the Geologic Environment: From Theory to Practice. American Society of Civil Engineers, Madison, WI, pp. 49–75.

Maddock T, 1973. Management Model as a Tool for Studying the Worth of Data. Water Resources Research, 9(2): 270–280.

McNulty G, Deshler B, Dove H, IT Corporation, 1997. Value of Information Analysis; Nevada Test Site. CONF-970335-37, USA.

Patel S, Dahlström L-O, Stenberg L, 1997. Characterisation of the rock mass in the prototype repository at Äspö HRL stage 1. Progress report HRL-97-24, Svensk Kärnbränslehantering AB

Rhén I (ed), 1995. Documentation of tunnel and shaft data. Tunnel section 2874–3600 m, hoist and ventilation shafts 0–450 m. SKB Progress report 25-95-28, Svensk Kärnbränslehantering AB

SKB, 2004. RD&D-Programme 2004. Programme for research, development and demonstration of methods for the management and disposal of nuclear waste, including social science research. SKB TR-04-21. Svensk Kärnbränslehantering AB.

SKB, 2005. Preliminary site description. Simpevarp subarea – version 1.2. SKB R-05-08. Svensk Kärnbränslehantering AB.

SKB, 2005b. Äspö Hard Rock Laboratory. Annual Report 2004. SKB TR-05-10. Svensk Kärnbränslehantering AB.

Staub I, Janson T, Fredriksson A, 2003. Geology and properties of the rock mass around the experiment volume. Äspö Pillar Stability Experiment. Äspö Hard Rock Laboratory. SKB IPR-03-02, Svensk Kärnbränslehantering AB.

Sundberg J, 1988. Thermal Properties of Soils and Rocks. Dissertation Thesis, Chalmers University of Technology and UNiversity of Göteborg (Gothenburg), Göteborg, 310 pp.

Sundberg J, Gabrielsson A, 1999. Laboratory and field measurements of thermal properties of the rocks in the prototype repository at Äspö HRL. SKB IPR-99-17, Svensk Kärnbränslehantering AB.

Sundberg J, 2002. Determination of thermal properties at Äspö HRL. Comparison and evaluation of methods and methodologies for borehole KA 2599 G01. SKB R-02-27, Svensk Kärnbränslehantering AB.

Sundberg J, 2003. Thermal properties at Äspö HRL. Analysis of distribution and scale factors. SKB R-03-17, Svensk Kärnbränslehantering AB.

Sundberg J, Back P-E, Bengtsson A, Ländell M, 2005. Thermal modelling. Preliminary site description Simpevarp subarea – version 1.2. SKB R-05-24, Svensk Kärnbränslehantering AB.

Tarbuck E, Lutgens F, 2005. Earth: introduction to physical geology. 8th ed. Pearson Higher Education, Upper Saddle River, NJ.

Wahlgren C-H, 2004. SGU (Geological survey of Sweden). Personal communication.

Appendix A

TPS measurements of thermal properties, two different sensor sizes. Hot Disk 2004

Sample 1 Sample	Sensor		TC [W/mK]	TD [mm²/s]	Cp [MJ/m³K]
1	4921	Average	2.39	1.13	2.11
		Stdav	0.02	0.04	0.07
		Stdav %	0.80	3.22	3.24
	5501	Average	2.155	1.31	1.64
		Stdav	0.008	0.02	0.03
		Stdav %	0.358	1.75	2.04
		Diff. 4921/5501 (%)	**9.8**	**–16.1**	**22.4**

Sample 2 Sample	Sensor		TC [W/mK]	TD [mm²/s]	Cp [MJ/m³K]
2	4921	Average	2.927	1.272	2.30
		Stdav	0.003	0.019	0.03
		Stdav %	0.119	1.472	1.38
	5501	Average	2.869	1.322	2.170
		Stdav	0.004	0.008	0.010
		Stdav %	0.149	0.575	0.441
		Diff. 4921/5501 (%)	**2.0**	**–3.9**	**5.7**

Sample 3 Sample	Sensor		TC [W/mK]	TD [mm²/s]	Cp [MJ/m³K]
3	4921	Average	3.00	1.32	2.28
		Stdav	0.02	0.02	0.02
		Stdav %	0.76	1.48	1.03
	5501	Average	3.054	1.323	2.31
		Stdav	0.006	0.005	0.01
		Stdav %	0.209	0.400	0.51
		Diff. 4921/5501 (%)	**–1.7**	**–0.5**	**–1.2**

Sample 4 Sample	Sensor		TC [W/mK]	TD [mm²/s]	Cp [MJ/m³K]
4	4921	Average	2.860	1.33	2.15
		Stdav	0.007	0.02	0.02
		Stdav %	0.229	1.17	0.95
	5501	Average	2.66	1.46	1.82
		Stdav	0.02	0.03	0.04
		Stdav %	0.57	1.92	2.32
		Diff. 4921/5501 (%)	**6.9**	**–10.0**	**15.3**

Sample 5 Sample	Sensor		TC [W/mK]	TD [mm²/s]	Cp [MJ/m³K]
5	4921	Average	2.91	1.47	1.97
		Stdav	0.04	0.01	0.04
		Stdav %	1.31	0.67	1.80
	5501	Average	2.5	1.8	1.4
		Stdav	0.1	0.2	0.2
		Stdav %	4.1	10.5	16.6
		Diff. 4921/5501 (%)	**13.5**	**–19.5**	**26.6**

Sample 6 Sample	Sensor		TC [W/mK]	TD [mm²/s]	Cp [MJ/m³K]
6	4921	Average	2.551	1.10	2.31
		Stdav	0.002	0.02	0.03
		Stdav %	0.072	1.40	1.36
	5501	Average	2.61	1.120	2.33
		Stdav	0.01	0.005	0.02
		Stdav %	0.45	0.445	0.68
		Diff. 4921/5501 (%)	**–2.4**	**–1.5**	**–0.9**

Sample 7 Sample	Sensor		TC [W/mK]	TD [mm²/s]	Cp [MJ/m³K]
7	4921	Average	2.62	1.16	2.27
		Stdav	0.02	0.01	0.01
		Stdav %	0.59	1.19	0.60
	5501	Average	2.667	1.124	2.374
		Stdav	0.001	0.005	0.009
		Stdav %	0.044	0.430	0.395
		Diff. 4921/5501 (%)	**–1.7**	**2.8**	**–4.7**

Sample 8 Sample	Sensor		TC [W/mK]	TD [mm²/s]	Cp [MJ/m³K]
8	4921	Average	2.57	1.15	2.24
		Stdav	0.02	0.01	0.01
		Stdav %	0.67	1.13	0.49
	5501	Average	2.564	1.129	2.27
		Stdav	0.004	0.008	0.02
		Stdav %	0.142	0.708	0.79
		Diff. 4921/5501 (%)	**0.1**	**1.6**	**–1.5**

Sample 9 Sample	Sensor		TC [W/mK]	TD [mm²/s]	Cp [MJ/m³K]
9	4921	Average	2.534	1.12	2.26
		Stdav	0.004	0.04	0.08
		Stdav %	0.177	3.63	3.53
	5501	Average	2.542	1.130	2.25
		Stdav	0.004	0.009	0.02
		Stdav %	0.160	0.804	0.81
		Diff. 4921/5501 (%)	**–0.299**	**–0.417**	**0.215**

Sample 10 Sample	Sensor		TC [W/mK]	TD [mm²/s]	Cp [MJ/m³K]
10	4921	Average	2.496	1.086	2.298
		Stdav	0.010	0.006	0.004
		Stdav %	0.398	0.546	0.183
	5501	Average	2.526	1.083	2.33
		Stdav	0.002	0.006	0.01
		Stdav %	0.081	0.581	0.52
		Diff. 4921/5501 (%)	**–1.2**	**0.2**	**–1.4**

Sample 11 Sample	Sensor		TC [W/mK]	TD [mm²/s]	Cp [MJ/m³K]
11	4921	Average	2.61	1.13	2.31
		Stdav	0.01	0.02	0.04
		Stdav %	0.52	2.19	1.71
	5501	Average	2.764	1.127	2.45
		Stdav	0.005	0.010	0.02
		Stdav %	0.199	0.868	0.72
		Diff. 4921/5501 (%)	**–5.8**	**0.2**	**–6.0**

Sample 12 Sample	Sensor		TC [W/mK]	TD [mm²/s]	Cp [MJ/m³K]
12	4921	Average	2.55	1.16	2.19
		Stdav	0.03	0.04	0.05
		Stdav %	1.22	3.54	2.23
	5501	Average	2.475	1.095	2.260
		Stdav	0.003	0.005	0.008
		Stdav %	0.107	0.421	0.374
		Diff. 4921/5501 (%)	**3.0**	**5.9**	**–3.1**

Sample 13 Sample	Sensor		TC [W/mK]	TD [mm²/s]	Cp [MJ/m³K]
13	4921	Average	2.599	1.115	2.33
		Stdav	0.009	0.005	0.02
		Stdav %	0.349	0.421	0.65
	5501	Average	2.573	1.071	2.402
		Stdav	0.003	0.002	0.005
		Stdav %	0.108	0.221	0.212
		Diff. 4921/5501 (%)	**1.0**	**4.0**	**–3.1**

Sample 14 Sample	Sensor		TC [W/mK]	TD [mm²/s]	Cp [MJ/m³K]
14*	4921	Average	2.786	1.323	2.11
		Stdav	0.008	0.009	0.02
		Stdav %	0.285	0.671	0.93
	5501	Average	2.65	1.36	1.95
		Stdav	0.02	0.04	0.06
		Stdav %	0.64	2.66	3.20
		Diff. 4921/5501 (%)	**5.0**	**–2.7**	**7.4**
14	4921	Average	2.81	1.30	2.16
		Stdav	0.01	0.03	0.04
		Stdav %	0.46	2.27	1.86
	5501	Average	2.720	1.240	2.19
		Stdav	0.010	0.008	0.02
		Stdav %	0.367	0.620	0.91
		Diff. 4921/5501 (%)	**3.3**	**4.8**	**–1.5**

Sample 15 Sample	Sensor		TC [W/mK]	TD [mm²/s]	Cp [MJ/m³K]
15	4921	Average	3.70	1.57	2.36
		Stdav	0.01	0.03	0.04
		Stdav %	0.37	1.96	1.62
	5501	Average	3.56	1.65	2.16
		Stdav	0.01	0.03	0.05
		Stdav %	0.31	1.80	2.12
		Diff. 4921/5501 (%)	**3.8**	**–5.3**	**8.7**

Appendix B

Porosity and density measurements of core samples

1002
ISO 17025

RAPPORT
utfärdad av ackrediterat laboratorium

Sida
1 (3)

Anna Bengtsson
Geo Innova AB
Teknikringen 1
583 30 Linköping

Handläggare, enhet
Marjo Savukoski
Bygg och Mekanik
033-16 51 63, marjo.savukoski@sp.se

Datum
2004-08-27

Beteckning
P402339

Provning av natursten
(1 bilaga)

Uppdrag

Provning av 30 prover från borrkärna KA2599G01. Providentifikation och de egenskaper som har provats framgår under rubriken "Provfakta/provningsomfattning" nedan.

Provtagning och ankomstdatum

Proverna togs ut och skickades till SP genom uppdragsgivarens försorg. SP saknar kännedom om provtagningen. Proverna ankom till SP 2004-08-10.

Provfakta/provningsomfattning

Tabell 1: Provfakta

Borrkärna	Märkning	Kärnans placering i meter
KA2599G01	1A	4,33-4,38
	1B	4,38-4,43
	2A	4,53-4,58
	2B	4,58-4,63
	3A	4,73-4,78
	3B	4,78-4,83
	4A	4,93-4,98
	4B	4,98-5,03
	5A	5,13-5,18
	5B	5,18-5,23
	6A	15,10-15,15
	6B	15,15-15,20
	7A	15,30-15,35
	7B	15,35-15,40
	8A	15,50-15,55
	8B	15,55-15,60

SP Sveriges Provnings- och Forskningsinstitut AB

Postadress
SP
Box 857
501 15 Borås

Tfn / Fax / E-post
033-16 50 00
033-13 55 02
info@sp.se

Org.nummer
556464-6874

Borrkärna	Märkning	Kärnans placering i meter
KA2599G01	9A	15,70-15,75
	9B	15,75-15,80
	10A	15,90-15,95
	10B	15,95-16,00
	11A	24,02-24,07
	11B	24,07,24,12
	12A	24,22-24,27
	12B	24,27-24,32
	13A	24,42-24,47
	13B	24,47-24,52
	14A	24,62-24,67
	14B	24,67-24,72
	15A	24,82-24,87
	15B	24,87-24,92

Tabell 2: Provningsomfattning

Egenskap	Metod [1)]	Prov-identitet	Provstorlek (mm)	Antal delprov	Provnings-datum
Vattenabsorp-tion och densitet	SS EN 13755, ISRM (1973), avsnitt 3, samt SKB MD 160.002 version 1.0	1A tom 15B	Ø 50*60	30	2004-08-16 tom 2004-08-27

[1)] Om inget annat anges avses den senaste utgåvan av metoden.

Provningsresultat

De provade bergarternas egenskaper redovisas bilaga 1.

Mätosäkerhet

Provningsresultaten anges med en expanderad mätosäkerhet om faktor 2 (95 % konfidens intervall):

Densitet	± 4 kg/m3
Porositet	± 0,09 %
Vattenabsorption	± 0,05 %

SP Sveriges Provnings- och Forskningsinstitut
Bygg och Mekanik - Byggnadsmaterial

Lotta Liedberg
Tekniskt ansvarig

Marjo Savukoski
Teknisk handläggare

Bilaga
1 Densitet och porositet

Densitet och porositet

				Uppdrags nr:	P402339
				Metod:	EN 13755, ISRM (1973), avsnitt 3 samt SKB MD 160.002 version 1.0
Vattnets temperatur (°C):	19,5	Våg, inv.nr:	102291	Provad av:	Lej
Vattnets densitet (°C):	0,9983	Termometer, inv.nr	100877	Datum:	2004-08-25-27

	Provmärkning:	Vikt i vatten, Msub (g)	Yttor vikt, Msat (g)	Torr vikt, Ms (g)	Bulk volym, V (cm3)	Por volym, Vv (cm3)	Porositet, n (%)	Porositet AB (%)	Torr Densitet, ρd (g/cm3)	Torr Densitet AB (g/cm3)	Våt densitet (g/cm3)	Våt densitet AB (g/cm3)
1	1A	248,82	387,27	386,66	138,69	0,61	0,4	0,4	2,79	2,77	2,79	2,78
2	1B	253,38	396,52	395,91	143,38	0,61	0,4		2,76		2,77	
3	2A	238,98	376,13	375,58	137,38	0,55	0,4	0,4	2,73	2,72	2,74	2,73
4	2B	245,32	387,77	387,22	142,69	0,55	0,4		2,71		2,72	
5	3A	238,15	376,61	376,11	138,70	0,50	0,4	0,4	2,71	2,71	2,72	2,71
6	3B	234,56	371,35	370,84	137,02	0,51	0,4		2,71		2,71	
7	4A	238,49	375,24	374,72	136,98	0,52	0,4	0,4	2,74	2,72	2,74	2,73
8	4B	237,44	375,53	375,04	138,33	0,49	0,4		2,71		2,71	
9	5A	229,7	363,22	362,67	133,75	0,55	0,4	0,4	2,71	2,71	2,72	2,71
10	5B	242,24	383,2	382,67	141,20	0,53	0,4		2,71		2,71	
11	6A	243,62	380,71	380,09	137,32	0,62	0,5	0,4	2,77	2,77	2,77	2,77
12	6B	254,05	396,71	396,09	142,90	0,62	0,4		2,77		2,78	
13	7A	249,5	390,83	390,21	141,57	0,62	0,4	0,4	2,76	2,76	2,76	2,76
14	7B	246,59	386,1	385,58	139,75	0,52	0,4		2,76		2,76	
15	8A	246,84	385,12	384,66	138,52	0,46	0,3	0,4	2,78	2,77	2,78	2,78
16	8B	247,62	387,12	386,59	139,74	0,53	0,4		2,77		2,77	
17	9A	240,59	376,34	375,78	135,98	0,56	0,4	0,4	2,76	2,77	2,77	2,77
18	9B	252,12	394,09	393,48	142,21	0,61	0,4		2,77		2,77	
19	10A	250,03	391,03	390,47	141,24	0,56	0,4	0,4	2,76	2,77	2,77	2,77
20	10B	252,07	393,79	393,23	141,96	0,56	0,4		2,77		2,77	
21	11A	242,25	379,74	379,16	137,72	0,58	0,4	0,5	2,75	2,75	2,76	2,76
22	11B	255,36	400,05	399,33	144,94	0,72	0,5		2,76		2,76	
23	12A	252,32	394,24	393,6	142,16	0,64	0,5	0,5	2,77	2,77	2,77	2,77
24	12B	244,27	381,64	380,97	137,60	0,67	0,5		2,77		2,77	
25	13A	249,62	389,01	388,24	139,63	0,77	0,6	0,5	2,78	2,80	2,79	2,81
26	13B	257,62	397,84	397,14	140,46	0,70	0,5		2,83		2,83	
27	14A	251,43	392,18	391,58	140,99	0,60	0,4	0,4	2,78	2,74	2,78	2,74
28	14B	232,31	368,69	368,08	136,61	0,61	0,4		2,69		2,70	
29	15A	230,31	366,93	366,32	136,85	0,61	0,4	0,4	2,68	2,69	2,68	2,69
30	15B	245,56	389,34	388,73	144,02	0,61	0,4		2,70		2,70	

P402339 dens Flik: Blad1

Appendix C

TPS measurements of thermal properties, five repeated measurements on the same sample

Results: File:	Sample 9 first (Points)	Temperature	Number of Rows: 21 Th.Conductivity	Th.Diffusivity	Spec.Heat	Pr.Depth	Temp.Incr.	Temp.Drift	Total/Char.Time	Time Corr.	Mean Dev.
Sample 1	(104- 200,tc)	Room temp, 21°C	2.48562892	1.058849475	2.347480903	9.185694575	0.617341022	0 (No corr.)	0.513871537	0.060369213	6.008E-05
Sample 1	(113- 200,tc)	Room temp, 21°C	2.451328879	1.100709935	2.227043476	9.365507833	0.543396177	0 (No corr.)	0.534186888	0.028677107	5.75349E-05
Sample 1	(98- 200,tc)	Room temp, 21°C	2.457440102	1.095449572	2.243316501	9.343101854	0.682347102	0 (No corr.)	0.531633975	0.093614129	0.000103073
Sample 1	(111- 200,tc)	Room temp, 21°C	2.486604994	1.099715683	2.261134429	9.36127703	0.552223213	0 (No corr.)	0.533704366	0.1	0.000100801
Sample 1	(113- 200,tc)	Room temp, 21°C	2.511974131	1.068896952	2.35006202	9.229173442	0.531028815	0 (No corr.)	0.51874769	0.023369549	7.16501E-05
			2.478595405	**1.084724323**	**2.285807466**						
			0.024590514	**0.019463588**	**0.058736079**						
Sample 5	(92- 200,tc)	Room temp, 21°C	2.999379761	1.346619209	2.227340692	10.35898707	0.60037	0 (No corr.)	0.653529419	0.079837388	9.2172E-05
Sample 5	(92- 200,tc)	Room temp, 21°C	2.989081298	1.364133979	2.191193347	10.42613638	0.597423441	0 (No corr.)	0.662029533	0.1	0.000127456
Sample 5	(90- 200,tc)	Room temp, 21°C	2.991130233	1.347800457	2.219267857	10.3635295	0.619350557	0 (No corr.)	0.654102692	0.07964545	8.44931E-05
Sample 5	(90- 200,tc)	Room temp, 21°C	2.984519401	1.357145554	2.199115189	10.39939567	0.61962836	0 (No corr.)	0.658637972	0.064242585	7.28762E-05
Sample 5	(92- 200,tc)	Room temp, 21°C	3.004411794	1.376061444	2.183341309	10.47161826	0.598434391	0 (No corr.)	0.667818066	0.084094635	0.000119172
			2.993704497	**1.358352129**	**2.204051679**						
			0.008050181	**0.012221954**	**0.018658345**						
Sample 8	(40- 200,tc)	Room temp, 21°C	2.493525402	1.212693643	2.056187411	9.830383002	1.479053357	0 (No corr.)	0.588533838	0.018993678	3.88972E-05
Sample 8	(40- 200,tc)	Room temp, 21°C	2.501877519	1.212416642	2.063546005	9.829260222	1.474675842	0 (No corr.)	0.588399407	0.023222922	4.24561E-05
Sample 8	(42- 200,tc)	Room temp, 21°C	2.49649073	1.206508387	2.069186387	9.805281376	1.436877348	0 (No corr.)	0.585532064	0.029563482	4.13691E-05
Sample 8	(42- 200,tc)	Room temp, 21°C	2.495949536	1.202278185	2.076016655	9.78807688	1.438739521	0 (No corr.)	0.5834791	0.038891039	3.45074E-05
Sample 8	(49- 200,tc)	Room temp, 21°C	2.485859905	1.211961958	2.051103905	9.827416951	1.306018666	0 (No corr.)	0.588178744	0.011766742	3.69672E-05
			2.494740618	**1.209171763**	**2.063208073**						
			0.005826739	**0.004618795**	**0.009946291**						
Sample 9	(62- 200,tc)	Room temp, 21°C	2.528407639	1.088847491	2.322095298	9.314904692	1.078017047	0 (No corr.)	0.528429911	0.1	8.76771E-05
Sample 9	(61- 200,tc)	Room temp, 21°C	2.562346437	1.088998124	2.352939257	9.31554899	1.08213856	0 (No corr.)	0.528503015	0.071825393	7.08608E-05
Sample 9	(60- 200,tc)	Room temp, 21°C	2.581241866	1.099997147	2.346589602	9.362474926	1.088556649	0 (No corr.)	0.533840964	0.071633455	6.6955E-05
Sample 9	(60- 200,tc)	Room temp, 21°C	2.574896744	1.077643011	2.389378225	9.266854552	1.090414627	0 (No corr.)	0.522992251	0.067568146	6.85724E-05
Sample 9	(78- 200,tc)	Room temp, 21°C	2.575913861	1.079972462	2.385166244	9.276864839	0.85855801	0 (No corr.)	0.524122759	0.090480506	4.26629E-05
			2.56456131	**1.087091647**	**2.359233725**						
			0.021365487	**0.00884914**	**0.028106687**						

Appendix D

Supporting tables to Section 5.2.3 magma composition and mineralogy

Table D-1. Mineral composition of schematically created samples from diagram presented in Figure 5-5. Mineral components are in percent.

Sample	Quartz	K-feldspar	Muscovite	Biotite	Plagioclase	Amphibole	Pyroxene	Olivine
1	18	62	3		17			
2	22	56	3	1	17	1		
3	24	50	3	2.5	18	2.5		
4	22	47	3	4	18	6		
5	20	40	3	5	21	11		
6	15	30	1	4	32	18		
7	10	12		3	49	26		
8	5			1	61	33		
9					62	34	4	
10					59	31	10	
11					55	29	16	
12					51	24	25	
13					48	14	34	4
14					43	2	45	10
15					32		48	20
16					22		44	34
17					14		36	50
18					8		22	70
19					4		11	85
20					1		4	95
21								100

Table D-2. Mineral properties used in calculation of sample densities (kg/m³) and thermal conductivities (W/(m×K)).

Mineral	Density	Thermal conductivity
Quartz	2.647	7.69
K-feldspar	2.566	2.29
Muscovite	2.852	2.32
Biotite	2.981	2.02
Plagioclase	2.656	1.70
Amphibole	3.176	3.39
Pyroxene	3.248	3.20
Olivine	3.501	4.57

Table D-3. Adjusted mineral property of the thermal conductivity (W/(m×K)) due to chemical composition for the different schematically created samples.

Sample	Plagioclase	Olivine
1	2.34	
2	2.34	
3	1.92	
4	1.92	
5	1.63	
6	1.63	
7	1.46	
8	1.46	
9	1.46	
10	1.46	
11	1.46	
12	1.46	5.10
13	1.46	5.10
14	1.46	4.27
15	1.59	3.60
16	1.59	3.60
17	1.59	3.18
18	1.72	3.18
19	1.72	3.05
20	1.72	3.05
21	1.72	3.14

Table D-4. Calculated densities (kg/m³) and thermal conductivities (W/(m×K)) for schematically created samples.

Sample	Density	Thermal conductivity (fixed mineral properties)	Thermal conductivity (adjusted mineral properties of plagioclase and olivine)
1	2.604	2.71	2.86
2	2.618	2.85	3.01
3	2.636	2.92	2.99
4	2.662	2.89	2.95
5	2.698	2.84	2.82
6	2.736	2.67	2.63
7	2.789	2.46	2.29
8	2.830	2.31	2.10
9	2.856	2.20	2.01
10	2.876	2.24	2.05
11	2.902	2.30	2.11
12	2.929	2.35	2.17
13	2.964	2.42	2.26
14	3.017	2.53	2.35
15	3.109	2.81	2.62
16	3.204	3.14	2.86
17	3.292	3.50	2.89
18	3.378	3.90	3.03
19	3.439	4.22	3.00
20	3.482	4.46	3.04
21	3.501	4.57	3.14

Appendix E

Inverse modelling of prototype repository.

E1 Location of temperature sensors

Table E1-1. Sensor locations in the local numerical grid. The distances from a sensor location to the symmetry axes of deposition boreholes 1 to 6 are denoted D1 to D6 respectively. The right-hand column gives the smallest distance to any of the deposition boreholes symmetry axis. The vertical z-axis starts from the bottom level of the canisters and is positive in the upward direction.

Sensor label	Sensor label	X (m)	Y (m)	Z (m)	D1 (m)	D2 (m)	D3 (m)	D4 (m)	D5 (m)	D6 (m)	Min D1–D6
TROA310	PXPTA0310	0.00	–9.08	–1.72	**9.08**	**15.08**	**21.08**	**27.08**	**45.08**	**51.08**	9.08
TROA320	PXPTA0320	0.00	–9.08	0.99	**9.08**	**15.08**	**21.08**	**27.08**	**45.08**	**51.08**	9.08
TROA330	PXPTA0330	0.00	–9.08	3.38	**9.08**	**15.08**	**21.08**	**27.08**	**45.08**	**51.08**	9.08
TROA340	PXPTA0340	0.00	–9.08	5.78	**9.08**	**15.08**	**21.08**	**27.08**	**45.08**	**51.08**	9.08
TROA350	PXPTA0350	0.00	–9.08	7.78	**9.08**	**15.08**	**21.08**	**27.08**	**45.08**	**51.08**	9.08
TROA610	PXPTA0610	0.00	–4.95	–1.48	**4.95**	**10.95**	**16.95**	**22.95**	**40.95**	**46.95**	4.95
TROA620	PXPTA0620	0.00	–4.96	1.12	**4.96**	**10.96**	**16.96**	**22.96**	**40.96**	**46.96**	4.96
TROA630	PXPTA0630	0.00	–4.97	3.52	**4.97**	**10.97**	**16.97**	**22.97**	**40.97**	**46.97**	4.97
TROA640	PXPTA0640	0.00	–4.98	5.92	**4.98**	**10.98**	**16.98**	**22.98**	**40.98**	**46.98**	4.98
TROA650	PXPTA0650	0.00	–4.99	7.92	**4.99**	**10.99**	**16.99**	**22.99**	**40.99**	**46.99**	4.99
TROA1010	PXPTA1010	–0.04	–2.05	–1.84	**2.05**	**8.05**	**14.05**	**20.05**	**38.05**	**44.05**	2.05
TROA1020	PXPTA1020	–0.04	–2.04	0.86	**2.04**	**8.04**	**14.04**	**20.04**	**38.04**	**44.04**	2.04
TROA1030	PXPTA1030	–0.04	–2.03	3.26	**2.03**	**8.03**	**14.03**	**20.03**	**38.03**	**44.03**	2.03
TROA1040	PXPTA1040	–0.04	–2.02	5.66	**2.02**	**8.02**	**14.02**	**20.02**	**38.02**	**44.02**	2.02
TROA1050	PXPTA1050	–0.04	–2.01	7.66	**2.01**	**8.01**	**14.01**	**20.01**	**38.01**	**44.01**	2.01
TROA1810	PXPTA1810	0.04	8.54	–1.16	**8.54**	**2.54**	**3.46**	**9.46**	**27.46**	**33.46**	2.54
TROA1820	PXPTA1820	0.04	8.49	2.14	**8.49**	**2.49**	**3.51**	**9.51**	**27.51**	**33.51**	2.49
TROA1830	PXPTA1830	0.00	8.43	6.09	**8.43**	**2.43**	**3.57**	**9.57**	**27.57**	**33.57**	2.43
TROA1840	PXPTA1840	0.00	8.41	7.59	**8.41**	**2.41**	**3.59**	**9.59**	**27.59**	**33.59**	2.41
TROA1850	PXPTA1850	0.00	9.98	7.80	**9.98**	**3.98**	**2.02**	**8.02**	**26.02**	**32.02**	2.02
TROA2110	PXPTA2110	0.10	10.06	1.17	**10.06**	**4.06**	**1.95**	**7.94**	**25.94**	**31.94**	1.95
TROA2120	PXPTA2120	0.07	10.04	2.84	**10.04**	**4.04**	**1.96**	**7.96**	**25.96**	**31.96**	1.96
TROA2130	PXPTA2130	0.07	10.02	4.23	**10.02**	**4.02**	**1.98**	**7.98**	**25.98**	**31.98**	1.98
TROA2140	PXPTA2140	0.03	10.00	5.98	**10.00**	**4.00**	**2.00**	**8.00**	**26.00**	**32.00**	2.00
TROA2150	PXPTA2150	2.36	14.28	7.96	**14.48**	**8.61**	**3.29**	**4.41**	**21.85**	**27.82**	3.29
TROA2310	PXPTA2310	6.73	14.32	4.64	**15.82**	**10.69**	**7.11**	**7.67**	**22.70**	**28.49**	7.11
TROA2320	PXPTA2320	1.79	12.00	6.63	**12.13**	**6.26**	**1.79**	**6.26**	**24.07**	**30.05**	1.79
TROA2330	PXPTA2330	2.19	12.00	7.92	**12.20**	**6.39**	**2.19**	**6.39**	**24.10**	**30.08**	2.19
TROA2410	PXPTA2410	3.91	11.93	–3.30	**12.56**	**7.11**	**3.91**	**7.22**	**24.38**	**30.32**	3.91
TROA2420	PXPTA2420	2.74	11.95	1.45	**12.26**	**6.55**	**2.74**	**6.64**	**24.20**	**30.17**	2.74
TROA2430	PXPTA2430	2.19	12.00	4.32	**12.20**	**6.39**	**2.19**	**6.39**	**24.10**	**30.08**	2.19
TROA2440	PXPTA2440	3.39	14.29	7.17	**14.68**	**8.95**	**4.09**	**5.03**	**21.98**	**27.92**	4.09
TROA3010	PXPTA3010	–0.11	15.95	–1.78	**15.95**	**9.95**	**3.95**	**2.05**	**20.05**	**26.05**	2.05
TROA3020	PXPTA3020	–0.07	15.96	0.87	**15.96**	**9.96**	**3.96**	**2.04**	**20.04**	**26.04**	2.04
TROA3030	PXPTA3030	–0.07	15.97	3.27	**15.97**	**9.97**	**3.97**	**2.03**	**20.03**	**26.03**	2.03
TROA3040	PXPTA3040	–0.04	15.98	5.67	**15.98**	**9.98**	**3.98**	**2.02**	**20.02**	**26.02**	2.02
TROA3050	PXPTA3050	0.00	15.99	7.67	**15.99**	**9.99**	**3.99**	**2.01**	**20.01**	**26.01**	2.01

E2 Results for evaluation period 160–365 days

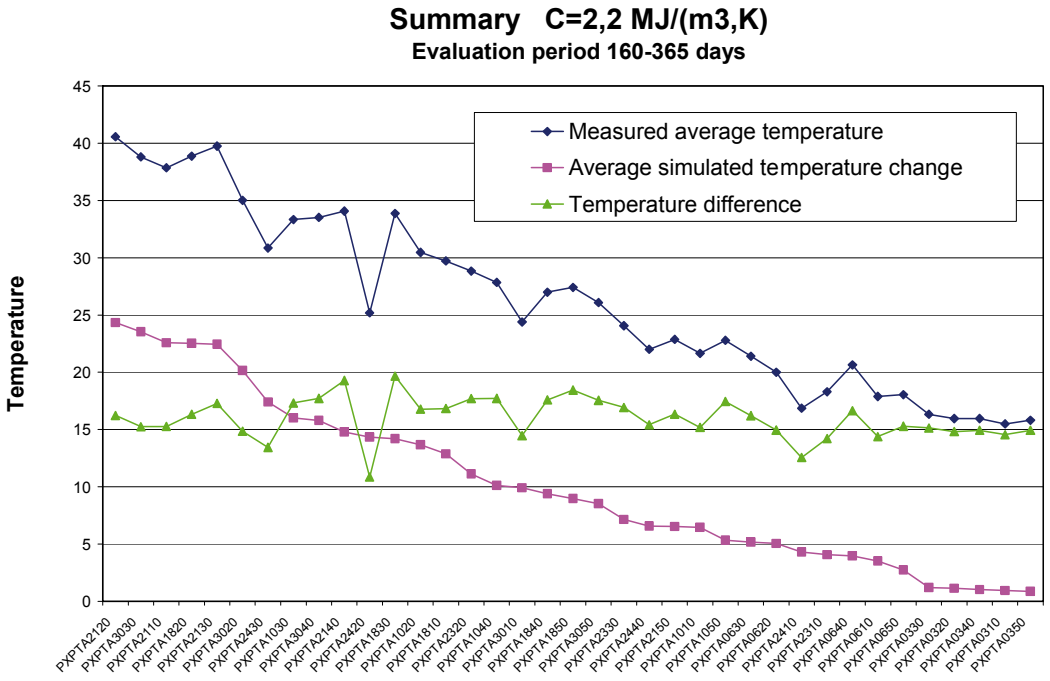

Figure E2-1. *Average measured rock temperature, average simulated temperature increase and difference between these values during the evaluation period 160–365 days for each of the 37 temperature sensors.*

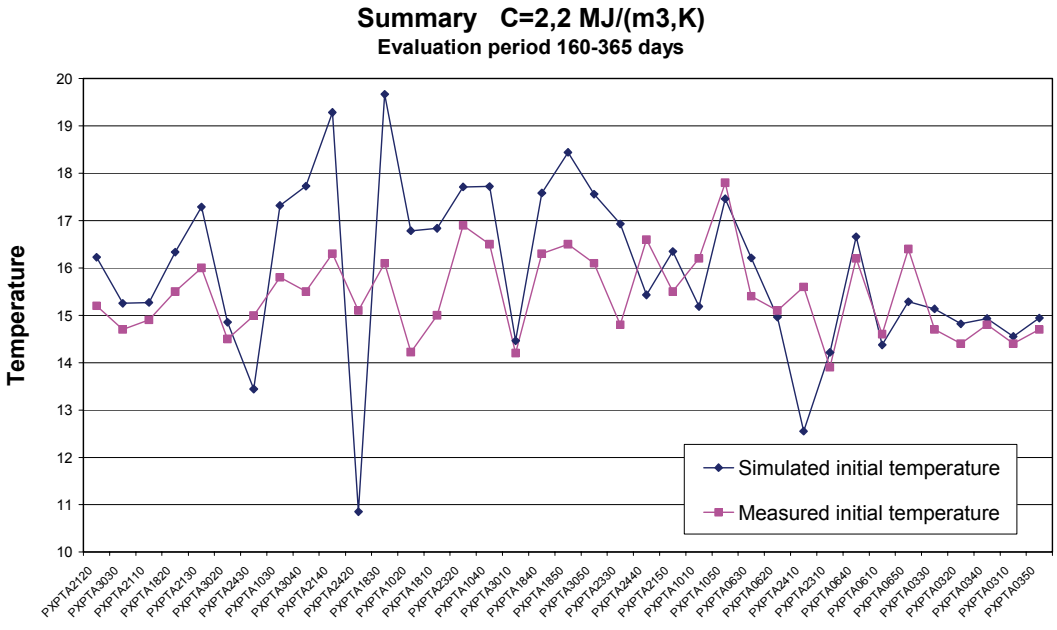

Figure E2-2. *Measured initial temperature and fitted "initial" temperature for each of the 37 temperature sensors. The period 160–365 days is used for fitting the measured and simulated response.*

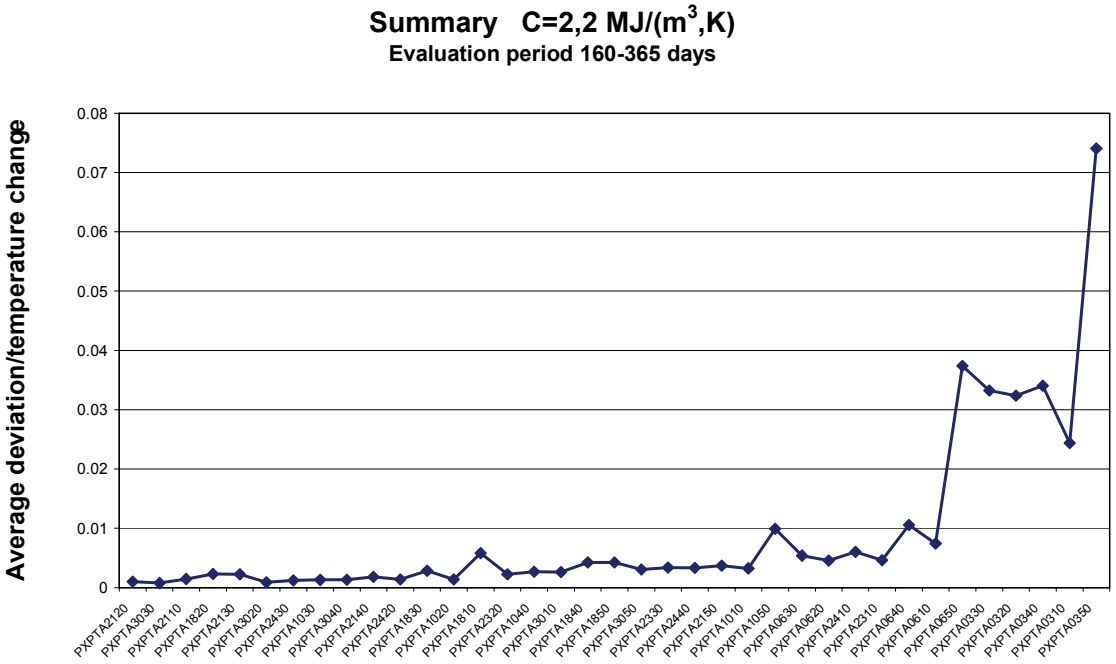

Figure E2-3. *Average deviation between measured and simulated temperatures in relation to simulated temperature increase. The period 160–365 days is used for fitting the measured and simulated response.*

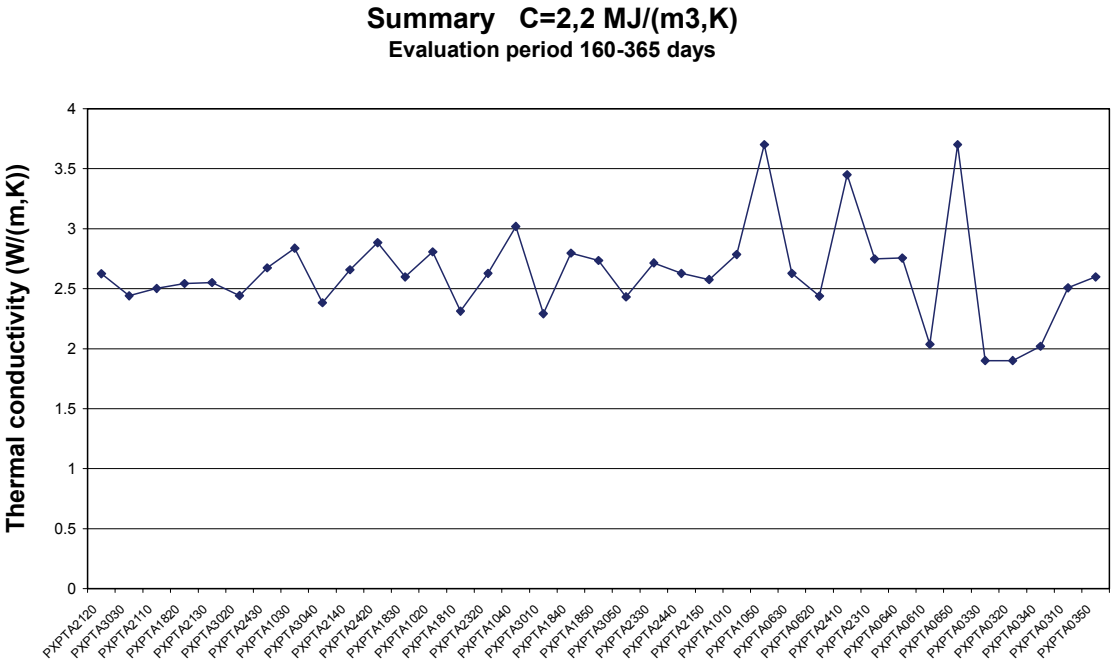

Figure E2-4. *Rock thermal conductivity that gives the best fit between measured and simulated temperatures during the evaluation period 160–365 days for each of the 37 temperature sensors.*

E3 Results for evaluation period 160–525 days

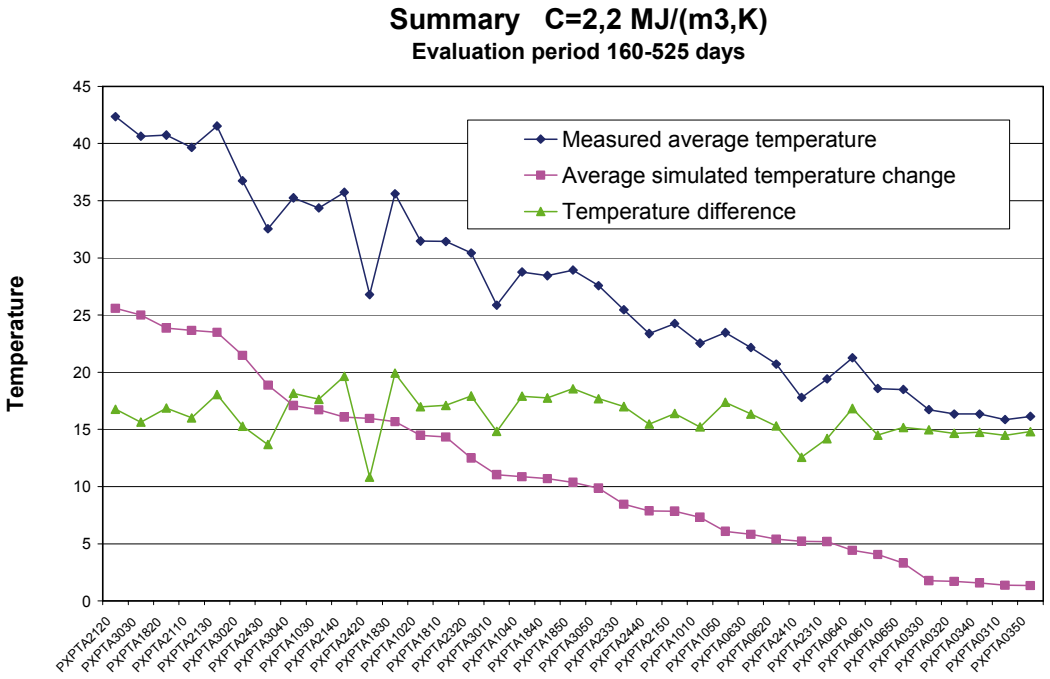

Figure E3-1. *Average measured rock temperature, average simulated temperature increase and difference between these values during the evaluation period 160–525 days for each of the 37 temperature sensors.*

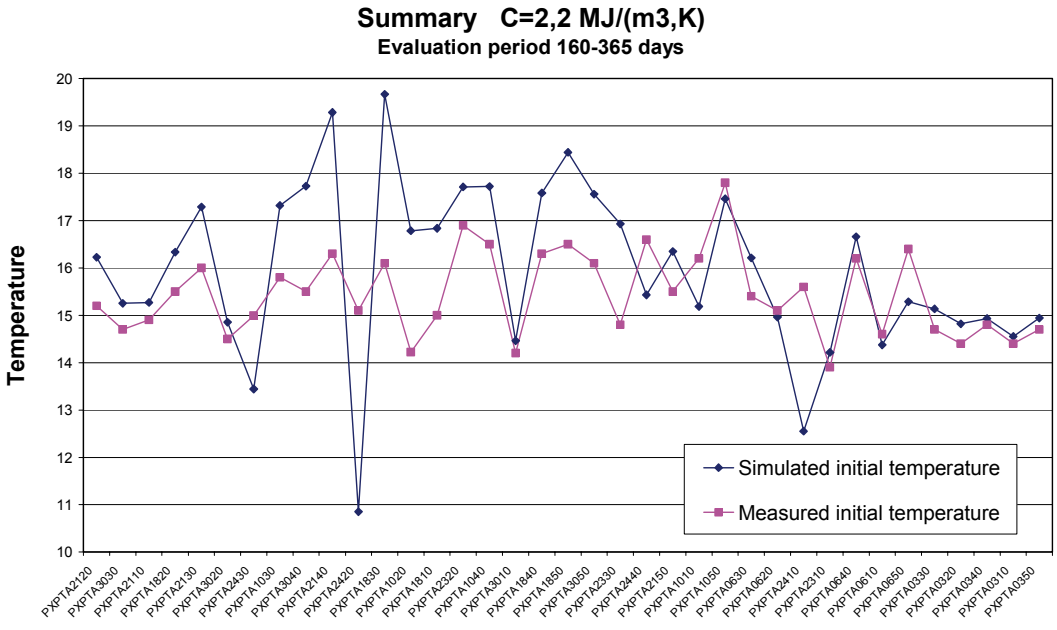

Figure E3-2. *Measured initial temperature and fitted "initial" temperature for each of the 37 temperature sensors. The period 160–525 days is used for fitting the measured and simulated response.*

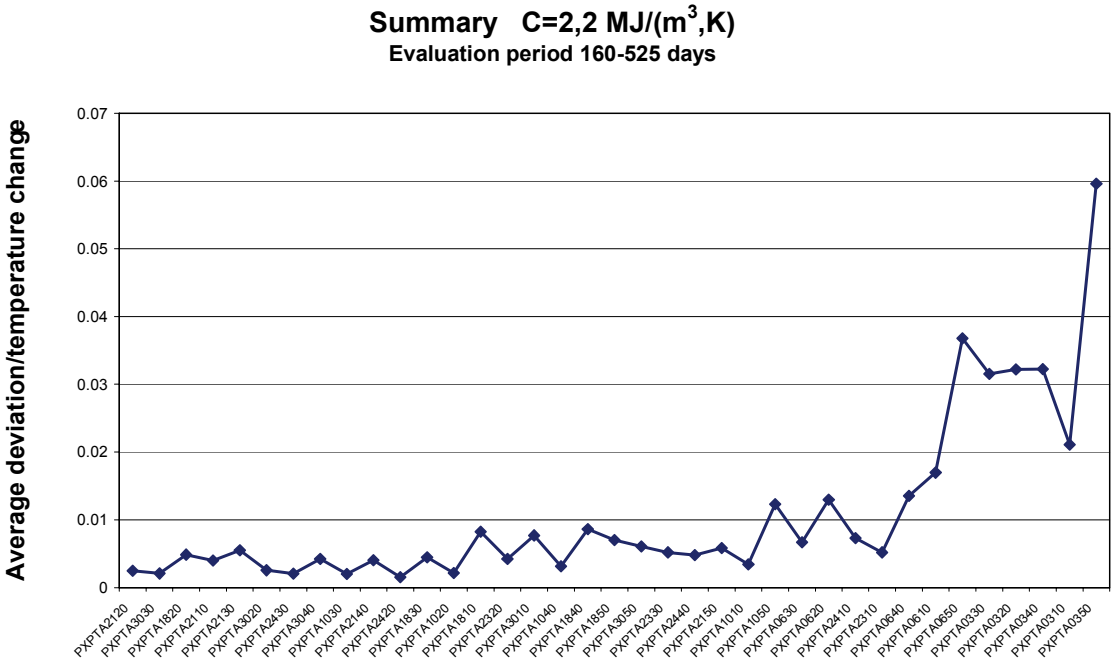

Figure E3-3. *Average deviation between measured and simulated temperatures in relation to simulated temperature increase. The period 160–525 days is used for fitting the measured and simulated response.*

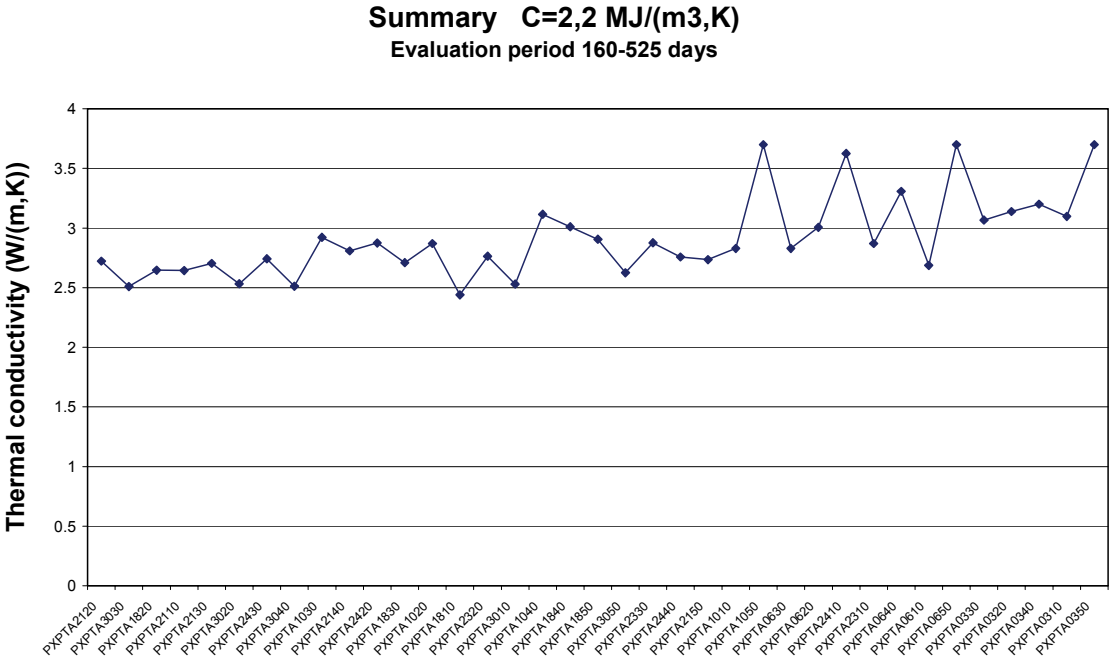

Figure E3-4. *Rock thermal conductivity that gives the best fit between measured and simulated temperatures during the evaluation period 160–525 days for each of the 37 temperature sensors.*